Scuola Internazionale Superiore di Studi Avanzati - Trieste

Investigation on spatio-temporal dynamics of RhoGTPases and their role in neuronal growth cone and actin wave motility

Thesis submitted for the degree of Doctor Philosophiae

Neuroscience Area

PhD in Neurobiology

October 2016

Candidate

Federico Iseppon

Supervisors

Vincent Torre, Dan Cojoc

SISSA - Via Bonomea 265 - 34136 TRIESTE - ITALY

Scuola Internazionale Superiore di Studi Avanzati – Trieste

Investigation on spatio-temporal dynamics of RhoGTPases and their role in neuronal growth cone and actin wave motility

Thesis submitted for the degree of Doctor Philosophiae

Neuroscience Area

PhD in Neurobiology

October 2016

Candidate

Federico Iseppon

Supervisors

Vincent Torre, Dan Cojoc

SISSA – Via Bonomea 265 – 34136 TRIESTE – Italy

INDEX

DECLARATION

All the work described in this thesis arises exclusively from my own experiments, with exception made for the parts regarding myosin and β-cyclodextrin inhibition in actin waves, and was carried out at the International School for Advanced Studies, SISSA and at the Optical Manipulation Lab, IOM-CNR in Basovizza between November 2012 and October 2016, under the supervision of Professor Vincent Torre and Doctor Dan Cojoc.

LIST OF PUBLICATIONS

Published or accepted papers

Iseppon, F., Napolitano, L. M. R., Torre, V., Cojoc, D. Cdc42 and RhoA reveal different spatio-temporal dynamics upon local stimulation with Semaphorin-3A. *Fron. Cell. Neurosci.* **9**(333), doi: 10.3389/fncel.2015.00333, (2015).

Papers under review

Iseppon, F., Napolitano, L. M. R., Torre, V., Cojoc, D. Combining FRET and Optical Tweezers to study RhoGTPases spatio-temporal dynamics upon local stimulation. *Journal of Biological Methods*

Papers in preparation

Iseppon, F., Mortal, S., Napolitano, L. M. R., Torre, V., Acto-myosin contractility and membrane tension regulate growth cone-like actin waves morphology and dynamics.

ABSTRACT

Neurons are highly polarised cells that migrate elongating their axon to reach distant synaptic targets. In the developing nervous system they travel along highly conserved trajectories defined by the molecules present in the surrounding environment, the so-called guidance cues. They can exert the function either at short range by direct contact or at long range, secreted by surrounding and target cells to create gradients that can be sensed by migrating axons.

During the PhD course I focused on investigating the spatio-temporal properties of neurons in response to chemical signals. I have studied in detail the morphology changes of Growth Cones (GC) upon local stimulation and the dynamics of signalling cascades regulating actin dynamics, with a particular attention on Rho-GTPases. Moreover I investigated the morphology, molecule composition of axonal Actin Waves (AWs), as well as the role of Rho-GTPases in their inception and movement kinetics. In these studies I adopted various techniques: from live-cell imaging of the actin dynamics in AWs to a combination of FRET imaging and optical manipulation to image the Rho-GTPases activation in GCs real time upon local chemical stimulus delivery.

The cellular module designed to perceive the guidance stimuli is the Growth Cone (GC), a specialised structure at the tip of the growing axon divided into three regions. The central region contains organelles and has a structural function, the transition region is formed by acto-myosin contractile arcs and the peripheral region, formed by thin filopodia and veil-like lamellipodia structures, that sustain dynamic protrusion and retraction cycles and express on the surface all the receptors to sense the presence of guidance molecules gradients.

The major component of these structures is actin, a molecule that polymerises to form filaments that can be arranged, with the cooperation of a wide variety of actin-binding molecules, into different architectures. Actin filaments are polarised structure with the “barbed” end oriented towards the leading edge and a “pointed” end towards the central region. Filaments undergo continuous cycles of polymerisation at the barbed end and depolymerisation at the pointed end, creating two dynamic behaviours called treadmilling and retrograde flow. The relative prominence of one process over the other is regulated by external signals that are sensed by receptors and initiate different intracellular signalling cascades. These pathways involve a lot of diverse proteins at various levels, but almost all of them pass through a “bottleneck” step: the Rho family of Guanosine Tri-Phosphatases (Rho-GTPases).

Rho-GTPases are molecular switches that cycle between activated, GTP-bound state and an inactivated, GDP-bound state. Their dynamics are modulated by upstream signals, and in turn they

interact with downstream effectors to propagate the signal transduction to the actin cytoskeleton. A single Rho-GTPase can be regulated by many different molecules, called Guanosine Exchange Factors (GEFs), GTPase domain Activator Proteins (GAPs) and Guanine Nucleotide Dissociation Inhibitors (GDIs), and activate a wide range of cellular responses, depending on the cell type and the stimulus received. They are best known for their roles in the modulation of cytoskeleton rearrangements, cell motility and polarity and axon guidance. They exert their effect mainly by affecting actin dynamics, not only in the growth cone but also in the axon shaft.

A particular behaviour of the polarising neuronal cells is the extrusion of GC-like structures that travel along the neurite shaft towards the tip and fuses with the GC to promote elongation. These structures are called Actin Waves (AWs): they have a mean velocity of 2-3 μm/min and appear in a stochastic manner in all the growing neurites with a frequency of about 1-2 waves per hour. Their propagation is strongly dependent on the dynamic behaviour of the actin filaments, with the balance between barbed end polymerisation and pointed end de-polymerisation at its basis. Therefore all those proteins involved in the regulation of actin might have a prominent role in their structure and function, including the RhoGTPases.

The main achievements and findings of my PhD are the following:

1. I combined successfully for the first time FRET imaging with optical tweezers to provide a strong tool to study dynamics of intracellular signalling molecules upon local delivery of chemical attractants and repellants. The versatility of the optical tweezers, that have the possibility to exert both contact stimulation and local gradient delivery, along with the precision and high spatio-temporal resolution of the FRET, allowed us to highlight fine spatio-temporal dynamics of Rho-GTPases in live cells.
2. Local repulsive stimulation by semaphorin-3A triggers local retraction of the side of the growth cone facing the stimulus, with distinct RhoGTPases spatio-temporal dynamics:
    a. I showed, in accordance to previous studies, that the stimulation triggers rapid activation of RhoA within 30 s in the central region of the growth cone, causing a delayed retraction (100-120 s from the stimulus application) that correlates with RhoA activation levels correlate with the induced morphological changes;
    b. I demonstrated that semaphorin-3A local delivery causes a decrease in Cdc42 activity within 60 s from the stimulation. Activity levels vary in a wave-like retrograde manner that proceeds almost in synchrony with the retraction. In few cases the stimulation induced the formation of active Cdc42 waves that propagate in a region away from

the local stimulus and promote the spawning of new filopodia and lamellipodia, suggesting a role of Cdc42 in travelling actin waves;

c. I showed that local stimulation with beads coated with semaphorin-3A induces the formation of active Cdc42 waves propagating from the GC edge to the central region with a mean period of 70 s. Same “travelling” waves have been found in some cases of spontaneous retraction in the neuronal cell culture, but they oscillate with a longer period (110 s).

These overall data show a more complex behaviour for Cdc42 than RhoA, and provide evidence for a higher degree of complexity in the Rho-GTPase signalling network.

3. Actin dynamics in neuronal actin waves are strongly dependent on Cdc42 and Rac1 activation dynamics. By means of immunofluorescence, STED nanoscopy and live cell imaging with inhibitors for different molecules, we showed that:
    a. In accordance with previous studies, actin waves are growth cone-like structures that generate at the proximal segment of neurites and then propagate along the shaft towards the growth cone. When it reaches its vicinity, the growth cone retracts and the two structure fuse together to form a new, bigger and more dynamic growth cone that elongates again;
    b. Myosin-IIB is localised at the rear of the propagating wave, suggesting a possible role of myosin in their dynamics. This role has been confirmed by further experiments in which myosin inhibition with 20 μM blebbistatin highlighted the disruption of the GC-like morphology of actin waves and the disappearing of the GC retraction upon wave incoming at the neurite tip, along with an effect on AW frequency and velocity;
    c. Membrane tension has a role in maintenance of AW morphology and affects also AW initiation and propagation. Addition of 250 μM of β-cyclodextrin disrupted the GC-like morphology and decreased the AW area of more than 50%. Moreover the treatment decreased the velocity and significantly the frequency of AW initiation, suggesting a major role of the membrane in AW dynamicity;
    d. Cdc42 and Rac1 have a strong impact on the initiation dynamics of the actin waves. The frequency of actin waves per hour is significantly reduced under 10 μM of both Cdc42 (ML141) and Rac1 (EHT1864) inhibition: from 2-3 waves per hour to about 0,5 and 1 wave per hour, respectively. Moreover, addition of a high concentration (30μM) of ML141 stopped the AW sprouting almost completely, demonstrating a prominent role of these Rho-GTPases in actin wave initiation at the initial segment of the neurite.

e. Cdc42 and Rac1 have a role also in the propagation dynamics of actin waves. Inhibition of both GTPases resulted in a significant decrease in the velocity of actin waves, from a mean of 2,2 μm/min to about 1,5 μm/min and 1,2 μm/min respectively. Moreover we observed a disruption of the GC-like morphology of AWs, as well as a reduction in the mean area of about 50%.

These results provide new insights for a prominent role of Rho-GTPases in the overall dynamics of the actin cytoskeleton within the travelling waves, in perfect accordance with previously reported data.

INTRODUCTION

The growth cone (GC) is a specialized structure located at the distal tip of growing axons which is fundamental for correct axonal migration and neuronal network formation. It was firstly discovered and described by Santiago Ramon y Cajal as “a concentration of protoplasm of conical form, endowed with amoeboid movements” (Ramon y Cajal, 1890). However, the proof that the growth cone is indeed a motile structure came in 1907, when Harrison, using long-term culture and time-lapse observation, demonstrated that axons elongate from a single cell body with the growth cone at its tip (Harrison, 1907, Dent and Gertler, 2003).

The highly organized but dynamic structure of the GC reflects his purpose: guiding the axon towards its correct post-synaptic target. Previous morphological studies have identified three distinct regions: the peripheral (P) domain, the transition (T) zone, and the central (C) domain, the internal region of the GC, where thicker structures and organelles are located (Dent and Gertler, 2003; Lowery and Van Vactor, 2009) (**Fig 1**). These regions and features can be distinguished in every GC, regardless the shape, because of the cytoskeletal elements that underlie its morphology. The P domain is enriched in actin that can organize into long bundled filaments (filopodia) as well as mesh-like networks (lamellipodia) that contribute to the dynamic motility of the GC. The C domain contains stable, bundled microtubules (MTs) that enter the GC from the axonal shaft. The T domain contains contractile acto-myosin structures (actin arcs) to form a transition ring between C and P domain that regulates relative C-P domains dynamics (Lowery and Van Vactor, 2009; Vitriol and Zheng, 2012) (**Fig. 1**).

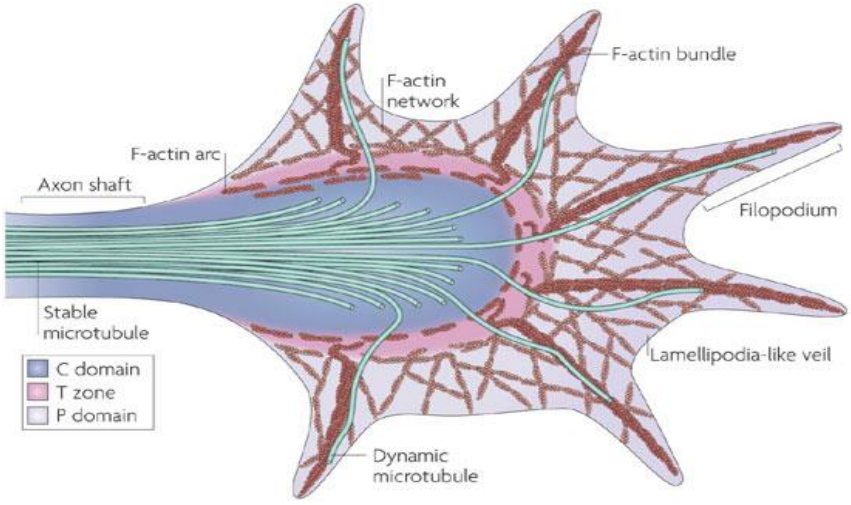

Figure 1: Schematic diagram of the Growth Cone and its cytoskeletal structure. *(Lowery and Van Vactor, 2009)*

The GC can change its shape dramatically by constant re-shaping of its P domain, where filopodia and lamellipodia constantly undergo rapid protrusion/retraction cycles generating the traction force necessary for neurite steering (Forscher and Smith, 1988; Zheng and Poo, 2007). Phase contrast studies in the early 80's showed a link between the GC rate of advance and its shape, particularly P domain dynamics (Argiro *et al.* 1984, 1985; Dent and Gertler, 2003). With the advent of video enhanced difference interferential contrast microscopy it was possible to distinguish and describe three morphologically different stages of GC maturation to extend axonal processes both *in vitro* (Glodberg and Burmeister, 1986; Dent and Gertler, 2003; Lowery and Van Vactor, 2009) and *in vivo* (Godement *et al.* 1994; Dent and Gertler, 2003). These stages are named protrusion, engorgement and consolidation. During protrusion, at first filopodia and lamellipodia elongate through actin filaments polimerization and membrane addition at the leading edges. Subsequently, during engorgemente, then the newly formed veils become invested with vesicles and organelles brought by both Brownian motion and directed transport by the MTs that invaded the P region. Finally during consolidation the proximal region of the GC assumes a cylindrical shape becoming part of the growing axon (Dent and Gertler, 2003; Lowery and Van Vactor, 2009; Mortimer et al, 2009; Vitriol and Zheng, 2012) (**Fig.2**).

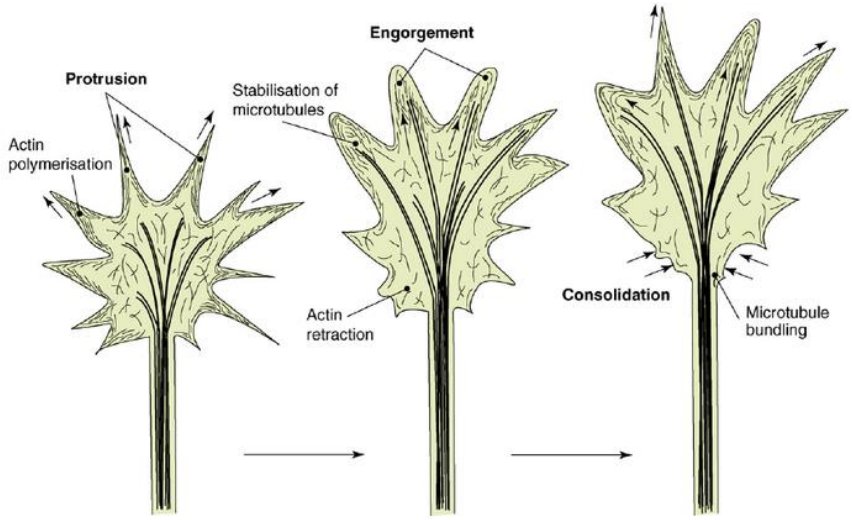

Figure 2: Scheme of GC maturation stages: protrusion, engorgement, consolidation. *(Mortimer et al., 2009)*

1. The intracellular machinery underneath Growth Cones: the cytoskeleton.

The shape of GC and its dynamic changes upon neuron migration and axon elongation are entirely dependent on the dynamics of the underlying cytoskeleton. Actin filaments are the primary element in maintaining shape, while microtubules are essential in giving the axon a stable structure and are important in axon extension (Dent and Gertler, 2003; Lowery and Van Vactor, 2009; Dent *et al.,* 2011).

1.1 Actin filaments

Actin filaments (F-Actin) are double-stranded helical polymers composed of globular actin monomers (G-Actin), a 42kDa protein. The filament elongation is rapid and proportional to the amount of available ATP-bound monomers, and filaments have two distinct ends: the barbed end, where polymerisation usually occurs at a rate of about 3000 subunits/s, and the pointed end, where depolymerisation of ADP-bound G-Actin usually occurs. The results of these reactions is a semi-flexible filament with a persistence length of about 10µm (**Fig.3**) (Dent and Gertler, 2003; Dent *et al.,* 2011; Blanchoin *et al.,* 2014).

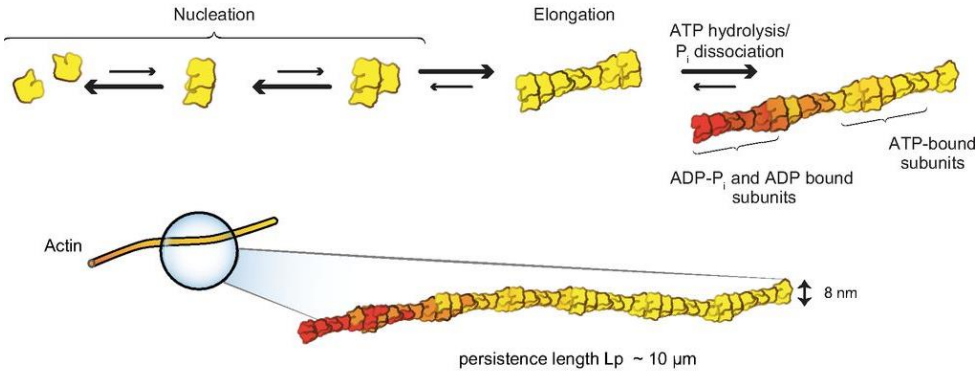

Figure 3: Actin Filaments structure. *Scheme of the polymerization of an actin filament and its mechanics (Blanchoin et al.. 2014).*

F-Actin content in the GC is maximum at the P and T regions, and drops towards the C region. Filaments can give rise to several structures, with the association of a plethora of actin-binding proteins: branched or cross-linked networks, parallel bundles and anti-parallel contractile structures, all of which are important for GC dynamics and navigation function (Blanchoin *et al.,* 2014).

Branched networks are complex mesh-like structures that form the moving lamellipodia in the P region of the GC. They are constructed by a seven protein complex: Arp2/3, which nucleates branches on the side of pre-existing filaments. Besides this “primer” filament, the complex needs a Nucleation Promoting Factor (NPF) to effectively elongate branches: this molecule connects Arp2/3 complex to the primer filament and releases the catalytic pocket to initiate extension (Pollard and Beltzner, 2002). This process is limited by capping proteins that bind and sequester filament barbed ends, stopping actin polymerisation. This interplay gives rise to a dynamic network with viscoelastic properties capable of exerting driving force for the cell membrane of the GC (Dent *et al.,* 2011; Blanchoin *et al.,* 2014).

Cross-linked networks are involved in controlling cell shape and mechanical integrity. Cross-linking proteins of the Formins superfamily link together pre-exsisting actin filaments to create complex shapes. These proteins differ in affinity towards F-Actin and in cross-linking distance: from 10 nm (e.g. fascin, fimbrin) to 160 nm (e.g. filamin, α-actinin), and give rise to different structures. The two structures of most interest for GC geometry and function are parallel and anti-parallel bundles. The former form filopodia in the P region of the GC: formins of the mDia family link together elongating parallel filaments to exert force on the membrane and sprout a micro-spike that, with the help of other structural proteins, will become a filopodium. The latter are important for contractile actin arcs formation in the T region: formins and myosin motors bind together all these filaments with different orientation to form a unique contractile semicircle (Dent *et al.,* 2011; Blanchoin *et al.,* 2014).

Filaments disassembly is fundamental in regulating dynamics of actin-based structures and overall the motility of the GC itself. Two key protein factors are involved in this process: ADF/Cofilin and Myosin, both acting on filament mechanics. ADF/Cofilin is a severing agent that fragments filaments leading to structure breakdown. This process is depending on its saturating concentration along filaments: low concentration leads to severing while high leads to filament stabilisation. It binds preferentially to ADP-bound rather than ATP-bound Actin and facilitate network turnover by dropping the persistence length of filaments to 2μm, and causes massive fracture. Myosin-based dissociation is a two step process: first bundle dissociation and then filament disassembly due to contraction. The filaments, put under high mechanical stress, buckle and then the high curvature favors fragmentation that can propagate to a mesoscopic scale (Blanchoin *et al.,* 2014).

Neuron guidance and GC motility and outgrowth depend on the dynamic properties of F-Actin: the actin structures forming lamellipodia and filopodia undergo continuous reshaping and movement, balancing two different dynamics: retrograde flow and treadmilling. The former keeps the length of actin filaments constant by monomers addition at the barbed end and disassembly at the pointed end, while the latter is the continuous movement of monomers towards the pointed end of the filaments. The retrograde flow is driven both by myosin-mediated contractility and by the push from freshly added monomers at the leading edge of filopodia and lamellipodia. When these structure are strengthened by adhesion to the membrane and the surface beneath, the retrograde flow is slowed down and then the treadmilling can exert the force needed to grow (Dent and Gertler, 2003; Lowery and Van Vactor, 2009; Dent *et al.,* 2011; Blanchoin *et al.,* 2014).

1.2 Microtubules

MTs are polarised structures composed of α- and β-tubulin heterodimers assembled into linear arrays: usually 13 dimer arrays form the MT wall, giving rise to a tubular structure with about 25nm

diameter and a persistence length of about 1mm. As actin filaments, MTs are polarised into a head-to-tail configuration, with a “plus” end that undergoes dynamic growth and rapid shrinkage (catastrophe) and a “minus” end that is inherently unstable and shrinks unless it’s stabilised (**Fig.4**) (Dent and Gertler, 2003; Dent *et al.,* 2011).

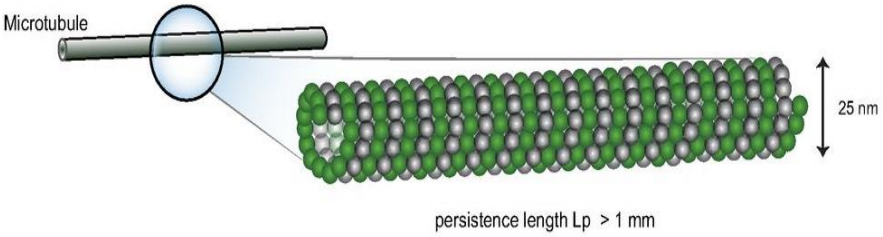

Figure 4: Microtubule structure. *Scheme of the microtubule structure and mechanics (Blanchoin et al., 2014).*

MTs can be functionally modified by several forms of post-translational modification, including tyrosination/de-tyrosination, acetylation, phosphorylation to cite some of them: neuronal MTs, for example, are highly acetylated and sparsely tyrosinated at their minus ends, with vice-versa a high acetylation and sparse tyrosination at the plus ends. These changes affect their binding with associated proteins and thus interaction with other cytoskeletal components and proteins downstream intracellular signalling pathways (Dent and Gertler, 2003). MT dynamics are regulated by diverse proteins that bind specific parts of the MTs, called Microtubule Associated Proteins (MAPs). They can specifically bind to plus end tips and help polymerisation and rescue after catastrophe, they can stabilise MTs and function during neuron outgrowth, branching and polarity, or they can de-stabilise and sever them, being mostly active at the minus end. Disassembly must be tightly regulated, since too much leads to few MTs and outgrowth inhibition, whereas too little leads to MT loop formation in the C region and growth pausing.

In neurons, MTs form a dense parallel array in the axon shaft, spreading apart when they enter the GC, often adopting a looped morphology, when GC is in a paused state. They usually remain confined in the central region of the GC, where they are kept by actin arcs and the dense meshwork in the T and P regions. However, during the protrusion phase, individual MTs actively explore the P region by cycling through a phase of rapid growth and catastrophe events, a property called “dynamic instability”. These MTs help as guidance sensors and provide molecules for directed growth and adhesion of the GC. The second major role occurs during engorgement, when the stable, bundled C region moves into the new area of growth, while consolidation behind fixes the axonal direction (Lowery and Van Vactor, 2009; Dent *et al.*, 2011). Furthermore, MTs are not only “bricks” in the axon shaft, but they are also “routes” which different motor proteins like myosins, kinesins an dyneins can

move along and transport vesicles, other cytoskeletal components and other proteins towards both the GC (anterograde movement) and the soma (retrograde movement) (Lowery and Van Vactor, 2009; Dent *et al.*, 2011).

2. Growth Cone navigation: the importance of guidance cues

When Santiago Ramon y Cajal first discovered GCs, he realized also that axons have the ability to grow efficiently towards their correct synaptic target, becoming one of the strongest advocates of the "neurotropic" hypothesis, or the directed axonal growth in response to chemical cues present in the environment (Ramon y Cajal, 1892, Raper and Mason, 2010). This intuition revealed itself true when it was shown that the first axons that grow in the developing nervous system travel along highly conserved trajectories and pass through well defined "choice points" to form a reproducible scaffold of nerves and tracts. These "pioneer neurons" fasciculate to form a pathway on which later growing neurons extend (Raper *et al.,* 1983a, Raper and Mason, 2010). Although they travel along a common pathway, axons can diverge their trajectory at reproducible choice points, highlighting that each can respond to the same chemical cue in a cell specific manner. The capability of axonal GCs to sense the surrounding environment while growing along specific routes is important in many stages of nervous system development, from midline crossing either in the spinal cord or in the optic chiasm to guidance in and out of the sub-plate region, a pause zone crucial for the correct cortex development (Catalano and Shatz, 1998; Raper and Mason, 2010). The cellular and chemical environment that surrounds navigating axons is crucial for its guidance, as it reflects the growth cone morphology and its dynamics. Depending on different substrata for growing GCs, three general morphologies were identified, that reflect also the growth rate. Torpedo-shaped GCs, often with small lamellipodia extending from a central shaft, are observed during progression through axonal bundles. Wide GCs with complex filopodia structure are observed at choice points, where axons pause from active extension to sense the complex chemical cues in order to proceed in the right direction. Small, condensed GCs were observed when encountering a repulsive chemical signal, and this structure is often followed by retraction: collapsed GCs then can re-extend, repeating the cycle and elongating in a new direction (Mason and Wang, 1997; Sakai and Halloran, 2006; Raper and Mason, 2010). The information present on the environment surrounding navigating axons must be specifically distributed, and it's the sequential response to these guidance cues as axons extend towards their targets that allows for such complex patterns to develop (Raper and Mason, 2010; Kolodkin and Tessier-Lavigne, 2010). Guidance information can take different forms, from electrical gradients to physical constraints and localized molecular cues: they can function either at long or short distance to mediate either attraction or repulsion, dependent mainly on the receptors pattern present on the

GC of the growing axon (Bashaw and Klein, 2010; Raper and Mason, 2010; Kolodkin and Tessier-Lavigne, 2010) (**Fig.5**).

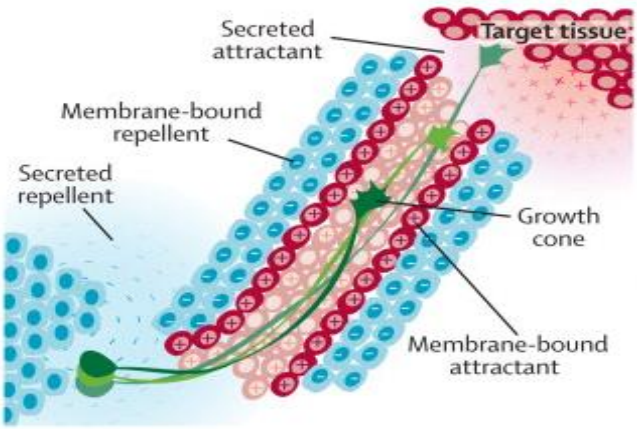

Figure 5: Scheme of different neuronal guidance mechanisms. *Color refers to either attractive (red) or repulsive (blue) mechanisms. (Van Battum et al., 2015)*

2.1 Adhesive Cues

Axons require a permissive substratum to extend in vitro and in vivo, a semi-rigid scaffold where they can adhere on and exert traction force through focal contacts and focal adhesions (Letourneau, 1975; Raper and Mason, 2010). Adhesive cues generally fall into two categories: Extracellular Matrix (ECM) components and Cell Adhesion Molecules (CAMs) expressed on neuronal and non-neuronal cells membranes (**Fig.6**) (Raper and Mason, 2010; Myers *et al.*, 2011).

ECM is composed of a heterogeneous mixture of molecules like collagen, laminin, fibronectin and vitronectin. Besides giving GCs a structure to adhere on, they can bind also smaller molecules and secreted proteins, thus working with soluble factors to promote axon outgrowth (Hynes, 2009; Myers *et al.*, 2012). Some of these components act only as scaffolding proteins, while others, like laminin, can also activate signalling cascades downstream of integrin receptors present on axon and GC surface both *in vitro* and *in vivo* (Myers *et al.*, 2011). They localize in spatially and temporally dynamic patterns in region of active morphogenesis, like spinal cord and cortical sub-plate regions, to modulate and sometimes alter response of growing axons for canonical guidance cues (Stewart and Perlman, 1987; Chun and Shatz, 1996; Myers *et al.*, 2011). Other ECM components, like tenascin, are mainly responsible for neuron-glia interactions: they are expressed on astrocytes, radial glia cells and some immature neurons (Brodkey *et al.,* 1995; Kawano *et al.*, 1995) and possess specific domains for specific cell sub-compartments (Dorries *et al.*, 1996; Myers *et al.*, 2011).

CAMs are expressed by neurons and glia in various combination to mediate adhesion of axons to themselves or other cellular processes. Some important CAMs for axon outgrowth are the Ig superfamily and the calcium-dependent cadherins. They can bind homophilically to serve as indirect physical linkers of the external structure to the internal cytoskeleton of the cell through focal contacts

and focal adhesions. However they are mainly responsible of outgrowth regulation by functioning as signalling molecules, often in heterophilic combinations. Some IgCAMs, like NrCAM and L1, have been implied in guidance as co-receptors in Semaphorin receptor complexes (Mann *et al.*, 2007) whereas others, like DsCAM mediate repulsion as homophilic binding strategy, and are thought to mediate axonal and dendritic self-avoidance (Kolodkin and Tessier-Lavigne, 2010). Thus, redundant utilisation of a small amount of adhesive cues, combined with different quantitative expression and spatio-temporal localisation can direct the formation of highly complex neuronal connections both *in vitro* and *in vivo* (Schwabe *et al.,* 2013).

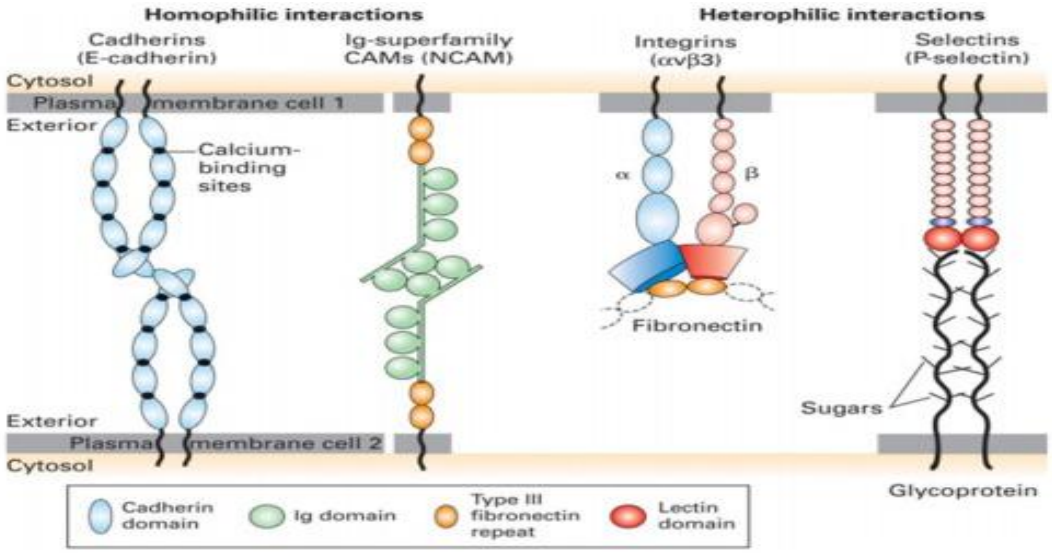

Figure 6: Examples of different adhesion cues and their receptors.

2.2 Morphogens and Trophic Factors

Signalling from morphogens of the Wnt, Hedgehog (Hh) and transforming growth factor b/bone morphogenic protein (TGFb/BMP) families, as well as growth factors like nerve growth factor (NGF), brain-derived neurotrophic factor (BDNF) and many others have been implicated in axon guidance. While the former can mediate for repulsion or attraction, depending on the diverse neural system or organism, the latter are found to be only attractive, promoting neuronal survival, GC motility and axon outgrowth (Kolodkin and Tessier-Lavigne, 2010; Raper and Mason, 2010). Wnts, for example, have been shown to repel axon away of the posterior commissure in Drosophila (Yoshikawa *et al.* 2003) as well as attraction of spinal commissural axons in vertebrates (Lyuksyutova *et al.,*2003) and are important in guiding migration, directing topographic mapping and regulating synapse formation (Kolodkin and Tessier-Lavigne, 2010). On the other hand, NGF and BDNF promote GC attraction and growth through signalling cascade initiated by the binding to receptors of the TrK family (Tojima *et al.,* 2011). Insulin-like growth factor (IGF) and hepatocyte growth factor (HGF) act as chemoattractants for olfactory and motor neurons respectively (Ebens *et al.,* 1996; Scolnick *et al.,*

2008; Raper and Mason, 2010). However, most of the neurotrophins did not elicit a high orientation response *in vitro*, since only steep gradients seem to orient the axonal outgrowth, and thus they may act as short range chemoattractants (Patel *et al.*, 2000) or promote the neuron survival after the connections have already been made (Reichardt, 2006; Raper and Mason, 2010).

2.3 Tropic Guidance Cues

Tropic guidance cues more than other ones impart a directional valence to GC motility, acting as attractants or repellants: the chemotactic cues hypothesized by Ramon y Cayal. They can be secreted by both neighbouring and distant cells and create gradients of information that steer axons "en route", or they can be tightly linked to cell surfaces to influence by direct contact (Raper and Mason, 2010). Using different experimental strategies (**Box 1**), four major families of these so-called "canonical" guidance cues have been identified (**Fig.7**) (Kolodkin and Tessier-Lavigne, 2010):

- Semaphorins;
- Netrins;
- Slits;
- Ephrins.

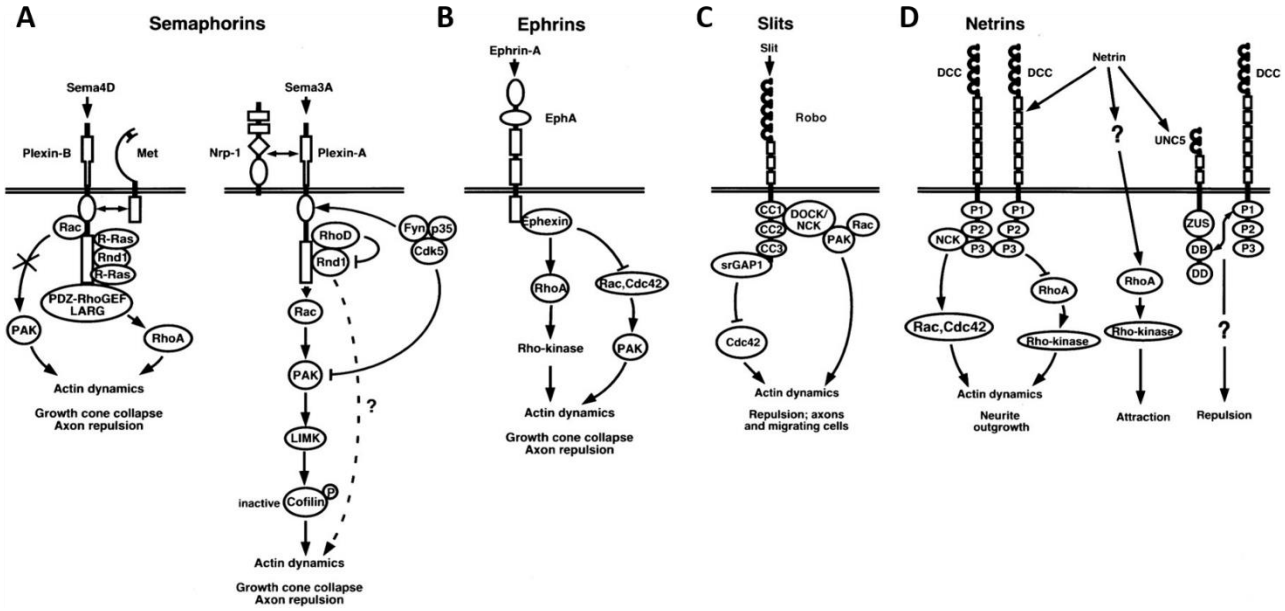

Figure 7: Canonical guidance cues families and their receptors and function. A *Semaphorins family (e.g. Sema4D and Sema3A)* ***B*** *Ephrins family (e.g. Ephrin-A)* ***C*** *Slits family (e.g. Slit)* ***D*** *Netrins (e.g. Netrin-1) (Govek et al., 2005).*

Semaphorins are a family of approximately 20 different molecules that contain a signature Semaphorin domain that plays a key role in association and binding with receptors belonging to the Plexin family, and that can function both at short and long range as potent inhibitory cues (Zhou *et al.,* 2008; Kolodkin and Tessier-Lavigne, 2010). Many of these proteins bind to Plexin receptors, but

some semaphorins, like the Semaphorin-3A (Sema3A), bind to Neuropilin class co-receptors, that link the semaphoring ligand to the plexin receptor and trigger activation through a conformational change of the holoreceptor complex (Antipenko *et al.,* 2003). They are normally expressed in tissues surrounding many peripheral nerves, constraining the growing axons on the correct path. They have a very important function in neuronal development, as for example Sema3A deficiency disrupt normal axon guidance in mice (Kitsukawa *et al.,* 1997). Moreover, many transmembrane semaphorins can act also as a repellent on axon bundles to facilitate unbundling of individual axons. (Tran *et al.,* 2007). Holoreceptor complexes can recruit also other receptors, as NCAM or other IgCAMs, to mediate repulsion by modulating actin cytoskeleton dynamics or disrupting adhesions (**Fig.7A**) (Zhou *et al.,* 2008). The multimeric receptors and receptor complexes justify the diversity of signalling cascades that are activated downstream of semaphorins: the different receptor composition determines the binding but also its functional outcome, creating almost unique signalling events for specific responses and cell type-specific behaviours (Zhou *et al.,* 2008; Kolodkin and Tessier-Lavigne, 2010).

Netrins are a small family of phylogenetically conserved guidance cues. In mammals three secreted molecules (Netrin-1, -3, -4) and two glycosylphosphatidylinositol (GPI)-anchored membrane proteins (Netrin G1, G2) have been identified (Moore *et al.,* 2007). They can be secreted from cells and act as long-range guidance cues for hundreds of microns, or they can be immobilized on the cells producing them and thus act as short-range cues. GCs react to Netrins along a continuum of behaviours that range from repulsion to non-responsiveness to attraction, and this depends on the receptors present on the GC itself (**Fig.7D**) (Moore *et al.,* 2007; Kolodkin and Tessier-Lavigne, 2010). The Deleted in Colorectal Cancer (DCC) receptor alone is responsible for engorgement in shape and area of the GC and for attraction, with DsCAM that might act as co-receptor in some systems (Shekarabe *et al.,* 2002), whereas receptors of the UNC5 family (UNC5A-D) mediate repulsion alone (for short-range repulsion) or in combination with DCC (for long-range repulsion) (Hong *et al.,* 1999; Keleman and Dickson, 2001; Moore *et al.,* 2007). Netrins are expressed on and released from many neuronal and non-neuronal cell types. Netrin-1 is released from floor-plate cells where acts as a chemoattractant for spinal commissural axons creating a circumferential attractive gradient that make them to surpass midline in vertebrates spinal cord (Kolodkin and Tessier-Lavigne, 2010), but as a chemorepellent it directs axon extension by subsets of neurons like cranial, trochlear and spinal accessory motor-neurons (Moore *et al.,* 2007).

Ephrins are a family of cell surface-bound signalling molecules that are divided in two sub-families: class A ephrins tethered to the cell membrane through GPI linkages, and class B ephrins that are

transmembrane proteins (**Fig.7B**). They exert an important role in development and axon guidance, ranging from topographic projections organization to synaptogenesis and trajectories pruning (Kullander and Klein, 2002; Fadheim and O'Leavy, 2010; Kolodkin and Tessier-Lavigne, 2010). They can act both as attractants and as repellent for specific axons subsets, but since they require clusterization and cell-cell contact to bind with receptors and activate, they act esclusively as short-range guidance cues (Kullander and Klein, 2002). Unlike other guidance cues, they exhibit bidirectional signalling:

- forward signalling through tyrosine kinase (TrK) receptors that auto-phosphorylate tyrosine residues in the cytoplasmic portion to activate through association of adaptor proteins like ephexin which can modulate RhoGTPases of Integrin signalling thorugh molecules like R-Ras or FAK (Kullander and Klein, 2002), fundamental for example to form the cortico-spinal tract, dependent on EphA4-Ephrin-B3 binding (Kullander et al., 2001);
- reverse signalling, when Ephrins become receptors for many modulators like Grb4, that triggers a phosphorylation-dependent loss of polymerized actin structures and focal adhesions disruption, and is linked with the proper formation of the anterior commissure, Eph-B2-dependent (Henkemeyer et al., 2002);

Slits are a family of large secreted proteins found originally in Drosophila that act through Robo receptors of the Ig superfamily (**Fig.7C**). They act as repulsive short-range cues that are important in axon repulsion at the midline crossing in vertebrates spinal cord (Brose and Tessier Lavigne, 2000; Kolodkin and Tessier-Lavigne, 2010). Robo receptors are expressed on commissural axons, and act in concert with Netrin/DCC signalling to promote midline crossing and impede the re-crossing of midline by these axons (Andrews *et al.,* 2007; Ypsilanti *et al.,* 2010). Robo receptor family comprises four different isoforms (Robo1-4), expressed in central and peripheral nervous system (CNS and PNS), that can also bind homophilically to regulate de-fasciculation of axon bundles (Andrews *et al.,* 2007). Heparin sulphate, a proteoglycan present in the ECM, can act as co-receptor both facilitating and abolishing Slit/Robo repulsive action (Hu *et al.,* 2001; Ypsilanti *et al.,* 2010). Slits can regulate other functions besides midline crossing: they regulate tangential migration in the forebrain, olfactory bulb and hindbrain (Ypsilanti *et al.,* 2010), axonal migration and targeting (Brose and Tessier Lavigne, 2000), and promote axonal branching activity and secondary collateral branching after first axonal targeting (Brose and Tessier Lavigne, 2000; Ypsilanti *et al.,* 2010).

BOX 1: Optical Manipulation as a tool to deliver localised stimuli.

Cell guidance is a dynamics process that depends on the precise sensing of the directionality of the external stimuli by cell receptors (Raper and Mason, 2010). This is achieved through strict spatial and temporal control of chemical interactions: the specific sub-cellular expression of receptors and proteins realises the compartmentalisation needed for selective pathways activation (Komarova *et al.,* 2005). Hence, a detailed study of these processes requires sub-cellular manipulation and single-molecule approaches (Greulich *et al.,* 2000; Jauffred *et al.,* 2008). Cell signalling experiments are normally performed by pipetting the guidance molecule directly into the growth medium. Such an approach has several limitations in controlling the experimental condition and the stimulation amplitude and timing (Difato *et al.,* 2013). Optical Manipulation (OM) significantly changes the situation: micro-vectors and small reservoirs carrying active molecules can be used to stimulate the cells with precise timing and sub-cellular precision. OM includes 3D particle trapping, manipulation via Optical Tweezers (OT) and photolysis of liposomes by laser ablation (Difato *et al.,* 2013). Optical trapping via OT is the fundamental method for manipulation of small objects: an InfraRed (IR) laser beam is introduced to the experimental setup, and it can trap beads, carriers and vesicles, as well as single cells and even sub-cellular organelles (Ashkin *et al.,* 1987(1); Ashkin *et al.,* 1987(2); Amin *et al.,* 2011; Pinato *et al.,* 2012). An optically trapped bead can be empolyed as a probe to measure the small forces exerted by different cell compartments under controlled stimuli or to apply small forces to the cell (Cojoc *et al.,* 2007), as well as a mean to deliver chemical signals by functionalization with guidance molecules (Difato *et al.,* 2013). This technique has the advantage of perfect localisation of the stimulus because there is no spillover of ligand from the site of contact since the molecules are covalently attached to the bead surface (**Fig.B1**). This is particularly important in neuronal studies: cellular responses are dependent on the precise localisation of the stimulus, due to the different receptor expression in different cell compartments (Gallo *et al.,* 1997; D'Este *et al.,* 2011). Local delivery of active molecules via micro-carrier manipulation brings forth new advantages. An Ultra-Violet laser is inserted for pulsed laser ablation of the lipid vesicle carriers that can trigger both chemical and electrical stimulation (Pinato *et al.,* 2011(1); Difato *et al.,* 2013; Iseppon *et al.,* 2015). The ability to encapsulate a wide variety of molecules and the possibility of moving and dissecting single loaded capsules using optical techniques go along the capability of creating small, brief and precise gradients to which the cell can react (Dholakia *et al.,* 2011; Pinato *et al.,* 2011(2); Pinato *et al.,* 2012; Iseppon *et al.,* 2015). Properly mimicking the physiological process of release of guidance molecules that characterizes the fast diffusion in confined areas is particularly important for studying neuronal cells, which possess polarised structures specific for information processing and signal transmission (axons, dendrites, spines, and synapses). Considering the complex nature of cell signalling mechanisms, optical manipulation techniques can allow the investigation of specific pathways at single cell and single molecule resolution with unprecedented precision and easiness (Difato *et al.,* 2013).

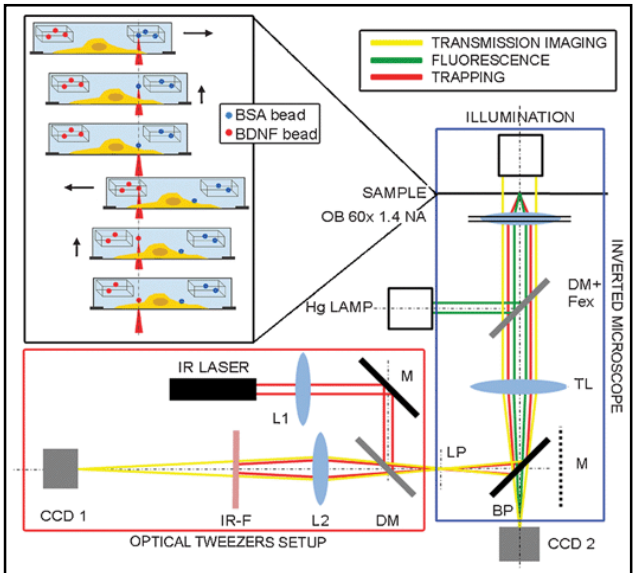

Figure B1: Example of Optical Manipulation setup (low right) and single cell beads stimulation (top left). The IR laser (1064nm) is aligned with both bright and fluorescence light on the sample focal plane for particle trapping. (*D'Este et al., 2012*)

3. Growth Cone navigation: intracellular signalling mechanisms downstream guidance cues.

As stated before, GC correct navigation is a fundamental step in network formation, and guidance cues gradients in the microenvironment play crucial role in controlling axonal direction acting through their receptors distributed in dynamic filopodia and lamellipodia in the P region of the GC. The side of the GC experiencing major cue concentration exhibits higher receptors occupancy: this asymmetry polarizes the entire GC providing the spatial bias in a given direction to grow towards (attraction) or against (retraction). The guidance receptors regulate various intracellular processes like cytoskeleton dynamics, adhesions, acto-myosin contractility and membrane and vesicles trafficking, by activating a plethora of different signalling cascades (Lowery and Van Vactor, 2009; Bashaw and Klein, 2010; Tojima *et al.,* 2011; Dent *et al.,* 2011).

During GC protrusion the F-Actin cytoskeleton is potentiated by activation of nucleating and crosslinking proteins that stimulate filopodia and lamellipodia extension, in concert with disassembly proteins that provide fresh actin monomers. Moreover, adhesion strengthening and retrograde flow inhibition are important steps in GC outgrowth, and exocytosis of vesicles may provide the additional membrane layer required for directed engorgement. On the other hand, a repulsive stimulus triggers an increase of myosin-based contractility at the T zone of the GC that potentiates retrograde flow. Moreover internalization of integrin receptors by endocytosis, which enfeebles the adhesion strength, leads to collapse of the stimulated region which can then grow back again in another direction (Lowery and Van Vactor, 2009; Bashaw and Klein, 2010; Vitriol and Zheng, 2012).

This polarisation of such complex dynamics is achieved by receptor-based intracellular generation of second messengers such as Ca^{2+} and cyclic nucleotides (Tojima *et al.,* 2011). In this manner even a shallow extracellular gradient can be transformed into a steeply graded or compartmentalized signal that orchestrates the various dynamic changes stated before to execute effectively GC bidirectional turning (**Fig.8**).

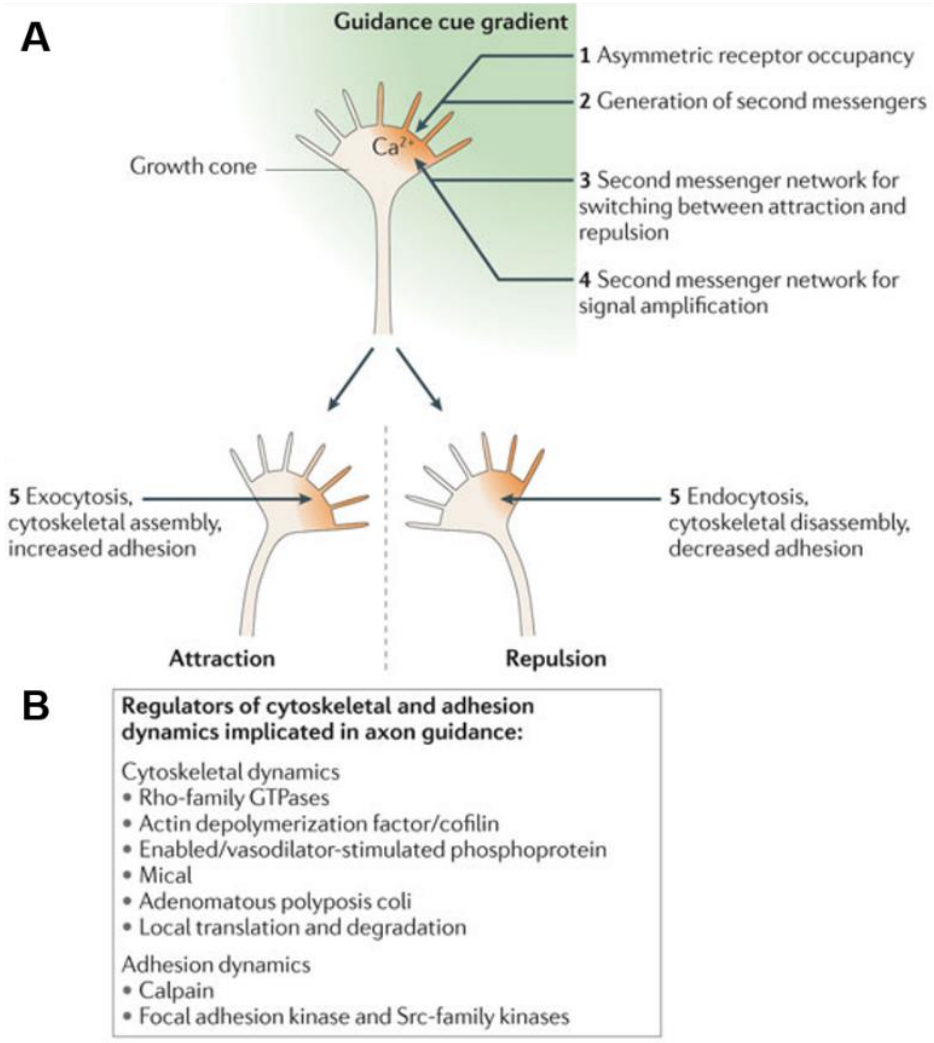

Figure 8: Overview of signalling cascade in cue-mediated GC guidance. A *Graded cue stimulus initiates second messengers signalling (1,2,3,4) that alters GC intracellular dynamics resulting in directional steering.* ***B*** *Examples of direct and indirect regulators of cytoskeleton, adhesion and trafficking dynamics. (Tojima et al., 2011).*

Ca^{2+} signals are a key factor in regulating GC guidance: asymmetric Ca^{2+} elevations occur in the side of the GC facing the cue gradient, regardless the cue being attractive or repulsive. Its mechanisms resides on the gating of differential Ca^{2+} channels: high amplitude Ca^{2+} transients are further amplified by Calcium-Induced Calcium Release (CICR) by ryanodine (RyR) or inositol-1,4,5-triphosphate ($InsP_3$) receptors on the endoplasmic reticulum and mediates cue induced attraction. On the contrary repulsion is mediated by lower amplitude transients, mostly generated by membrane Ca^{2+} channels like transient receptor potential channels family C (TRPC) and L-type voltage-dependent Ca^{2+} channels (VDCC). These differences can be recognized by various Ca^{2+} effectors like Ca^{2+}/Calmodulin-dependent protein kinase II (CaMKII) or the Ca^{2+}/Calmodulin-dependent protein phosphatase, calcineurin. The former has a higher affinity for Ca^{2+} and it diffuses into the cytoplasm, while the latter has a lower affinity for Ca^{2+} and is localised in the proximity of the

endoplasmic reticulum, ready to trigger CICR in response to high amplitude attractive signals (Zheng and Poo, 2007; Tojima *et al.,* 2011). BDNF and Netrin-1, for example, trigger depolarisation of the membrane with TRPC activation and rapid Ca^{2+} release from internal stores, whereas Sema3A signalling mediates hyperpolarisation and repulsion through Cyclic Nucleotides-Gated channels (CNG) activation and cross-regulation of Ca^{2+} through cyclic nucleotides (Nishiyama *et al.,* 2008; Togashi *et al.,* 2008; Bashaw and Klein, 2010).

Cyclic nucleotides, mainly cyclic Adenosine MonoPhosphate (cAMP) and cyclic Guanosine MonoPhosphate (cGMP), can also mediate axon guidance. The asymmetrical changes in intracellular concentration, and the ratio between the two determines the nature of the cues response. cAMP facilitates activation of endoplasmic reticulus Ca^{2+} channels to mediate an attractive response, whereas cGMP blocks CICR to mediate repulsion. They modulate the gating of RyR and $InsP_3$ receptors by phosphorylation by the cAMP and cGMP- dependent kinases PKA and PKG. Such regulation of the Ca^{2+} signal can be mutual, since Ca^{2+} in turn stimulates the production of cAMP by activating adenilate cyclases like AC1 and AC8, creating a positive feedback amplifying attractive signals (Bashaw and Klein, 2010; Tojima *et al.,* 2011). Negative feedbacks, on the other hand, are generated by Ca^{2+} self-inhibition of channels opening probability and cyclic nucleotide-dependent PhosphoDiEsterases (PDEs). Cyclic Nucleotides can also reciprocally inhibit themselves through activation of specific PDEs: this contributes to steeper intracellular gradients of second messengers. These gradient amplification mechanisms, referred to as “local augmentation” and “global inhibition” are fundamental in forcing the GC to a clear-cut decision between attraction and repulsion. cAMP rise on one side of the GC inhibits cGMP locally while increasing its concentration on the other side of the GC, blocking the generation of secondary Ca^{2+} transients and guidance impairment (Tojima *et al.,* 2011).

The second messengers dynamics and interplay are only one step of the complex signalling cascade leading to cue- mediated GC movement. Some of their key targets include the kinases and phosphatases, proteases and more importantly Rho-family GTPases and their regulators. These last ones act as key navigation signalling nodes to integrate the various upstream signals and coordinate the cytoskeletal rearrangements downstream (Lowery and Van Vactor, 2009; Bashaw and Klein, 2010; Tojima *et al.,* 2011).

4. The integration Step: RhoGTPases

The Rho-family of p21 small GTPases is one of six sub-families of the Ras-GTPases, and consist of 20 members, that can be classified into 8 sub-groups. They are best known for their roles in regulating cytoskeleton rearrangements, cell motility and polarity, axon guidance and cell cycle (Ridley, 2006). Their alteration leads to malignant transformation, neurological abnormalities and immunological diseases. They function as molecular switches that receives regulation from upstream signalling cascades and interact with downstream effectors to propagate the signal transduction. A single Rho-GTPase can activate a wide range of cellular responses, depending on the stimulus and cell type (Bourne *et al.,* 1990; Nobes and Hall, 1995; Hall and Nobes, 2000; Govek *et al.,* 2005; Hall and Lalli, 2010; Spiering and Hodgson, 2011; Hodge and Ridley, 2016). Within this plethora of signalling molecules, researchers have focused their attention on three, mainly for their prominent roles in regulating cytoskeletal dynamics: RhoA, Cdc42 and Rac1.

4.1 Rho-GTPases cycle and regulation by upstream factors

Most Rho-GTPases cycle between a GTP-bound active form and a GDP-bound inactive form (Bourne *et al.,* 1990). When active, the Rho-GTPases localise to the cell membrane, where they can activate multiple effectors (**Fig.9**) (Nobes and Hall, 1995; Michaelson *et al.,* 2001; Pertz, 2010). This cycling is mainly regulated by three protein types. Guanine Nucleotide Exchange Factors (GEFs) activate the GTPase by facilitating the GDP-to-GTP exchange, while GTPase-Activating Proteins (GAPs) inactivate the GTPase by increasing its intrinsic GTP hydrolysis rate. Guanine Nucleotide Dissociation Inhibitors (GDIs) sequester the GDP-bound GTPase in the cell cytosol, impeding their association with the membrane and activation by GEFs (Hodge and Ridley, 2016). The binding with GEFs and GAPs takes place at the same site for effector binding, and provokes slight conformational changes that act to displace the Mg^{2+} and release the bound GDP and insert a H_2O molecule into the catalytic pocket of the Rho-GTPase to facilitate by 4000-fold the GTP hydrolysis, respectively (Spiering and Hodgson, 2011). GDIs extract membrane-bound GTPases that have a lipid moiety at the C-terminus, which inserts into the hydrophobic pocket of the GDIs. This interaction brings into contact the N-terminal regulatory portion of the GDI and the effector site of the Rho-GTPase, preventing any spurious binding (Spiering and Hodgson, 2011). The addition of a lipid moiety, which regulates GDI binding, is part of a variety of Post Translational Modifications (PTMs) that includes phosphorylation, ubiquitylation and sumoylation and adds a further complexity level in the Rho-GTPases regulation (Hodge and Ridley, 2016).

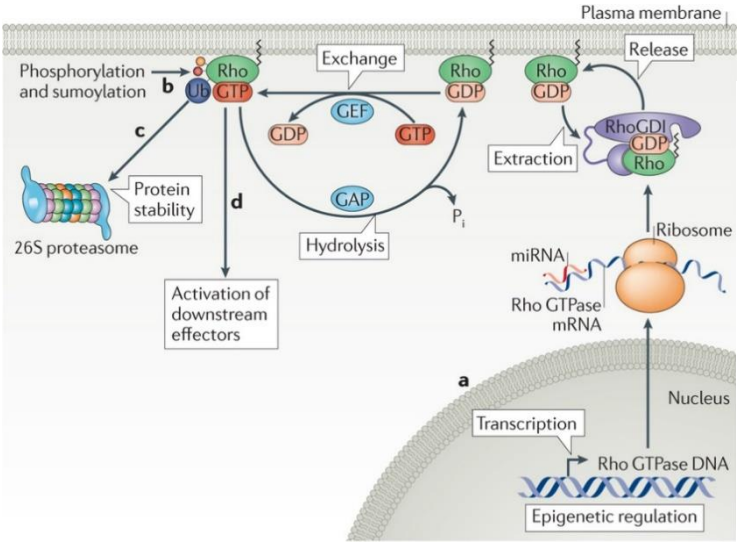

Figure 9: Overview of RhoGTPases cycling and regulation. *GTP-GDP cycle of Rho-GTPases can be regulated by GEFs, GAPs and GDIs.* ***a*** *Expression levels can be controlled by transcriptional level.* ***b*** *PTMs can modulate activity levels.* ***c*** *Protein levels can be acutely regulated by degradation* ***d*** *All these regulation patterns ensure the appropriate spatio-temporal regulation of Rho-GTPases (Hodge and Ridley, 2016).*

Lipid modifications have a crucial role in determining the sub-cellular localisation of Rho-GTPases to distinct membrane compartments, thus influencing their interaction with specific GEFs and signalling pathways. Two types of lipid modifications involve RhoGTPases: C-terminal prenylation and S-palmitoylation. The former is an irreversible process in which a farnesyl or geranylgeranyl moiety is added at a Cys residue in the C-terminal of the RhoGTPase; chaperone proteins like Small GTPase Guanosine Diphosphate Dissociation Stimulator (SmgGDS) can regulate different prenylation pathways. The latter is a reversible process that enables RhoGTPases to interact with the membrane and potentiates their activity: as an example, it increases the stability of Rac1 in its activated state and furthermore, subsequent prenylation and palmitoylation of Cdc42 render the protein unable to bind GDIs (Hodge and Ridley, 2016).

Phosphorylation regulates both the GTPase localisation on the membrane and the overall activity, when it occurs at the lipid modification or at the effector binding site, respectively. RhoA can be phosphorylated by PKA and PKG to inhibit its activation by increasing its binding with GDIs. This process is dual, because it inhibits RhoA but at the same time sequester it from the ubiquitin-dependent degradation, revealing a complex dynamic that is required in leading edge actin protrusion. Rac1 is phosphorylated by Src, FAK or AKT, that inhibit its activity by creating a steric hindrance at the GTP-binding site which increases concentration of GDP-bound GTPase. GEFs and GAPs also can be phosphorylated, modification that results in an increased activity in the majority of the cases. GDI phosphorylation by various kinases like Src, PKCα, PAK1 promotes the its dissociation from the RhoGTPase and therefore GEF-dependent activation (Hodge and Ridley, 2016).

Sumoylation is a PTM that is not necessary for the RhoGTPase activity but helps maintain the activated state, increasing its duration: for now Rac1 is the only GTPase known to undergo sumoylation (Spiering and Hodgson, 2011; Hodge and Ridley, 2016).

Ubiquitylation is a three-step process that most GTPases, GEFs and GAPs share: it marks the proteins for degradation by the 26S proteasome, controlling their expression levels with precise sub-cellular resolution. RhoA and Rac1 can ubiquitylated by different complexes: this is important for its regulation in different cell compartments and in response to different external signals (Hodge and Ridley, 2016).

4.2 Rho-GTPases downstream targets

RhoGTPases regulate many different downstream effectors that affect mainly the cytoskeletal dynamics. They include kinases, phosphatases, actin nucleators and cross-linkers, actin capping proteins, MT-binding proteins and other scaffolding molecules (Burridge and Wennerburg, 2004; Govek et al., 2005; Lowery and Van Vactor, 2009; Pertz, 2010; Spiering and Hodgson, 2011). These effectors can be specific for a single RhoGTPase or affected by different ones in different ways. Among all, some effectors has received extensive attention and their signalling cascade is clearer.

Rho-associated protein kinase (ROCK) is the most known and studied effector downstream of RhoA (Luo, 2000; Burridge and Wennerburg, 2004; Govek et al., 2005; Hall and Lalli, 2010). It's a serine/threonine kinase that, one activated, triggers phosphorylation of many actin-related proteins. It can phosphorylate the regulatory Myosin Light Chain (MLC) and inhibit the MLC Phosphatase (MLCP) to promote contractile activity and increase in retrograde flow both in GC and in migrating cells (Luo, 2000; Govek et al., 2005, Gallo, 2006). ROCK phosphorylates also LIMKinases (LIMK) that in turn inactivates by phosphorylation the actin filaments severing protein ADF/Cofilin: this stabilises actin filaments to allow focal adhesions and stress fibers formation in fibroblasts and cancer cells (**Fig.10**) (Nobes and Hall, 1995; Hall and Nobes, 2000; Luo, 2000; Burridge and Wennerburg, 2004; Hall and Lalli, 2010).

A broader target of the RhoGTPases is the formin family of mDiaphanous proteins (mDia-1, 2, 3): in fact, while mDia-1 binds only to RhoA, mDia-2 binds to RhoA and Cdc42, and mDia-3 shows no preferences binding to all three major RhoGTPases (Govek et al., 2005). Formins are cross-linkers that produce long, unbranched filaments by binding profilin-bound actin monomers and adding to barbed ends of F-actin filaments: the binding with RhoGTPases relieve an auto-inhibitory interaction between the N-terminal and C-terminal domains and activates their function (Nobes and Hall, 1995; Burridge and Wennerburg, 2004; Spiering and Hodgson, 2011). Interestingly, mDia-1 has been

shown to stabilise also MT tips and adhesions by association with the capping complex EB1/APC (**Fig.10**) (Spiering and Hodgson, 2011).

Proteins of the p-21-Activated Kinase (PAK) family are one of the most known effectors downstream of Rac1 and Cdc42. PAK1 and 3 are activated by disruption of an autoinhibitory N-terminal domain: their activation can regulate various effectors. They activate LIMK to inhibit ADF/Cofilin like ROCK, but also inhibits MLCK lowering acto-myosin contractility. Their phosphorylation activates filamin, an F-actin cross-linker important in promoting ruffling events at the leading edge of cells, paxillin, a scaffolding protein important for cell adhesion, and also stathmin, which promotes MT growth (Burridge and Wennerburg, 2004, Govek et al., 2005). Its activation can trigger also a Cdk5-dependent inhibition of PAK that is Rac-dependent and generates a negative feedback to modulate the duration of PAK activity. PAK proteins can also mediate the cross-talk with the other GTPases: PAK5, for example, is a Rac effector that inhibits RhoA activation, controlling the reciprocal Rho/Rac levels that are shown to be fundamental in persistent migration in fibroblasts (**Fig.10**) (Hall and Nobes, 2000; Burridge and Wennerburg, 2004; Govek et al., 2005; Hall and Lalli, 2010; Pertz, 2010).

Another important effector of Cdc42 and Rac1 is the WASp family of proteins: WASp and its neuronal isoform N-WASp are Cdc42- and Rac-dependent, whereas WAVE1/2 are activated by Rac1 but require the previous binding of the GTPase with the adaptor protein IRSp53 (Burridge and Wennerburg, 2004, Govek et al., 2005; Lowery and Van Vactor, 2009; Spiering and Hodgson, 2011). The activation of these proteins results in actin filaments nucleation via the Arp2/3 complex: once active, WASP and WAVE proteins bind to the Arp2/3 complex and bring it to the side of the filament, which activates the nucleation and promotes dendritic actin network formation. This mesh network assembly, in concert with other nucleation promoting factors like IQGAP is important in the dynamics of lamellipodia and membrane ruffles (**Fig.10**) (Govek et al., 2005; Hall and Lalli, 2010; Pertz, 2010; Wallrabe et al., 2015).

IRSp53 is not only an adaptor protein for Rac1-dependent WAVE activation, but is also a direct effector of Cdc42. Its activation localise the mammalian Ena (MEna) actin cross-linking proteins to the leading edge to trigger actin parallel bundles assembly and filopodia formation alongside mDia-1 and other scaffolding proteins (**Fig.10**) (Govek et al., 2005; Ahmed and Goh, 2010; Goh et al., 2012).

4.3 Rho-GTPases localisation and role in motility and guidance

Different RhoGTPases have a different localisation in the cell depending on the cell type and dynamics. Rac1 is predominantly localised in the plasma membrane, as well as Cdc42, that also

localises into the organelles membranes. RhoA, on the contrary, localises almost exclusively in the cytosol, that is indicative of a stable inactivation by GDIs. Upon GTP addition, all GTPases have been shown to translocate to the membrane (Michaelson *et al.,* 2001).

What is fundamental in mediating RhoGTPases cell location are their dynamics and their upstream regulatory proteins. Activation brings the GTPases to the membrane, whereas inactivation by GDIs sequester them in the cytosol (Nobes and Hall, 1995; Michaelson *et al.,* 2001). The different PTMs, GEFs, GAPs, GDIs, all collaborate and antagonise each other in a cell compartment- and stimulus-dependent manner to allow fine spatio-temporal regulation of RhoGTPases. (Spiering and Hodgson, 2011; Hodge and Ridley, 2016). Thus, the most important question to be answered is the sub-cellular localisation of active GTPases, which in the last years have been addressed with live imaging techniques alongside mathematical models and analysis algorithms (**Box 2**).

Most of the early work on RhoGTPases dynamics has been made in non-neuronal cells, studying their polarity, migration and leading edge motility. In actively migrating cells the polarity and direction is regulated by Rac1 and RhoA: the former is active at the leading edge of the cell promoting actin polymerisation via WAVE-dependent Arp2/3 nucleation, and the latter is active at the back of the cell, where it stimulates contractility of the cell rear through the ROCK-MLCK-MLC pathway. This antagonistic correlation is essential for correct directional migration (Itoh *et al.,* 2002; Burridge and Wennerburg, 2004; Pertz, 2010; Ridley, 2011; Kutys and Yamada, 2014). However the scenario is much more complicated, because active Rac1 has been localised also at the trail back of the cell, active RhoA at the leading edge of protruding lamellae, and Cdc42 activation occurs at the leading edges and filopodia tips as well as the Golgi compartment. These results show that one GTPase can be activated simultaneously at multiple cell locations, where it regulates distinct functions through distinct pathways. Effector proteins, as well as GEFs and GAPs, can associate to form complexes that affect the tuning of localized active Rho-GTPases (Govek *et al.,* 2005; Pertz, 2010). G-Protein βγ subunits locate a complex Pix/PAK/Cdc42 at the leading edge during neutrophil migration, similar to the complex IRSp53-Tiam1-Rac1-WAVE2 in the lamellipodia. These “signalling modules” are finely tuned both spatially and temporally and regulate not only Rho-GTPases localisation, but also their ability to transduce the signal downstream and control cross-talk (Luo, 2000; Pertz, 2010; Martin *et al.,* 2016).

Since a neuronal GC is present many of the same morphological structures of a full, migrating cell that explores the environment, Rho-GTPases has been implicated in axonal outgrowth and guidance dynamics (Luo, 2000). Rac1 and Cdc42 are positive regulators of axonal and dendrite outgrowth

and branching, whereas RhoA inhibits elongation of both structures. The RhoGTPases localisation in hippocampal neurons changes with the cell maturation and is GTPase-dependent. Cdc42 is ubiquitous even in fully mature neurons, while Rac1 has the same pattern of Cdc42 until fully mature neurons, where it localises into axons and preferably those who run in close proximity to dendrites of other cells. RhoA also changes its patterns in fully mature neurons, localising only into the dendritic tree: RhoA and Rac, in fact does not co-localise into fully mature neurons (Da Silva *et al.,* 2004).

BOX 2: Imaging RhoGTPases spatio-temporal dynamics: FRET

Imaging spatio-temporal activation of RhoGTPases has been intriguing since the discovery of their implication in cytoskeletal dynamics, cell migration and guidance. However, their localisation and low dynamics range are two major problems: the high cytosolic pool of GTPases impedes the correct visualisation of the active, membrane-bound fraction, that, in any case, is usually less than 5% of the total GTPase cell pool (Pertz, 2010). To enhance the signal-to-noise ratio, ratiometric probes based on Förster Resonance Energy Transfer (FRET) were designed that enable to specifically detect the localisation of active RhoGTPase. The most used are bi- and uni-molecular probes in which the RhoGTPase is fused with the donor fluorophore, and a Rho-Binding Domain (RBD) of a specific effector is fused with the acceptor fluorophore. When the GTPase is modulated by GEFs and GAPs an increase and decrease of the FRET ratio signal is detected, respectively (**Fig.B2**) (Pertz, 2010; Spiering and Hodgson, 2011). The uni-molecular probes, which maintain a 1:1 stoichiometry between donor and acceptor molecules, facilitate FRET efficiency quantification. The "Raichu" probes (Yoshizaki *et al.,* 2003) have been extensively utilised for monitoring RhoGTPase activity and dynamics in different cell types for the imaging of different cell behaviours with or without stimulation (Itoh *et al.,* 2002; Nakamura *et al.,* 2005; Picard *et al.,* 2009; Kunida *et al.,* 2012; Myers *et al.,* 2012). What emerged from these studies is that one RhoGTPase can be activated simultaneously at multiple cell locations, where it regulates distinct functions: thus the need to correlate the activation patterns of the RhoGTPases between each other and with the cytoskeleton and cell dynamics. This can be done either with mathematical modelling (Jilkine *et al.,* 2007; Weiner *et al.,* 2007; Holmes *et al.,* 2012) or, since imaging multiple RhoGTPases activation in the same cell with FRET is nearly impossible, by developing algorithms of analysis that allow the computational multiplexing of multiple RhoGTPase activities imaged in different cells and correlation with leading edge velocity (Machachek and Danuser, 2006; Machachek *et al.,* 2009). This approach has been further optimized for studying the role of RhoGTPases during cell migration and even predicting their relative "weight" in modulating different migration behaviours (Yamao *et al.,* 2015; Martin *et al.,* 2016). The knowledge of the RhoGTPases dynamics and their regulation mechanisms is becoming clearer and clearer, especially with the help of high spatio-temporal resolution imaging techniques and local stimulation techniques that can deliver gradients to precise cell locations, mimicking better the in vivo environment. However, since fluctuations in RhoGTPase activities occurs with a seconds-to-minutes time scale, adequate dissection of these mechanisms will require tools that apply perturbations and allow imaging at these specific time scales (Pertz, 2010).

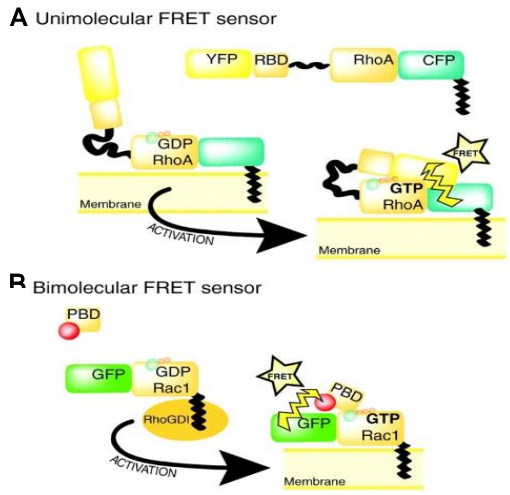

Figure B2: FRET sensors designs. A Uni-molecular sensor **B** Bi-molecular sensor *(Pertz, 2010).*

Within the GC, active Rac1 localises widely into the P region, Cdc42 shows a gradual increase towards the leading edge and RhoA, when active, localises into the P and T regions of the GC where it can control actin depolymerisation and myosin-based contractility (Nakamura *et al.,* 2005; Govek *et al.,* 2005; Gallo, 2006). Rho-GTPases regulation is important also for neuronal polarization, as it was for non-neuronal cells. Tight Cdc42 regulation is required for axonal specification: it acts downstream of Rap1B GTPase that localises a complex mPar3/mPar6/aPKC that interacts with Cdc42 and Rac1 active forms. They promote a local actin depolymerisation required for initial axon formation, and their activation enhances PI3Kinase activity that can activate Rac1 thorugh the Tiam1 GEF in a positive feedback loop that can help break the symmetry and polarise the cell (Govek *et al.,* 2005; Hall and Lalli, 2010). Axon extension requires a precise spatio-temporal regulation of Rho-GTPases and a balance between their activity levels. In cultured cerebellar granule cells SDF-1X promotes extension at low RhoA levels through mDia1 and Rac-dependent extension, while it inhibits growth at high RhoA levels through ROCK and increased contractility. Rac1 levels are also important for proper axon growth: too low levels result in overshooting beyond the proper synaptical target, whereas too high levels stall the axonal growth (Luo, 2000; Arakawa *et al.,* 2003; Govek *et al.,* 2005).

RhoGTPases are important for regulating GC dynamics and guiding axon to their correct synaptic target (**Fig.10**). They are known to be downstream of every canonical guidance cue and many trophic factors (Govek *et al.,* 2005; Hall and Lalli, 2010; Bashaw and Klein, 2010; Kolodkin and Tessier-Lavigne, 2010). BDNF stimulates FAK and Src activation, which in turn activate Cdc42 via GEFs like p130Cas or GRAF in lamellipodia and filopodia in the P region of the GC (Myers *et al.,* 2012). NGF stimulates protrusion and attractive turning via simultaneous Rac1 activation and RhoA inactivation. Its receptor, TrkA, localises and activates Ras-GTPase that activates in turn PI3K and then Rac1 downstream. RhoA-ROCK pathway is inhibited by Rac1 activation, possibly through some specific effectors like PAK5, resulting in increased actin polymerisation and decreased contractility at the leading edge of the GC (Govek *et al.,* 2005).

GC collapse induced by Sema3A depends on Rac1 and RhoA activation. The former interacts directly with Plexin-A1 and Plexin-B1 receptors: this may be a form of sequestration of Rac, rendering its binding with GEFs unlikely, or a way to promote the receptor endocytosis required for Sema-3A mediated collapse (Bashaw and Klein, 2010: Hall and Lalli, 2010). Sema-3A can also trigger a localisation of RhoA mRNA translation to the developing axons and GCs upon stimulation, sufficient to trigger GC collapse (Hall and Lalli, 2010). RhoA is activated downstream of Sema-3A and Sema-4D by many GEFs like PDZ-RhoGEF. It enhances contractility through ROCK and promotes actin stabilisation through LIMK activation and subsequent ADF/Cofilin inhibition (Govek

et al., 2005: Hall and Lalli, 2010). Also in this case an antagonistic relationship between Rac and RhoA has been observed, highlighting the presence of conserved cross-talk mechanisms to allow fine directional regulation of axon extension (Govek *et al.,* 2005; Bashaw and Klein, 2010).

Ephrin-dependent GC collapse is mediated by an unbalance in Rho-GTPases activation levels. In the absence of stimulation ephexin1 is bound to the EphA4 receptor and activates all GTPases, but ephrin-induced receptor clustering promotes ephexin1 phosphorylation, which shifts the GEF activity toward RhoA causing local actin depolymerisation. Rac1 inactivation can be mediated also by the Rac GAP α-chimaerin that enhances RhoA activation. This yet again antagonistic relationship between RhoA and Rac1 is enhanced by the cooperative actions of the two GEFs, and sufficient to induce GC collapse and axon retraction. However, ephrin signalling can trigger local transient Rac1 activation, important for mediating endocytosis and allow cell detachment during retraction (Govek *et al.,* 2005; Bashaw and Klein, 2010).

Slits act through Robo receptors to mediate repulsion at the midline of the nervous system, and increased Cdc42 and Rac1 activities cause deficiencies in axonal ability to cross the midline (Govek *et al.,* 2005). Slit stimulation triggers the activation of specific Rac and Cdc42 GAPs called srGAPs that downregulate their activity and enhance RhoA activation. On the other hand, Dock is an adaptor protein that can bind PAK and Robo cytoplasmic domain. This binding increase modestly Rac1 activity, probably through the dual Ras-RhoGEF Sos. The coordinated activities of GEFs and GAPs may promote precise spatio-temporal cycling of Rac activity, which may be more important than the overall levels of active Rac in the motile GC (Govek *et al.,* 2005; Lowery and Van Vactor, 2009; Bashaw and Klein, 2010).

Netrin-1 with its receptor DCC induces cytoskeletal rearrangements downstream of Rac1 and Cdc42 that promotes both axon growth and attractive turning (Govek *et al.,* 2005; Picard *et al.,* 2009). Netrin induces the rapid activation of Rac1, Cdc42 and PAK1, maybe through the direct association of a dual GEF like Trio with the receptor. DOCK180 is another Rac GEF that is required for Netrin-dependent axonal outgrowth that can interact with the DCC receptor. Rac1, Cdc42 and PAK1 activation in the GC result in WASP and WAVE-dependent Arp2/3 recruitment and increase in actin polymerisation (Hall and Lalli, 2010; Bashaw and Klein, 2010).

In conclusion, Rho-GTPases play a fundamental role in integrating many different external signals, both chemical and mechanical, with the superimposed intracellular machinery that steers GCs, extends axons and favours cell migration. The GTPase step is the bottleneck of many signalling cascades mediating so many different effects on cell dynamics that has to be regulated tightly in

both spatial and temporal manners. The discovery of the possible organisation of marco-complexes containing GEFs/GAPs, Rho-GTPases and effectors highlights a much more complex scenario than the simple receptor-GTPase-effector that was brought to light by early studies.

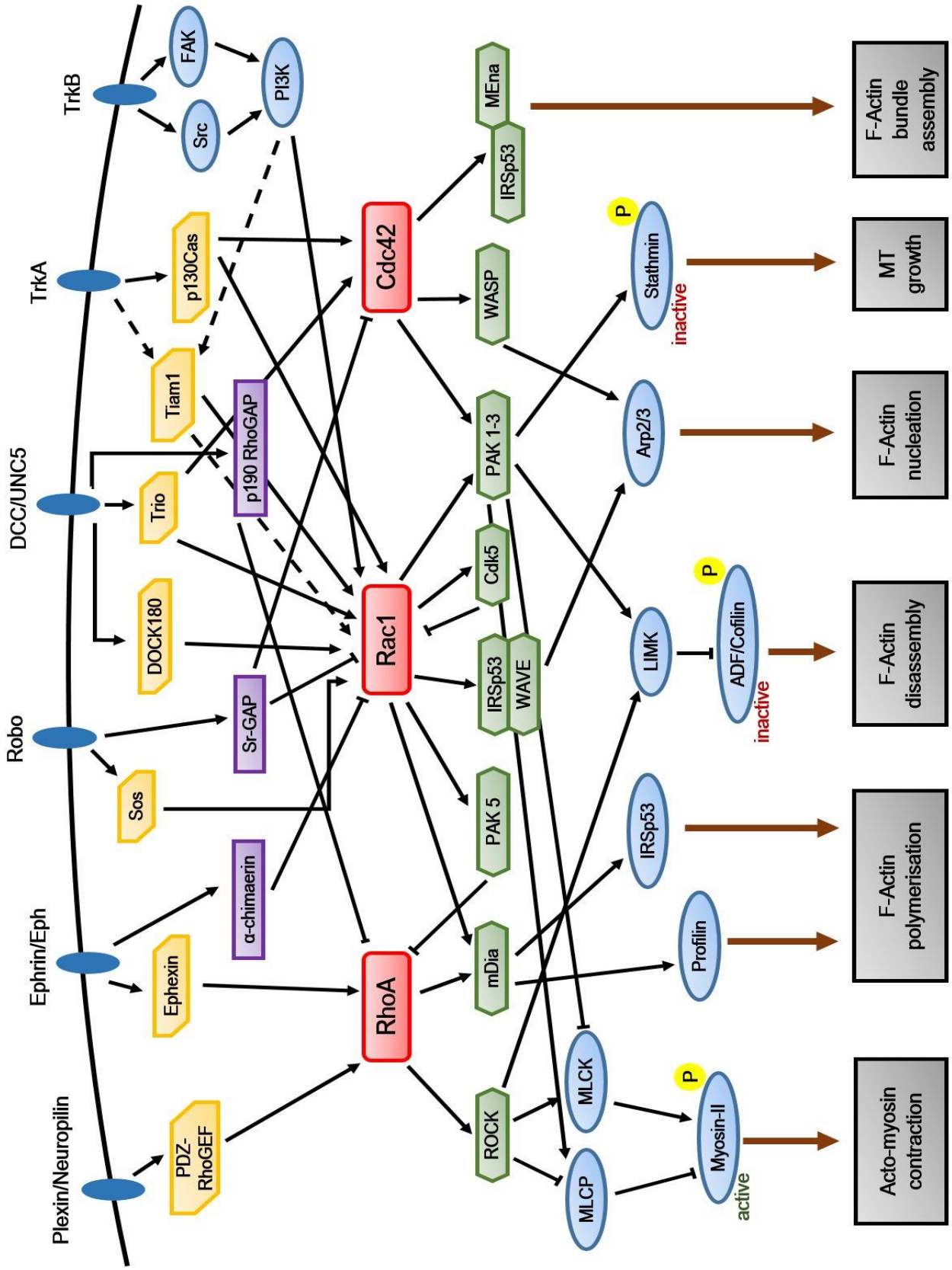

Figure 10: Scheme of RhoGTPases signalling cascade downstream of major guidance molecules.

5. Actin in Axon: waves, rings, trails and patches of actin regulate axonal extension and structure.

In the neuronal axon, actin is enriched mainly at the GC site, where is involved in navigation, signalling and stabilisation upon target contact. In contrast, actin localisation in the axonal shaft has remained obscure and somewhat uninteresting. However, recent super-resolution and live-cell imaging studies have uncovered various peculiar modalities of actin organization and dynamics inside the axonal shaft. These newly discovered features are called waves, rings, patches and trails (**Fig. 11**) (Arnold and Gallo, 2014; Roy, 2016).

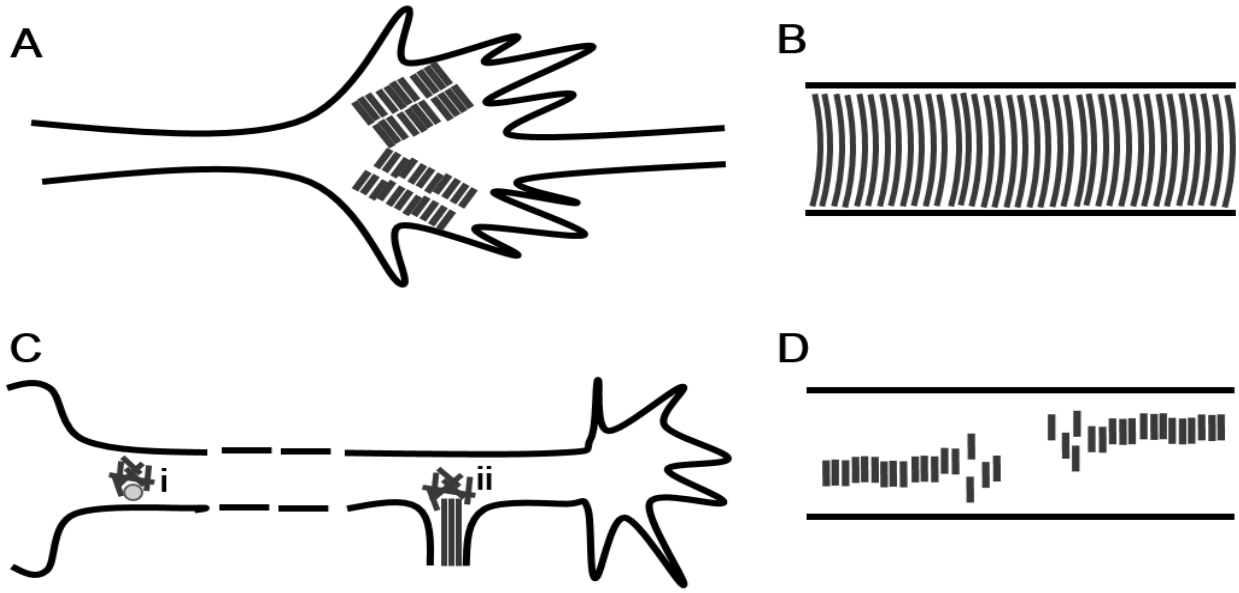

Figure 11: Actin structures in the axon. A *Actin Waves (AWs).* ***B*** *Actin Rings (ARs)* ***C*** *Actin Patches (APs) in the proximal* ***(i)*** *and distal* ***(ii)*** *axon.* ***D*** *Actin Trails (ATs). (Adapted from Roy, 2016)*

5.1 Actin Waves

Actin Waves (AWs) (**Fig.11A**) are growth cone-like structures that emerge at the base of neurites and travel towards the tip with a mean velocity of 2-3μm/min. Upon arrival in the proximity of the neurite tip, the GC retracts and fuses with the incoming AW creating a bigger and more dynamic GC that starts back neurite protrusion (Ruthel and Banker, 1998,1999; Flynn *et al.,* 2009; Katsuno *et al.,* 2015; Winans *et al.,* 2016). AWs appear in a stochastic manner in all neurites at early stages of neuronal development and then concentrate in the process that will become the axon. They have been observed also in non-neuronal cells, where they usually migrate along the cell perimeter and have been called “travelling (t-) waves” (Kunida *et al.,* 2012; Allard and Molginer, 2013; Roy, 2016). The principal motor of AWs are the actin filaments, which fan out the neurite shaft, orientating at acute angles with the barbed ends towards the GC and with each filament undergoing directional treadmilling (Katsuno *et al.,* 2015; Roy, 2016). Despite being critically dependent on actin dynamics,

AWs are also disrupted by MT-depolymerising agents (Ruthel and Banker, 1998; Winans *et al.,* 2016). Single MTs enriched in doublecortin (cytoskeleton stabilising protein) extend into AWs, and their number is increased in and behind the proceeding wave, along with an increase in the neurite area: there may be a reciprocal interplay between actin and MT in the form of a positive feedback, where the widening of the neurite allows for more MTs to elongate (Ruthel and Banker, 1998; Tint *et al.,* 2009; Winans *et al.,* 2016; Roy, 2016).

Actin and MTs are not the only constituents of AWs: many other proteins are found in AWS, like cortactin, shootin-1, ADF/cofilin, Arp2/3 complex, Rac1 and Cdc42. All these proteins cooperate to build the intracellular machinery that AWs use to migrate along the neurite shaft. Cortactin activates the Arp2/3 complex-dependent nucleation of actin filaments and branches inside the AWs, while ADF/cofilin produces fresh G-Actin monomers for elongation at the barbed ends of filaments. Shootin-1 slows down the retrograde movement by coupling filaments to L1-CAM adhesions to the substrate and Rac1 and Cdc42 coordinate all the various effectors (Flynn *et al.,* 2009; Toriyama *et al.,* 2013; Katsuno *et al.,* 2015; Winans *et al.,* 2016). It's possible that Cdc42 spatio-temporal activation, found in and beyond the AWs, may be responsible for their constantly anterograde movement, whereas Rac1 may be its starting trigger at the soma-to-neurite junction (Flynn *et al.,* 2009; Winans *et al.,* 2016). Another important player in the dynamics and impact of AWs on the neurite is myosin II: its inhibition reduces the retraction induced by proximity of the AW with the GC and increases filopodia dynamics and neurite outgrowth and branching, while decreasing the frequency of AW appearance (Flynn *et al.,* 2009; Katsuno *et al.,* 2015).

AWs are observed also *in vivo* in cortical neurons as well as hippocampal neurons of the dentate gyrus and CA3, CA1 regions: they seem to retain the same characteristics and dynamics of the ones studied *in vitro* (Flynn *et al.,* 2009; Katsuno *et al.,* 2015).

Consistent with their concentration on the axonal shaft upon polarisation and their impact on neurite growth both *in vitro* and *in vivo*, they have been implied in neurite outgrowth and symmetry breaking in early stages of neuron maturation: they promote competition between neurites generating large stochastic fluctuations in multiple neurites as they explore the environment for cues, while enhancing actin- and MT-based transport of axon-promoting factors to the tip of the neurite that will polarise into the final axon (Ruthel and Banker, 1998,1999; Flynn *et al.,* 2009; Katsuno *et al.,* 2015; Winans *et al.,* 2016).

5.2 Actin Rings

Actin Rings (ARs) (**Fig.12B**) are periodic, quasi-1D circumferential lattices of actin and spectrin underneath the axonal plasma membrane visible only by super-resolution microscopy (Xu *et al.,* 2013; D'Este *et al.,* 2015; Roy, 2016; Leite and Sousa, 2016). F-Actin arranges in short filaments capped by adducin and aligned to form a circle, whereas spectrin proteins associate to form a tetrameric spacer between different rings, forming this coordinated network with a spatial period of about 190nm that is elastic and stable to give mechanical support to the plasma membrane (Xu *et al.,* 2013; D'Este *et al.,* 2015). Adducin has also the role of stabilising the structure by binding both to actin and spectrin: loss of this protein results in fact in increase in the ring diameter and axonal degeneration with major impairments in nerve formation (Leite *et al.,* 2016). ARs interact also with MTs: in fact MT loss leads to ring structure loss in neurons, and this cross-talk may be important in creating periodic docking sites for the regulation of the myosin-based axonal transport (Zhong *et al.,* 2014; Leite and Sousa, 2016).

ARs are firstly formed in early neurons at 2 Days In Vitro (DIV), into what will become the Axon Initial Segment (AIS): actin rings intercalate with neurofascin, a protein expressed exclusively in the AIS, and are assembled in a proximal to distal fashion (Xu *et al.,* 2013; D'Este *et al.,* 2015). Up to 5 DIV, they have spread to the entire axonal shaft and branches, with except of thin filopodia and synaptic boutons, where they remain during further maturation and can be observed even at 30 DIV. They are observed in particular in thicker axons in both the CNS and the PNS, but they recently have been observed also in a percentage of dendrites from 5 up to 17 DIV (D'Este *et al.,* 2015).

ARs seem to be not only a mechanical structure that stabilises the plasma membrane, but this precise periodicity implies also functions in regulating protein and vesicle transport and also in ordering important trans-membrane and membrane-bound proteins along the axon. As an example, the voltage-gated Na^+ channels exhibit the same periodicity as actin filaments, with cross-linking proteins like ankyrin (which exhibits the same periodicity) binding them to the ARs (D'Este *et al.,* 2015; Leite and Sousa, 2016).

5.3 Actin Patches and Trails

Actin filaments in axons are not only at the cell membrane forming rings, but are also deep into the axonal lumen, when they assume diverse organisations.

Actin Patches (APs) (**Fig.11C**) are mesh-like F-Actin assemblies similar to GC lamellipodia, but they are non protrusive structures (Loudon *et al.,* 2006, Gallo, 2013; Arnold and Gallo, 2014). They can be distinguished based on their location along the axonal shaft:

- APs in the AIS are stable structures that co-localise with myosin Va and have the function of capturing cargos entering the axon and excluding non-axonal ones, and are regulated by PI3K signalling that forms micro-domains in the AIS (Ketschek and Gallo, 2010; Arnold and Gallo, 2014);
- APs in the distal axon are dynamic structures that appear and disappear with a mean period of 20-30s. They co-localise with myosin II and require Arp2/3 complex, cortactin and WAVE to form and exert their function of precursors to the formation of axonal filopodia (Ketschek and Gallo, 2010; Arnold and Gallo, 2014).

Actin Trails (ATs) (**Fig.11D**) are hotspots of Actin polymerisation and depolymerisation that appear in neurons from 7 to 10 DIV, with a spacing of about 3-4µm and a time period of about 30s (Ganguly *et al.,* 2015, Roy, 2016). They are foci of rapid assembly, independent of MTs, from which long filaments elongate in a formin-dependent manner without clear polarisation. However, the overall frequency in anterograde oriented ATs is higher, implying a slow, biased actin transport in neurites. Moreover they co-localise with stationary endosomes, where the initial nucleation takes place, before formin-dependent assembly, implying another function as actin supplier for pre-synaptic boutons (Ganguly *et al.* 2015; Roy et al 2016).

REFERENCES

Ahmed, S., Goh, W. I. & Bu, W. I-BAR domains, IRSp53 and filopodium formation. *Semin. Cell Dev. Biol.* **21,** 350–356 (2010).

Allard, J. & Mogilner, A. Traveling waves in actin dynamics and cell motility. *Curr. Opin. Cell Biol.* **25,** 107–115 (2013).

Antipenko, A. *et al.*Structure of the semaphorin-3A receptor binding module. *Neuron***39,** 589–598 (2003).

Arakawa, Y. *et al.* Control of axon elongation via an SDF-1alpha/Rho/mDia pathway in cultured cerebellar granule neurons. *J. Cell Biol.***161,** 381–391 (2003).

Argiro, V., Bunge, M. B. & Johnson, M. I. A quantitative study of growth cone filopodial extension. *J. Neurosci. Res.* **13,** 149–162 (1985).

Argiro, V., Bunge, M. B. & Johnson, M. I. Correlation between growth form and movement and their dependence on neuronal age. *J. Neurosci.* **4,**3051–3062 (1984).

Arnold, D. B. & Gallo, G. Structure meets function: actin filaments and myosin motors in the axon. *J. Neurochem.***129,** 213–220 (2014).

Ashkin, A. & Dziedzic, J. M. Optical trapping and manipulation of viruses and bacteria. *Science* **235,** 1517–1520 (1987).

Ashkin, A., Dziedzic, J. M. & Yamane, T. Optical trapping and manipulation of single cells using infrared laser beams. *Nature* **330,**769–771 (1987).

Bashaw, G. J. & Klein, R. Signaling from axon guidance receptors. *Cold Spring Harb Perspect Biol***2,** a001941 (2010).

Bashaw, G. J., Hu, H., Nobes, C. D. & Goodman, C. S. A novel Dbl family RhoGEF promotes Rho-dependent axon attraction to the central nervous system midline in Drosophila and overcomes Robo repulsion. *J. Cell Biol.***155,** 1117–1122 (2001).

Blanchoin, L., Boujemaa-Paterski, R., Sykes, C. & Plastino, J. Actin dynamics, architecture, and mechanics in cell motility. *Physiol. Rev.* **94,**235–263 (2014).

Bourne, H. R., Sanders, D. A. & McCormick, F. The GTPase superfamily: a conserved switch for diverse cell functions.*Nature* **348,** 125–132 (1990).

Brodkey, J. A. *et al.* Focal brain injury and upregulation of a developmentally regulated extracellular matrix protein. *J. Neurosurg.* **82,** 106–112 (1995).

Burridge, K. & Wennerberg, K. Rho and Rac take center stage. *Cell* **116,** 167–179 (2004).

Cajal S. R. Notas anatómicas I. Sobre la aparición de las expansiones celulares en la médula embrionaria. *Gac. Sanit. Barc.* **12,** 413–419 (1890).

Catalano, S. M. & Shatz, C. J. Activity-dependent cortical target selection by thalamic axons. *Science* **281,** 559–562 (1998).

Cojoc, D. *et al.* Properties of the force exerted by filopodia and lamellipodia and the involvement of cytoskeletal components. *PLoS ONE* **2,** e1072 (2007).

Cowan, C. A. & Henkemeyer, M. Ephrins in reverse, park and drive. *Trends Cell Biol.* **12,** 339–346 (2002).

D'Este, E. *et al.* Use of optical tweezers technology for long-term, focal stimulation of specific subcellular neuronal compartments. *Integr Biol (Camb)* **3,** 568–577 (2011).

D'Este, E., Kamin, D., Göttfert, F., El-Hady, A. & Hell, S. W. STED nanoscopy reveals the ubiquity of subcortical cytoskeleton periodicity in living neurons. *Cell Rep* **10,** 1246–1251 (2015).

Dent, E. W. & Gertler, F. B. Cytoskeletal dynamics and transport in growth cone motility and axon guidance. *Neuron* **40,**209–227 (2003).

Dent, E. W., Gupton, S. L. & Gertler, F. B. The growth cone cytoskeleton in axon outgrowth and guidance. *Cold Spring Harb Perspect Biol* **3,**(2011).

Dholakia, K. & Čižmár, T. Shaping the future of manipulation. *Nat Photon* **5,** 335–342 (2011).

Difato, F., Pinato, G. & Cojoc, D. Cell signaling experiments driven by optical manipulation. *Int J Mol Sci* **14,** 8963–8984 (2013).

Dörries, U. *et al.* Distinct effects of recombinant tenascin-C domains on neuronal cell adhesion, growth cone guidance, and neuronal polarity. *J. Neurosci. Res.* **43,** 420–438 (1996).

Ebens, A. *et al.*Hepatocyte growth factor/scatter factor is an axonal chemoattractant and a neurotrophic factor for spinal motor neurons. *Neuron* **17,** 1157–1172 (1996).

Flynn, K. C., Pak, C. W., Shaw, A. E., Bradke, F. & Bamburg, J. R. Growth cone-like waves transport actin and promote axonogenesis and neurite branching. *Dev Neurobiol* **69,** 761–779 (2009).

Forscher, P. & Smith, S. J. Actions of cytochalasins on the organization of actin filaments and microtubules in a neuronal growth cone. *J. Cell Biol.* **107,** 1505–1516 (1988).

Gallo, G. RhoA-kinase coordinates F-actin organization and myosin II activity during semaphorin-3A-induced axon retraction. *J. Cell. Sci.* **119,** 3413–3423 (2006).

Gallo, G., Lefcort, F. B. & Letourneau, P. C. The trkA receptor mediates growth cone turning toward a localized source of nerve growth factor. *J. Neurosci.* **17,** 5445–5454 (1997).

Ganguly, A. *et al.* A dynamic formin-dependent deep F-actin network in axons. *J. Cell Biol.* **210,** 401–417 (2015).

Gerisch, G. *et al.* Mobile actin clusters and traveling waves in cells recovering from actin depolymerization. *Biophys. J.* **87,** 3493–3503 (2004).

Godement, P., Wang, L. C. & Mason, C. A. Retinal axon divergence in the optic chiasm: dynamics of growth cone behavior at the midline. *J. Neurosci.***14,** 7024–7039 (1994).

Goh, W. I. *et al.* mDia1 and WAVE2 proteins interact directly with IRSp53 in filopodia and are involved in filopodium formation. *J. Biol. Chem.***287,** 4702–4714 (2012).

Goldberg, D. J. & Burmeister, D. W. Stages in axon formation: observations of growth of Aplysia axons in culture using video-enhanced contrast-differential interference contrast microscopy. *J. Cell Biol.***103,** 1921–1931 (1986).

Govek, E.-E., Newey, S. E. & Van Aelst, L. The role of the Rho GTPases in neuronal development. *Genes Dev.* **19,** 1–49 (2005).

Greulich, K. O. *et al.* Micromanipulation by laser microbeam and optical tweezers: from plant cells to single molecules. *J Microsc* **198,**182–187 (2000).

Hall, A. & Lalli, G. Rho and Ras GTPases in axon growth, guidance, and branching. *Cold Spring Harb Perspect Biol* **2,**a001818 (2010).

Hall, A. & Nobes, C. D. Rho GTPases: molecular switches that control the organization and dynamics of the actin cytoskeleton. *Philos. Trans. R. Soc. Lond., B, Biol. Sci.* **355,** 965–970 (2000).

Harrison R. G. The outgrowth of the nerve fibers as a mode of protoplasmic movement. *J. Exp. Zool.* **9,** 787–846 (1910).

Hodge, R. G. & Ridley, A. J. Regulating Rho GTPases and their regulators. *Nat. Rev. Mol. Cell Biol.* **17,** 496–510 (2016).

Holmes, W. R., Carlsson, A. E. & Edelstein-Keshet, L. Regimes of wave type patterning driven by refractory actin feedback: transition from static polarization to dynamic wave behaviour. *Phys Biol***9,** 046005 (2012).

Hong, K. *et al.* A ligand-gated association between cytoplasmic domains of UNC5 and DCC family receptors converts netrin-induced growth cone attraction to repulsion. *Cell* **97,** 927–941 (1999).

Hynes, R. O. The extracellular matrix: not just pretty fibrils. *Science***326,** 1216–1219 (2009).

Iseppon, F., Napolitano, L. M. R., Torre, V. & Cojoc, D. Cdc42 and RhoA reveal different spatio-temporal dynamics upon local stimulation with Semaphorin-3A. *Front Cell Neurosci* **9,** 333 (2015).

Itoh, R. E. *et al.*Activation of rac and cdc42 video imaged by fluorescent resonance energy transfer-based single-molecule probes in the membrane of living cells. *Mol. Cell. Biol.* **22,**6582–6591 (2002).

Jauffred, L., Richardson, A. C. & Oddershede, L. B. Three-dimensional optical control of individual quantum dots. *Nano Lett.* **8,** 3376–3380 (2008).

Jilkine, A., Marée, A. F. M. & Edelstein-Keshet, L. Mathematical model for spatial segregation of the Rho-family GTPases based on inhibitory crosstalk.*Bull. Math. Biol.* **69,**1943–1978 (2007).

Katsuno, H. *et al.* Actin Migration Driven by Directional Assembly and Disassembly of Membrane-Anchored Actin Filaments. *Cell Rep***12,** 648–660 (2015).

Kawano, H., Ohyama, K., Kawamura, K. & Nagatsu, I. Migration of dopaminergic neurons in the embryonic mesencephalon of mice.*Brain Res. Dev. Brain Res.* **86,** 101–113 (1995).

Keleman, K. & Dickson, B. J. Short- and long-range repulsion by the Drosophila Unc5 netrin receptor. *Neuron* **32,**605–617 (2001).

Ketschek, A. & Gallo, G. Nerve growth factor induces axonal filopodia through localized microdomains of phosphoinositide 3-kinase activity that drive the formation of cytoskeletal precursors to filopodia. *J. Neurosci.* **30,** 12185–12197 (2010).

Kitsukawa, T. *et al.*Neuropilin-semaphorin III/D-mediated chemorepulsive signals play a crucial role in peripheral nerve projection in mice.*Neuron* **19,** 995–1005 (1997).

Kolodkin, A. L. & Tessier-Lavigne, M. Mechanisms and molecules of neuronal wiring: a primer. *Cold Spring Harb Perspect Biol***3,** (2011).

Komarova, N. L., Zou, X., Nie, Q. & Bardwell, L. A theoretical framework for specificity in cell signaling. *Mol. Syst. Biol.* **1,** 2005.0023 (2005).

Kullander, K. & Klein, R. Mechanisms and functions of Eph and ephrin signalling. *Nat. Rev. Mol. Cell Biol.* **3,**475–486 (2002).

Kullander, K. *et al.* Kinase-dependent and kinase-independent functions of EphA4 receptors in major axon tract formation in vivo.*Neuron* **29,** 73–84 (2001).

Kunida, K., Matsuda, M. & Aoki, K. FRET imaging and statistical signal processing reveal positive and negative feedback loops regulating the morphology of randomly migrating HT-1080 cells.*J. Cell. Sci.* **125,** 2381–2392 (2012).

Kutys, M. L. & Yamada, K. M. An extracellular-matrix-specific GEF-GAP interaction regulates Rho GTPase crosstalk for 3D collagen migration. *Nat. Cell Biol.* **16,** 909–917 (2014).

Leite, S. C. & Sousa, M. M. The neuronal and actin commitment: Why do neurons need rings? *Cytoskeleton (Hoboken)* **73,** 424–434 (2016).

Leite, S. C. *et al.* The Actin-Binding Protein α-Adducin Is Required for Maintaining Axon Diameter. *Cell Rep* **15,**490–498 (2016).

Letourneau, P. C. Cell-to-substratum adhesion and guidance of axonal elongation. *Dev. Biol.* **44,**92–101 (1975).

Lorenzo, D. N. *et al.* A PIK3C3-ankyrin-B-dynactin pathway promotes axonal growth and multiorganelle transport. *J. Cell Biol.* **207,** 735–752 (2014).

Loudon, R. P., Silver, L. D., Yee, H. F. & Gallo, G. RhoA-kinase and myosin II are required for the maintenance of growth cone polarity and guidance by nerve growth factor. *J. Neurobiol.* **66,**847–867 (2006).

Lowery, L. A. & Van Vactor, D. The trip of the tip: understanding the growth cone machinery. *Nat. Rev. Mol. Cell Biol.* **10,** 332–343 (2009).

Luo, L. Rho GTPases in neuronal morphogenesis. *Nat. Rev. Neurosci.* **1,**173–180 (2000).

Lyuksyutova, A. I. *et al.* Anterior-posterior guidance of commissural axons by Wnt-frizzled signaling. *Science* **302,**1984–1988 (2003).

Machacek, M. & Danuser, G. Morphodynamic profiling of protrusion phenotypes. *Biophys. J.* **90,** 1439–1452 (2006).

Machacek, M. *et al.* Coordination of Rho GTPase activities during cell protrusion. *Nature* **461,** 99–103 (2009).

Mann, F., Chauvet, S. & Rougon, G. Semaphorins in development and adult brain: Implication for neurological diseases. *Prog. Neurobiol.* **82,** 57–79 (2007).

Martin, K. *et al.* Spatio-temporal co-ordination of RhoA, Rac1 and Cdc42 activation during prototypical edge protrusion and retraction dynamics. *Sci Rep* **6,**21901 (2016).

Mason, C. A. & Wang, L. C. Growth cone form is behavior-specific and, consequently, position-specific along the retinal axon pathway. *J. Neurosci.* **17,** 1086–1100 (1997).

Michaelson, D. *et al.* Differential localization of Rho GTPases in live cells: regulation by hypervariable regions and RhoGDI binding. *J. Cell Biol.* **152,** 111–126 (2001).

Moore, S. W., Tessier-Lavigne, M. & Kennedy, T. E. Netrins and their receptors. *Adv. Exp. Med. Biol.* **621,** 17–31 (2007).

Mortimer, D., Fothergill, T., Pujic, Z., Richards, L. J. & Goodhill, G. J. Growth cone chemotaxis. *Trends Neurosci.* **31,** 90–98 (2008).

Myers, J. P., Robles, E., Ducharme-Smith, A. & Gomez, T. M. Focal adhesion kinase modulates Cdc42 activity downstream of positive and negative axon guidance cues. *J. Cell. Sci.* **125,** 2918–2929 (2012).

Myers, J. P., Santiago-Medina, M. & Gomez, T. M. Regulation of axonal outgrowth and pathfinding by integrin-ECM interactions. *Dev Neurobiol* **71,** 901–923 (2011).

Nakamura, T., Aoki, K. & Matsuda, M. FRET imaging in nerve growth cones reveals a high level of RhoA activity within the peripheral domain. *Brain Res. Mol. Brain Res.* **139,**277–287 (2005).

Nishiyama, M., von Schimmelmann, M. J., Togashi, K., Findley, W. M. & Hong, K. Membrane potential shifts caused by diffusible guidance signals direct growth-cone turning. *Nat. Neurosci.***11,** 762–771 (2008).

Nobes, C. D. & Hall, A. Rho, rac, and cdc42 GTPases regulate the assembly of multimolecular focal complexes associated with actin stress fibers, lamellipodia, and filopodia. *Cell* **81,** 53–62 (1995).

Pertz, O. Spatio-temporal Rho GTPase signaling - where are we now? *J. Cell. Sci.* **123,** 1841–1850 (2010).

Picard, M. *et al.* Spatial and temporal activation of the small GTPases RhoA and Rac1 by the netrin-1 receptor UNC5a during neurite outgrowth. *Cell. Signal.* **21,** 1961–1973 (2009).

Pinato, G. *et al.* Less than 5 Netrin-1 molecules initiate attraction but 200 Sema3A molecules are necessary for repulsion. *Sci Rep* **2,** 675 (2012).

Pinato, G., Raffaelli, T., D'Este, E., Tavano, F. & Cojoc, D. Optical delivery of liposome encapsulated chemical stimuli to neuronal cells. *J Biomed Opt* **16,** 095001 (2011).

Pinato, G.; Lien, L.T.; D'Este, E.; Torre, V.; Cojoc, D. Neuronal chemotaxis by optically manipulated liposomes. *J. Eur. Opt. Soc. Rapid Publ.* **6,** 11042 (2011).

Piper, M., Georgas, K., Yamada, T. & Little, M. Expression of the vertebrate Slit gene family and their putative receptors, the Robo genes, in the developing murine kidney. *Mech. Dev.* **94,** 213–217 (2000).

Plachez, C. *et al.* Robos are required for the correct targeting of retinal ganglion cell axons in the visual pathway of the brain. *Mol. Cell. Neurosci.* **37,** 719–730 (2008).

Pollard, T. D. & Beltzner, C. C. Structure and function of the Arp2/3 complex. *Curr. Opin. Struct. Biol.* **12,** 768–774 (2002).

Raper, J. & Mason, C. Cellular Strategies of Axonal Pathfinding. *Cold Spring Harb Perspect Biol***2,** (2010).

Raper, J. A., Bastiani, M. & Goodman, C. S. Pathfinding by neuronal growth cones in grasshopper embryos. I. Divergent choices made by the growth cones of sibling neurons. *J. Neurosci.* **3,** 20–30 (1983).

Raper, J. A., Bastiani, M. & Goodman, C. S. Pathfinding by neuronal growth cones in grasshopper embryos. II. Selective fasciculation onto specific axonal pathways. *J. Neurosci.* **3,**31–41 (1983).

Reichardt, L. F. Neurotrophin-regulated signalling pathways.*Philos. Trans. R. Soc. Lond., B, Biol. Sci.* **361,**1545–1564 (2006).

Ridley, A. J. Life at the leading edge. *Cell* **145,**1012–1022 (2011).

Ridley, A. J. Rho GTPases and actin dynamics in membrane protrusions and vesicle trafficking.*Trends Cell Biol.* **16,**522–529 (2006).

Roy, S. Waves, rings, and trails: The scenic landscape of axonal actin.*J. Cell Biol.* **212,** 131–134 (2016).

Ruthel, G. & Banker, G. Actin-dependent anterograde movement of growth-cone-like structures along growing hippocampal axons: a novel form of axonal transport? *Cell Motil. Cytoskeleton* **40,** 160–173 (1998).

Ruthel, G. & Banker, G. Role of moving growth cone-like 'wave' structures in the outgrowth of cultured hippocampal axons and dendrites. *J. Neurobiol.***39,** 97–106 (1999).

Sakai, J. A. & Halloran, M. C. Semaphorin 3d guides laterality of retinal ganglion cell projections in zebrafish. *Development***133,** 1035–1044 (2006).

Santos Da Silva, J., Schubert, V. & Dotti, C. G. RhoA, Rac1, and cdc42 intracellular distribution shift during hippocampal neuron development. *Mol. Cell. Neurosci.* **27,** 1–7 (2004).

Schwabe, T., Neuert, H. & Clandinin, T. R. A network of cadherin-mediated interactions polarizes growth cones to determine targeting specificity. *Cell* **154,** 351–364 (2013).

Scolnick, J. A. *et al.* Role of IGF signaling in olfactory sensory map formation and axon guidance. *Neuron* **57,**847–857 (2008).

Shekarabi, M. & Kennedy, T. E. The netrin-1 receptor DCC promotes filopodia formation and cell spreading by activating Cdc42 and Rac1. *Mol. Cell. Neurosci.***19,** 1–17 (2002).

Spiering, D. & Hodgson, L. Dynamics of the Rho-family small GTPases in actin regulation and motility. *Cell Adh Migr* **5,**170–180 (2011).

Stewart, G. R. & Pearlman, A. L. Fibronectin-like immunoreactivity in the developing cerebral cortex. *J. Neurosci.* **7,**3325–3333 (1987).

Tint, I., Jean, D., Baas, P. W. & Black, M. M. Doublecortin associates with microtubules preferentially in regions of the axon displaying actin-rich protrusive structures.*J. Neurosci.* **29,** 10995–11010 (2009).

Togashi, K. *et al.* Cyclic GMP-gated CNG channels function in Sema3A-induced growth cone repulsion. *Neuron* **58,**694–707 (2008).

Tojima, T., Hines, J. H., Henley, J. R. & Kamiguchi, H. Second messengers and membrane trafficking direct and organize growth cone steering.*Nat. Rev. Neurosci.* **12,**191–203 (2011).

Toriyama, M., Kozawa, S., Sakumura, Y. & Inagaki, N. Conversion of a signal into forces for axon outgrowth through Pak1-mediated shootin1 phosphorylation. *Curr. Biol.* **23,** 529–534 (2013).

Tran, T. S., Kolodkin, A. L. & Bharadwaj, R. Semaphorin regulation of cellular morphology.*Annu. Rev. Cell Dev. Biol.***23,** 263–292 (2007).

Vitriol, E. A. & Zheng, J. Q. Growth cone travel in space and time: the cellular ensemble of cytoskeleton, adhesion, and membrane. *Neuron***73,** 1068–1081 (2012).

Weiner, O. D., Marganski, W. A., Wu, L. F., Altschuler, S. J. & Kirschner, M. W. An actin-based wave generator organizes cell motility.*PLoS Biol.* **5,** e221 (2007).

Winans, A. M., Collins, S. R. & Meyer, T. Waves of actin and microtubule polymerization drive microtubule-based transport and neurite growth before single axon formation. *Elife* **5,**e12387 (2016).

Xu, K., Zhong, G. & Zhuang, X. Actin, spectrin, and associated proteins form a periodic cytoskeletal structure in axons. *Science* **339,**452–456 (2013).

Yamao, M. *et al.* Distinct predictive performance of Rac1 and Cdc42 in cell migration. *Sci Rep* **5,**17527 (2015).

Yoshikawa, S., McKinnon, R. D., Kokel, M. & Thomas, J. B. Wnt-mediated axon guidance via the Drosophila Derailed receptor. *Nature***422,** 583–588 (2003).

Yoshizaki, H. *et al.*Activity of Rho-family GTPases during cell division as visualized with FRET-based probes. *J. Cell Biol.* **162,** 223–232 (2003).

Ypsilanti, A. R., Zagar, Y. & Chédotal, A. Moving away from the midline: new developments for Slit and Robo. *Development***137,** 1939–1952 (2010).

Zheng, J. Q. & Poo, M.-M. Calcium signaling in neuronal motility. *Annu. Rev. Cell Dev. Biol.* **23,**375–404 (2007).

Zhou, Y., Gunput, R.-A. F. & Pasterkamp, R. J. Semaphorin signaling: progress made and promises ahead. *Trends Biochem. Sci.* **33,** 161–170 (2008).

RESULTS

This section is the sum of experiments carried out by different people.

For what concerns me:

- In the first article I performed all the local stimulation and delivery experiments and corresponding data analysis and figures preparation;
- In the second article I performed the FRET and Optical Tweezers setup validation, data analysis and figure preparation;
- In the third article I carried out the part of the actin live cell imaging and inhibition of RhoGTPases, the immunofluorescence and corresponding data analysis and figures preparation.

I actively participated in writing and designing all these works.

1

Cdc42 and RhoA reveal different spatio-temporal dynamics upon local stimulation with Semaphorin-3A.

Federico Iseppon, Luisa Maria Rosaria Napolitano, Vincent Torre and Dan Cojoc

Frontiers in Cellular Neuroscience

frontiers in Cellular Neuroscience

ORIGINAL RESEARCH
published: 26 August 2015
doi: 10.3389/fncel.2015.00333

Cdc42 and RhoA reveal different spatio-temporal dynamics upon local stimulation with Semaphorin-3A

Federico Iseppon[1], *Luisa M. R. Napolitano*[1,2], *Vincent Torre*[1]* *and Dan Cojoc*[3]*

[1] Neurobiology Sector, International School for Advanced Studies, Trieste, Italy, [2] Structural Biology Laboratory, Elettra-Sincrotrone Trieste S.C.p.A., Trieste, Italy, [3] Institute of Materials – National Research Council, Trieste, Italy

Small RhoGTPases, such as Cdc42 and RhoA, are key players in integrating external cues and intracellular signaling pathways that regulate growth cone (GC) motility. Indeed, Cdc42 is involved in actin polymerization and filopodia formation, whereas RhoA induces GC collapse and neurite retraction through actomyosin contraction. In this study we employed Förster Resonance Energy Transfer (FRET) microscopy to study the spatio-temporal dynamics of Cdc42 and RhoA in GCs in response to local Semaphorin-3A (Sema3A) stimulation obtained with lipid vesicles filled with Sema3A and positioned near the selected GC using optical tweezers. We found that Cdc42 and RhoA were activated at the leading edge of NG108-15 neuroblastoma cells during spontaneous cycles of protrusion and retraction, respectively. The release of Sema3A brought to a progressive activation of RhoA within 30 s from the stimulus in the central region of the GC that collapsed and retracted. In contrast, the same stimulation evoked waves of Cdc42 activation propagating away from the stimulated region. A more localized stimulation obtained with Sema3A coated beads placed on the GC, led to Cdc42 active waves that propagated in a retrograde manner with a mean period of 70 s, and followed by GC retraction. Therefore, Sema3A activates both Cdc42 and RhoA with a complex and different spatial-temporal dynamics.

Keywords: RhoA, Cdc42, FRET, local stimulation, Semaphorin-3A, GC retraction, NG108-15 cell line

OPEN ACCESS

Edited by:
Daniel Marcel Suter, Purdue University, USA

Reviewed by:
Timothy Gomez, University of Wisconsin, USA
Gianluca Gallo, Temple University, USA

***Correspondence:**
Vincent Torre, Neurobiology Sector, International School for Advanced Studies, via Bonomea 265, Trieste 34136, Italy torre@sissa.it;
Dan Cojoc, Institute of Materials – National Research Council, Area Science Park, Basovizza, Trieste 34149, Italy cojoc@iom.cnr.it

Received: *29 April 2015*
Accepted: *10 August 2015*
Published: *26 August 2015*

Citation:
Iseppon F, Napolitano LMR, Torre V and Cojoc D (2015) Cdc42 and RhoA reveal different spatio-temporal dynamics upon local stimulation with Semaphorin-3A. Front. Cell. Neurosci. 9:333. doi: 10.3389/fncel.2015.00333

Introduction

Axon outgrowth and guidance depend on the ability of growth cones (GCs) to detect molecular guidance cues in their extracellular environment and to respond with a dynamic remodeling of the cytoskeleton. It is well-established that repulsive GCs turning arises from the disruption and loss of F-actin superstructures and actomyosin contraction, while attractive GC turning entails asymmetrical incorporation of actin on the side of the GC close to the chemoattractant (Dent et al., 2011). The Rho protein family members of small GTPases act as molecular switches to control signal transduction pathways by cycling between a GDP-bound, inactive form, and a GTP-bound, active form (Raftopoulou and Hall, 2004). In their active state, they have a key role in the cytoskeleton reorganization as they act downstream of most guidance cue receptors (Hall, 1998; Luo, 2000; Dickson, 2001; Jaffe and Hall, 2005). In neurons, the Rho family members RhoA and Cdc42 regulate GC extension and axon outgrowth: RhoA triggers actin cytoskeleton rearrangement to support GC collapse and neurite retraction (Thies and Davenport, 2003; Wu et al., 2005),

whereas Cdc42 promotes neurite outgrowth and GC filopodia formation (Ahmed et al., 2006; Hall and Lalli, 2010). However, the activation of the RhoA pathway has growth-promoting effects in cortical and hippocampal cell axons (Ahnert-Hilger et al., 2004; Ohnami et al., 2008).

The secreted guidance cue is Semaphorin-3A (Sema3A), a repulsive guidance molecule that generally causes GC collapse in neurons through microtubule and actin reorganization (Fan and Raper, 1995; Goshima et al., 2002; Tran et al., 2007; Zhou et al., 2008), helping steer both axons and migrating cells along the correct trajectory. Sema3A is thought to act as a dimer (Wong et al., 1999) binding to the complex of receptors neuropilin1/plexinA1, to initiate signal transduction pathways (Adams et al., 1997; Takahashi et al., 1997). Intracellular signaling of Sema3A has been extensively studied, also quite recently (Jongbloets and Pasterkamp, 2014; Worzfeld and Offermanns, 2014). In DRG neurons, Sema3A stimulation induces GC collapse of sensory neurons through RhoA effector ROCK and intra-axonal translation of RhoA mRNA, which, through an axonal 3′UTR targeting element, is localized in developing axons and GCs (Wu et al., 2005; Hengst et al., 2006). This local translation is a condition necessary and sufficient to allow Sema3A-mediated GC collapse. In contrast, the role of Cdc42 in Sema3A collapse response is still unclear with reported contradictory results (Jin and Strittmatter, 1997; Kuhn et al., 1999).

Bath application of Sema3A has several drawbacks: the entire neuron is exposed to Sema3A and the response could involve both the entire neuron and the GC (Brown et al., 2009). In the present study, we combined the sensitized emission Förster Resonance Energy Transfer (FRET) technique with local stimulation to observe the spatial and temporal activation of RhoA and Cdc42 following localized stimulation with Sema3A. We used two types of vectors for local delivery of molecules: microbeads and micro-sized lipid vesicles. Silica microbeads have been covalently functionalized on their surface with Sema3A and placed on the GC of interest with a sub-micrometric precision, allowing a more localized stimulation for 30 s. Thus, Sema3A beads were able to induce a localized response to Sema3A, although the guidance molecule was not in its native form. We then used lipid vesicles encapsulating Sema3A that were trapped with optical tweezers in front of the exploring GC and broken with short UV laser pulse. In this way we studied the delivery of Sema3A in its native form but with a less precise spatial localization of its delivery.

In this paper, we examine the role of RhoA and Cdc42 in NG108-15 neuroblastoma cells and we show that they are both involved in Sema3A morphological changes with specific spatio-temporal dynamics; we also show that Cdc42 (but not RhoA) exhibits a complex wave behavior. Although the existence of different models that prove both a crosstalk and a negative feedback between the Rho GTPases (Holmes et al., 2012; Marèe et al., 2012) is confirmed, our data support a more dynamic pattern for Cdc42 that reflects a higher degree of complexity for the Rho GTPase signaling.

Materials and Methods

Cell Cultures and Transfection

NG108-15 neuroblastoma cells were purchased from Sigma Aldrich and grown in Dulbecco's modified Eagle's medium (DMEM) with 10% (v/v) fetal bovine serum (FBS) (Invitrogen), 100 μg/ml streptomycin and 100 units/ml in penicillin in a 5% CO_2atmosphere at 37°C. For live cell imaging studies, cells were seeded on glass coverslips, coated for 3 h with laminin (50 μg/ml, L2020 Sigma) in 12-multiwell plates. Cells were transfected 24 h later with intermolecular RhoA/Cdc42 FRET sensors (Murakoshi et al., 2011) using Metafectene reagent (Biontex Laboratories) following the manufacturer's protocol and imaged 1 day after transfection. mEGFP-RhoA-C1 (Addgene plasmid #29674), mEGFP-Cdc42-C1 (Addgene plasmid #29673), mCherry-Rhotekin(8–89)-mCherry-C1 (Addgene plasmid #29675) and mCherry-Pak3(60–113)/S74A/F84A-mCherry-C1 (Addgene plasmid #29676) were a gift from Ryohei Yasuda (Murakoshi et al., 2011).

Immunofluorescence

All these steps were performed at room temperature (20–22°C) and coverslips were rinsed with phosphate-buffered saline (PBS) between each step. Cells were fixed in freshly prepared 4% paraformaldehyde containing 0.15% picric acid in PBS, permeabilized in 0.1% Triton X-100 for 10 min and blocked with 0.5% BSA (all from Sigma-Aldrich, St.Louis, MO) in PBS for 1 h. Cells were then incubated with primary goat polyclonal antibody against neuropilin1 (Santa Cruz Biotechnology, Santa Cruz, CA) and rabbit polyclonal antibody against plexinA1 (Santa Cruz Biotechnology, Santa Cruz, CA) for 1 h. The secondary antibodies were donkey anti-rabbit 488 and donkey anti-goat 594 Alexa (Invitrogen, Life Technologies, Gaithersburg, MD, USA) and the incubation time was 30 min. Nuclei were stained with 2 μg/ml Hoechst 33342 (Sigma-Aldrich, St.Louis, MO) in PBS for 5 min. Coverslips were inverted and mounted on the glass side using Vectashield Mounting Medium and were then examined on a Leica DM6000 microscope (Leica Microsystems GmbH, Germany) using a 100× magnification and 1.42 NA oil-immersion objective. Fluorescent images were processed using Leica LCS Lite and Image J by W. Rasband (developed at the U.S. National Institutes of Health and available at http://rsbweb.nih.gov/ij/). For the colocalization analysis, each image was captured applying the same exposure and gain settings per channel and using Volocity 5.4 3D imaging software (PerkinElmer, Coventry, UK).

Vesicle Preparation

Detailed experimental procedures are described in our companion papers (Pinato et al., 2011, 2012). Single vesicles, with a diameter of 1–5 μm, were obtained with the lipid film hydration method using a hydration solution containing BSA or Sema3A, and were then identified, trapped and positioned at the location of interest (Ichikawa and Yoshikawa, 2001).

Beads Functionalization and Immunohistochemistry

1.5 μm large silica beads coated with COOH groups (Kisker-biotech, cat. PSi-1.5COOH) were functionalized using PolyLink

Protein Coupling Kit (Bangs Laboratories Inc., cat. PL01N), following the manufacturers protocol. Briefly, about 1.4×10^5 beads were incubated with 500 ng of Sema3A, in the presence of 20 μg/μL EDAC for 1 h, at room temperature and stored in Storage Buffer at 4°C.

Coated and un-coated microspheres were washed in PBS and incubated for 1 h, at room temperature, with anti-Sema3A (1:50, Sigma). Beads were then centrifuged, washed and incubated for 30 min, at room temperature, with donkey anti-goat Alexa 594 (Invitrogen) and finally analyzed using Fluorescence Microscopy (Nikon Eclipse TE-2000-E).

Optical Manipulation and FRET Microscopy Setup

Local delivery was achieved by optical trapping and manipulation of single vesicles at a specific position nearby the cells, followed by vesicles photolysis, to release active molecules. To increase the localization of the stimulus, single beads were optically trapped and maintained in contact with the GCs for 30 s. RhoGTPases activation was monitored by FRET microscopy. The setup, depicted in **Figure 1**, was developed around an inverted microscope (Nikon Eclipse TE-2000-E) adding three modules: (1) Infrared (IR) laser tweezers (custom built); (2) Ultraviolet (UV) laser micro-dissection system (MMI- CellCut Plus, MMI, Zurich, Switzerland); (3) Image splitter (OptoSplit II LS, Cairn Research, UK).

The first two modules are described in detail in our companion papers (Pinato et al., 2011, 2012). The trapping laser beam, generated by a 1064 nm fiber laser, is aligned with the micro-dissection UV beam and then focused on the sample through the same lens (Nikon, 60X water immersion, numerical aperture NA-1.2). The fluorescence path includes a 100 W Hg Lamp, excitation filters for EGFP (445/30 nm, Chroma, USA) and mCherry (550/30 nm). Light emitted by the sample is directed to the image splitter, where a dichroic mirror (585 nm) splits the light into Donor (EGFP) and Acceptor (mCherry) channels. After passing through the emission filters (EGFP: 515/30 nm; mCherry: 625/30 nm) each of the two beams is imaged on one of the two halves of a sCMOS sensor (Orca Flash 4.0, Hamamatsu), thus allowing the acquisition of the donor and of FRET emissions simultaneously. All live cells and FRET microscopy experiments were performed on the setup previously described. Imaging was performed in a Ringer's Solution and during the experiments cells were kept at 37°C, using a temperature controller (TempControl 37-2, PeCon, Germany). Experiments with the same coverslip always lasted less than 60 min. For bath applied stimulation assays time-lapse DIC images were acquired every 500 ms with a Nikon, 20X (NA: 0.25) objective in case of population studies, and with a Nikon, 60X (NA: 1.2) objective in case of single cell studies, from 90 s before adding the Sema3A to 20 min after it. For local stimulation assays, we trapped the lipid vesicle or the bead with the optical tweezers and we positioned it in front of, or in contact with, the selected GC. We then acquired simultaneously the Donor and Acceptor (FRET) channels for 15 min after the vesicle photolysis. All acquisitions were done with the sCMOS sensor at 16-bit depth. The exposure time for the FRET channels acquisition was 1 s at binning 4 × 4.

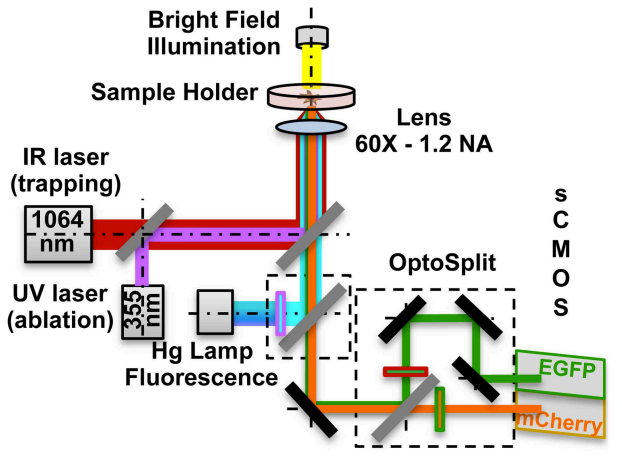

FIGURE 1 | Optical manipulation and FRET imaging setup. The IR laser beam (1064 nm) is aligned to the UV laser micro-dissection beam (355 nm) and then both are directed into the pupil of the microscope objective (60X - 1.2 NA). The sample is illuminated both by a white light source and a Hg fluorescence lamp. The light coming from the Donor and the Acceptor fluorophores in the sample is separated by a dual emission image splitter and the two images are formed on the two halves of the sCMOS camera sensor.

Ratiometric Corrections and Image Analysis

Ratiometric corrections and ratio calculations to generate activity images were performed using the Biosensors 2.1 MATLAB package (Danuser laboratory: http://lccb.hms.harvard.edu/software.html). All images were sequentially shading-corrected and background-subtracted; an optional photobleaching correction was also applied. Binary masks, with values equal to 1 inside the cells and 0 elsewhere, were extracted by thresholding the EGFP image (since it presented the highest signal-to-noise ratio). Control cells expressing either EGFP alone or mCherry alone were used to obtain bleedthrough coefficients necessary for the correction of the FRET image. The final ratio image, obtained dividing the completely corrected FRET image by the EGFP image, was used as a measure for the RhoA and Cdc42 activity.

Further image analysis was performed by ImageJ and custom-built codes were written in Matlab (Mathworks). To describe RhoA and Cdc42 activation, rectangular areas (size 10 × 20 μm) were generated selecting regions of interest in the normal direction with respect to the edge dynamics of the GCs; montage images were then composed by taking one image every 60 or 120 s for the entire duration of the experiment. The quantification of the FRET ratio was performed in stalling, protruding and retracting regions of the cell edge, and the results were normalized by the mean intensity of the ratio in the stalling regions. To measure the temporal dynamics of RhoA and Cdc42, a square area of 4 μm^2 was selected in the region of interest previously considered for image montages, so that no movement of the edge could interfere with the measurements; the intensity was calculated for every time point and then the measurements were normalized using the following equation:

$\Delta F = \frac{F-F_0}{F_0}$, where F is the intensity at the time point t and F_0 is the intensity at the first frame. Cell edges were detected for each frame by intensity-thresholding of the Ratio final image and edge dynamics were calculated along the central line of the rectangles, previously considered for the image montages. Edge and RhoGTPases activation dynamics were then plotted together in a graph, as a function of time. To measure the period of the waves in the different cases, one or more areas were selected in the retracting GCs, as previously described for temporal dynamics measurements, and then the wave period was calculated extrapolating the time between two maxima from the intensity vs. time plots.

Statistical Analysis

All quantitative results have been obtained from at least three independent experiments and expressed as the mean ± SEM. Experimental data were analyzed by Student's *t*-test and One-Way analysis of variance (ANOVA). Differences among samples were considered statistically significant when $p < 0.05$.

Results

The Spontaneous Dynamics of RhoA and Cdc42 in NG108-15 Cell Line

NG108-15 neuroblastoma cells are a good model system for neuronal signaling and growth (Smalheiser, 1991a,b; Goshima et al., 1993; Tsuji et al., 2011). In the absence of adherent or diffusive signaling gradients, NG108-15 cells exhibit both a complete collapse of the GC followed by a full or partial retraction of the neurite and the transient collapse of the GC structures (Rauch et al., 2013). Therefore, to measure the spontaneous activity of RhoA and Ccd42 in GCs, we transiently overexpressed in NG108-15 cells the intermolecular RhoA/Cdc42 probes based on FRET (Murakoshi et al., 2011). These probes consist of two components: wild type RhoA/Cdc42 tagged with monomeric enhanced green fluorescent protein (mEGFP) and their binding partner, Rho GTPase binding domain (RBD) of Rhotekin/Pak3, doubly tagged with mCherry (mCherry-RBD-mCherry) (Murakoshi et al., 2011). The expression of the intermolecular RhoA/Cdc42 probes was carefully titrated to levels that did not alter the normal neurite outgrowth. GFP, mCherry and FRET images were captured 18-20 h post-transfection using a Dual-view image splitting device. After background and spectral bleed-through correction, the GFP/mCherry ratio was measured and correlated with the activation levels of RhoA and Cdc42 during spontaneous protrusion and retraction events.

NG108-15 neuroblastoma cell line shows neurite outgrowth when plated on glass slides that have been coated with laminin. To examine the effect of RhoA and Cdc42 transfection on NG108-15 cells, we compared the morphologies of cells transfected with either RhoA or Cdc42 (Figures S1A,B). Transfection of Cdc42 induced significant neurite outgrowth compared with RhoA transfected cells that appeared more flatted (Figures S1A–D). Furthermore, most of the Cdc42-transfected cells were polarized with long neurite-like processes that were generally branched and exhibited micro-spikes along their length (Figures S1B–D).

In RhoA transfected cells, we observed that elevated RhoA activity (**Figures 2A,B**; mean FRET ratio: 1.109) correlates with edge retraction, whereas reduced RhoA activity (**Figures 2A,B**; mean FRET ratio: 0.831) leads to edge protrusion. To investigate how spontaneous RhoA activity relates to edge dynamics, we scanned RhoA activity in both protrusion (**Figures 2C,D**) and retraction regions (**Figures 2C,E**) of one representative cell at 60 s intervals. This confirmed that edge retraction coincides with a boost in RhoA activity compared with a protrusion event.

Cdc42 activity has been implicated in the regulation of filopodia and lamellipodia extension in many cell types (Nobes and Hall, 1995; Peng et al., 2003; Nalbant et al., 2004; Myers et al., 2012). We then imaged Cdc42 transfected cells and we found that membrane-ruffling and filopodia extension strongly correlate with hot spots of Cdc42 activity (**Figure 3B**; mean FRET ratio of 1.061) with respect to cell edges without protrusions

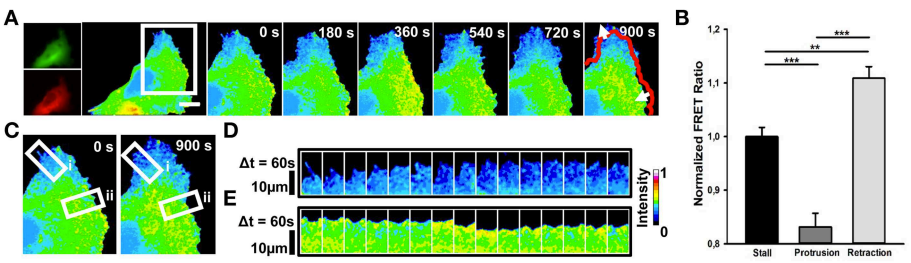

FIGURE 2 | Spontaneous RhoA dynamics in NG108-15 cells. **(A)** Ratiometric FRET live imaging of a representative RhoA-FRET neuroblastoma cell (n = six experiments). Consecutive frames were taken every second (left: generation of a ratiometric image) for 15 min. Insets on the right show a time series (1 frame every 3 min) of the magnified region denoted by the white box in the left image. Arrows indicate protrusion and retraction directions. The red line shows the initial edge profile. Scale Bar: 20 μm. **(B)** Quantification of mean RhoA activity (FRET ratio) in 50 stalling, protruding and retracting sections along the cell edge from RhoA neuroblastoma cells from two experiments. $^{**}p < 0.01$, $^{***}p < 0.001$ using ANOVA test (**C–E**) Montage images showing the dynamics of RhoA activation in protruding **(D)** and retracting sections **(E)** along the cell edge. **(C)** Images showing the regions of interest selected for the montage (white boxes) (i, protruding region; ii, retracting region). **(D,E)** Montage images highlighting a low RhoA activity in protruding regions **(D)** and a higher RhoA activity in retracting ones **(E)**. Intensity scale on the right in **(D)** applies to **(A,C–E)**.

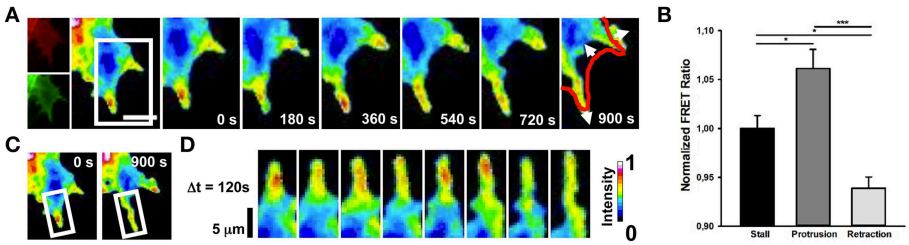

FIGURE 3 | Spontaneous Cdc42 dynamics in NG108-15 cells. **(A)** Ratiometric FRET live imaging of a representative Cdc42-FRET neuroblastoma cell (n = six experiments). Consecutive frames were taken every second (left: generation of a ratiometric image) for 15 min. Insets on the right show a time series (1 frame every 3 min) of the magnified region denoted by the white box in the left image. Arrows indicate protrusion and retraction directions. The red line shows the initial GC profile. Scale Bar: 20 μm. **(B)** Quantification of mean Cdc42 activity (FRET ratio) in 30 stalling, protruding and retracting sections along the cell edge from Cdc42 neuroblastoma cells from two experiments. $*p < 0.05$, $***p < 0.001$ using ANOVA test **(C,D)** Montage images showing the dynamics of Cdc42 activation in a protruding region of the cell. **(C)** Images showing the region of interest selected for the montage (white boxes). **(D)** Montage images highlighting hotspots of Cdc42 in the protruding region. Intensity scale on the right in **(D)** applies to **(A,C,D)**.

(**Figure 3B**; mean FRET ratio of 0.938) (**Figure 3**). Therefore, these findings indicate that a selective activation of RhoA and Cdc42 correlates spatially and temporally with retraction and extension events in NG108-15 cell line.

Sema3A Induces GC Retraction in NG108-15 Cell Line

In order to study the NG108-15 behavior after Sema3A stimulation, we first observed the distribution of Sema3A receptors neuropilin1 and plexinA1 using immunofluorescence microscopy after double staining with antibodies against neuripilin1 and plexinA1: both the Sema3A receptors were found in GCs of NG108-15 cell line (Figure S1E). This observation was consistent with the distribution of neuropilin1 and plexinA1 shown for hippocampal neurons (Pinato et al., 2012). Since bath application of Sema3A could have several drawbacks (Brown et al., 2009), we examined the effect of local stimulation with Sema3A filled lipid vesicles on GC in NG108-15 cells. We had previously demonstrated that local stimulation with vesicles encapsulating guidance molecules can allow a controlled spatiotemporal stimulation of hippocampal neurons that mimics better the natural behavior of the guidance molecules themselves (Pinato et al., 2012).

Lipid vesicles, with a diameter varying between 1 and 5 μm, were encapsulated with 10^3–10^4 molecules of Sema3A (Pinato et al., 2011, 2012). Local stimulation with lipid vesicles encapsulating Sema3A led to a rapid collapse and retraction of the GC (**Figures 4A,C**): retraction was already detectable at 100 s after stimulation with Sema3A and reached a plateau between 5 and 6 min. After local stimulation with BSA, no comparable retraction was observed (**Figures 4B,D**).

Local Stimulation by Sema3A Induces RhoA Activation Followed By the GC Retraction

To investigate the spatio-temporal activation of RhoA after local stimulation with Sema3A, we combined FRET with optical tweezers set-up to induce the local delivery of vesicles encapsulating Sema3A (**Figure 1**-see Methods section). Local application of Sema3A leads to an increase of RhoA activity in the central region of the GC followed by GC collapse and retraction (**Figure 5A** and Supplementary Movie 1). Ratiometric FRET imaging highlighted that RhoA activity increases rapidly, within 30 s after Sema3A local stimulation, reaching the maximum value within 400 s (**Figures 5B,C**). A more detailed analysis of the time dependence of RhoA activity and GC edge retraction showed that the GC begins to retract within 100–120 s after Sema3A local stimulation, reaching a complete collapse and retraction within 15 min (**Figure 5D**; data from five experiments). The delay between the increase of RhoA activity and the GC retraction can be explained with the recruitment of RhoA binding proteins necessary for cytoskeletal rearrangement. When we stimulated RhoA transfected cells with vesicles encapsulating

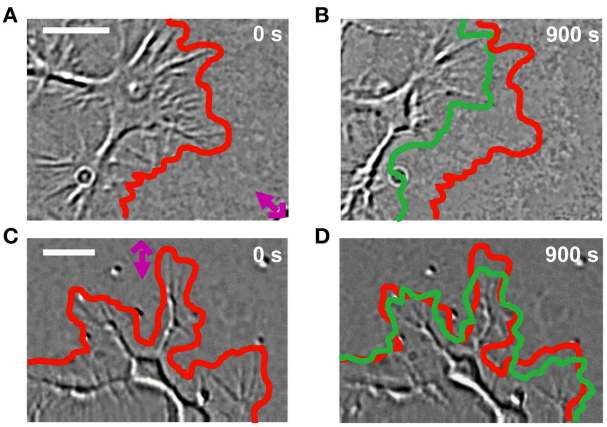

FIGURE 4 | GC behavior of NG108-15 cells stimulated with Sema3A. **(A,B)** DIC images of a representative cell locally stimulated with lipid vesicles encapsulating 1 μM of Sema3A at 0 **(A)** and 900 s **(B)** from the delivery. The red and green lines represent respectively the initial and final GC profile. The pink cross with the arrow represents the position of the liposome. **(C,D)** The same as in **(A,B)**, but the representative cell is locally stimulated with lipid vesicles encapsulating 1 μM of BSA. Frames were taken every second for 15 min in both cases. Contrast and brightness enhancement were applied to all images, followed by bandpass filtering of the spatial frequencies to enhance the edge contrast.

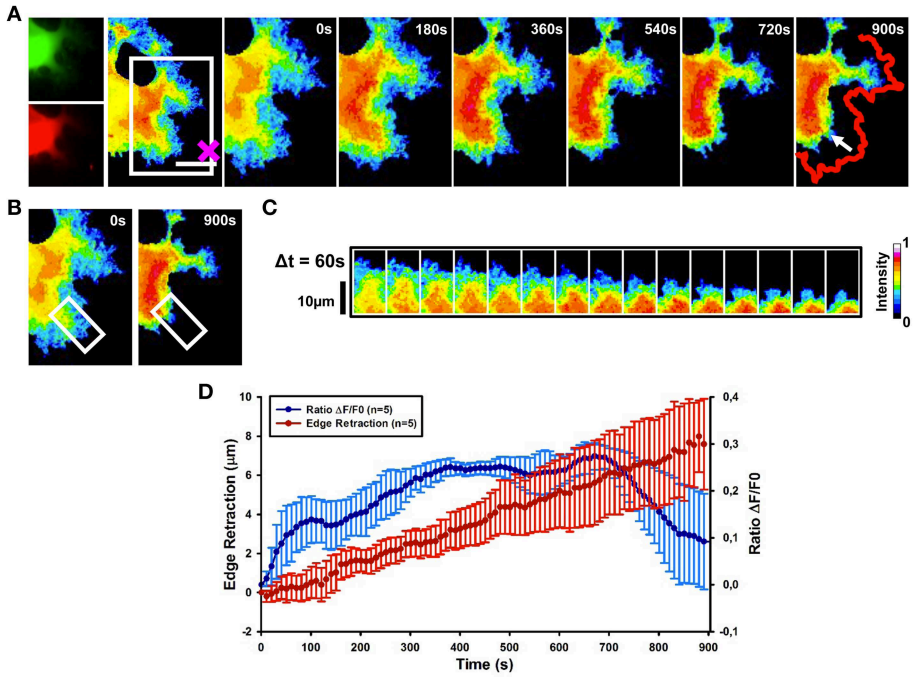

FIGURE 5 | RhoA activation dynamics upon local release of Sema3A. **(A)** Ratiometric FRET live imaging of a representative RhoA-FRET neuroblastoma cell upon Sema3A stimulation. Frames were taken every second (left: generation of a ratiometric image) for 15 min (the cross indicates the position of the lipid vesicle filled with Sema3A). Insets on the right show a time series (1 frame every 3 min) of the magnified region denoted by the white box in the left image. Arrow indicates the retraction direction. The red line shows the initial edge profile. Scale Bar: 20 μm. **(B,C)** Montage images showing the dynamics of RhoA activation in the stimulated cell GCs. **(B)** Images showing the region of interest selected for the montage (white boxes). **(C)** Montage images highlighting a progressive increase of RhoA activation in the retracting GC. Images were taken at 60 s intervals. Intensity scale on the right in **(C)** applies to **(A–C)**. **(D)** Plot of average RhoA activity ($\Delta F/F_0$) from five experiments. RhoA dynamics was followed for 15 min after Sema3A stimulation. FRET ratio is represented as a blue line; edge retraction is defined as a red line. Data are shown as Mean ± SEM.

BSA (Figures S2A–C), no comparable retraction (**Figure 2**) was observed.

Thus, our results strongly suggest that Sema3A local stimulation leads to an activation of RhoA associated to GC collapse and retraction.

Cdc42 Activation Exhibits a Wave-like Behavior

We then determined the spatial and temporal dynamics of activated Cdc42 in response to Sema3A local delivery (Supplementary Movie 2). Ratiometric FRET imaging showed that Cdc42 activity decreases within 60 s from Sema3A stimulation almost in synchrony with the cell edge retraction (**Figures 6A,B,D,E** and Figure S3; data from seven experiments).

In 43% of cases, we observed that in the region far from the stimulus Cdc42 activity increases within 120 s after Sema3A stimulation followed by edge advancement, lamellipodia ruffling and filopodia extension (**Figures 6A–C,F**). Plotting Cdc42 activity against time showed waves of active Cdc42 between the front and back of the protruding region, with a mean period of 155 ± 9 s (**Figures 7C,E**; data from three experiments). The delay between Cdc42 activation and Sema3A stimulation indicates that the protrusion event in the region far from the local release of Sema3A is a reaction to the repulsive stimulus. Consistently, BSA local stimulation seemed not to affect the activity of Cdc42 in transfected cells (Figures S2D–F).

In order to better characterize Cdc42 activity in response to Sema3A local stimulation, we used 1.5 μm microbeads coated with Sema3A that allow a more localized stimulation (D'Este et al., 2011) (Figure S4). Live FRET imaging of GCs transfected with Cdc42 and stimulated with Sema3A-beads showed the appearance of recurring waves of active Cdc42 almost in synchrony with the retraction of the GC (**Figure 7A**). Plotting Cdc42 intensity against time from three different areas of the stimulated GC revealed a burst of Cdc42 activity within 100–120 s from the local stimulation and highlighted the propagation of Cdc42 traveling waves from the front to the back of the retracting GC (**Figure 7B**). In spontaneous GC collapse and retraction we observed again Cdc42 active waves, but with a different periodicity (Beads: 70 ± 5 s vs. Spontaneous: 110 ± 10 s) (**Figures 7D,E**). Indeed, we found that Cdc42 active waves have different periods in all three cases described herein (Lipid vesicles, Spontaneous, and Coated Beads) reflecting the different cellular behavior in response to the stimulus applied (Holmes et al., 2012; Marèe et al., 2012).

Taken together, these findings show that (a) Cdc42 has a traveling wave behavior with a different periodicity, highlighting

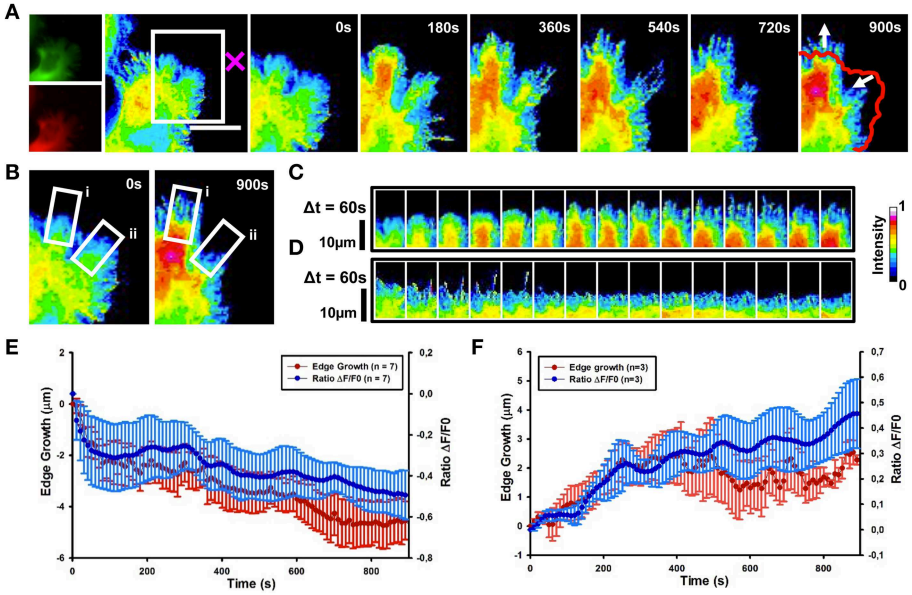

FIGURE 6 | Cdc42 dynamics upon local delivery of Sema3A. (A) Cdc42 activity determined by ratiometric FRET live imaging. Frames were taken every second (left: generation of a ratiometric image) for 15 min after stimulation (the cross indicates the position of the lipid vesicle encapsulating Sema3A). Insets on the right show a time series (1 frame every 3 min) of the magnified region denoted by the white box in the left image. Arrows indicate retraction and protrusion directions. The red line shows the initial edge profile. Scale Bar: 20 μm. **(B–D)** Montage images showing the dynamics of Cdc42 activity in protruding and retracting regions of the cell. **(B)** Images showing the regions of interest selected for the montage (white boxes) (i, protruding region; ii, retracting region). **(C,D)** Montage images highlighting a decrease of Cdc42 activity in the retracting region of the cell facing the lipid vesicle filled with Sema3A **(C)** and an increase of Cdc42 activity in the protruding region, away from the vesicle **(D)**. Images are taken at 60 s intervals. Intensity scale on the right in **(D)** applies to **(A–D)**. **(E)** Plot of average Cdc42 activity ($\Delta F/F_0$) vs. edge growth from seven experiments. Negative values are defined as retraction. FRET ratio is represented as a blue line; edge growth is defined as a red line. **(F)** The same as in **(E)**, but in this case data are obtained from three experiments. Positive values are defined as edge protrusion. Data are shown as Mean ± SEM.

its complex spatio-temporal dynamic; (b) that, in all the cases observed, a variation of Cdc42 activity upon Sema3A stimulation is accomplished with a leading edge retraction in the region of the stimulus; (c) that, in few cases, Sema3A local release induces the formation of active Cdc42 waves away from Sema3A stimulation that produced new lamellipodia and filopodia.

Discussion

By combining FRET with local stimulation we have demonstrated that local delivery of Sema3A induces an activation of RhoA followed by a rapid GC retraction. The use of two different approaches (beads and liposome vesicles) for Sema3A local stimulation of Cdc42 transfected cells, both based on optical manipulation, led to a better characterization of Cdc42 wave behavior. Sema3A release from the vesicles induced a decrease in Cdc42 activity followed by an edge retraction. In regions distant from the stimulus, active waves of Cdc42 resulted in a marked increase in cell dynamic with lamellipodia-ruffling and filopodia extension. Using 1.5-μm diameter Sema3A-immobilized microbeads, we observed again Cdc42 active waves that here resulted in GC retraction. In previous papers (Pinato et al., 2011, 2012), the local delivery was used to estimate the minimum number of Sema3A and Netrin1 molecules necessary to induce retraction and growth, respectively. The present study expands previous observations by combining for the first time local stimulation with the FRET technique underlying a fine spatial and temporal regulation of RhoGTPase activities after Sema3A stimulus.

RhoA and Cdc42 Have a Different Spontaneous Activity in NG108-15 Neuroblastoma Cells

Rho GTPases are key molecular switches that affect multiple cellular functions including cell migration and polarity, vesicle trafficking, cytokinesis and endocytosis (Etienne-Manneville and Hall, 2002; Govek et al., 2005; Boureux et al., 2007; Haesman and Ridley, 2008; Pertz, 2010). They are important players in the transmission and integration of signals that control the cytoskeleton: in response to extracellular signals, they induce changes in the organization of actin cytoskeleton to allow different biological processes like morphogenesis, chemotaxis, axonal guidance, and cell cycle progression (Ridley and Hall, 1992; Gallo and Letourneau, 2004; Sit and Manser, 2011; Gomez and Letourneau, 2014). In N1E-115 neuroblastoma cell line, Cdc42 promotes the formation of filopodia and lamellipodia, whereas RhoA causes GC collapse and neurite retraction (Kozma et al., 1997; van Leeuwen et al., 1997; Sarner et al., 1997). Consistent with this view, on a laminin

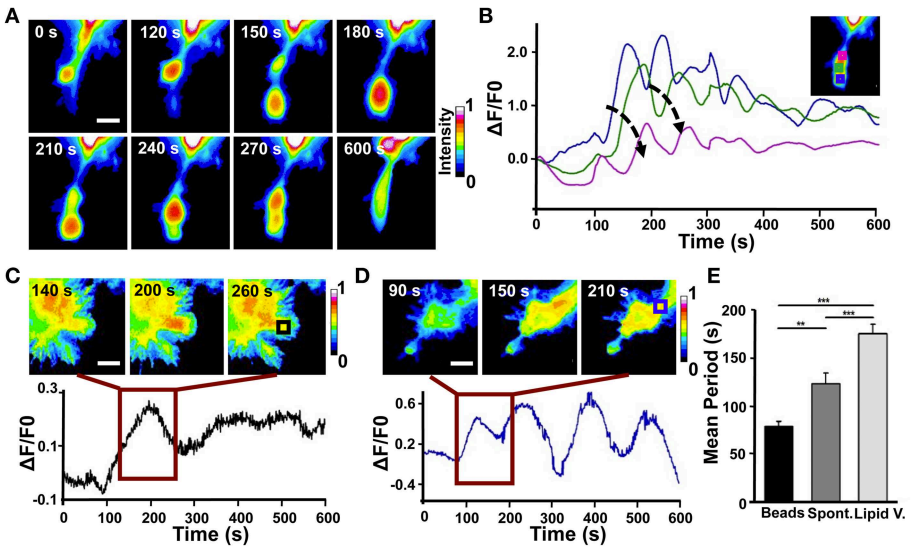

FIGURE 7 | Analysis of Cdc42 wave-like behavior. (A) Time series of the active Cdc42 retrograde waves upon local stimulation with Sema3A-coated beads (Representative of three experiments). **(B)** Plot of average Cdc42 activity ($\Delta F/F_0$) in the regions defined by the colored squares in the inset image at the top right. The analyzed cell is the same shown in **(A)**. Arrows indicate the temporal progression of the oscillations. **(C)** Top: Time series (1 frame every 60 s) of the Cdc42 oscillatory behavior upon local stimulation with lipid vesicles filled with Sema3A for the time defined by the dark red square in the bottom plot; Bottom: Plot of average Cdc42 activity ($\Delta F/F_0$) in the region defined as a black square in the image at the top right. **(D)** Top: Time series (1 frame every 60 s) of the Cdc42 wave behavior during spontaneous motion for the time defined by the dark red square in the bottom plot. Bottom: Plot of average Cdc42 activity ($\Delta F/F_0$) in the region defined as a blue square in the image at the top right. **(E)** Quantification of the period of the oscillations both during spontaneous motion and upon local stimulation. Mean period ± SEM of 10 periods from 3 experiments for bead stimulation, 10 periods from 2 experiments for spontaneous motion and 10 periods from 3 experiments for lipid vesicles stimulation. $^{**}p < 0.01$, $^{***}p < 0.01$ using ANOVA test. Scalebars in **(A,C,D)**: 10 μm.

substrate, NG108-15 cells expressing Cdc42 exhibited long processes with rather simple GCs and branched neurites with several actin microspikes along their length. On the contrary, expression of RhoA often resulted in cell rounding and flattening without the appearance of stress fibers or focal contact (Figure S1). Spatial and temporal monitoring of spontaneous activity of RhoA and Cdc42 in NG108-15 cells allowed us to directly compare cell motility with levels of active RhoA and Cdc42. We found that filopodia and lamellipodia protrusions correlate with Cdc42 activation in these subcellular domains (**Figure 3**), whereas RhoA activity increases and decreases in synchrony with cell leading edge retraction and protrusion (**Figure 2**).

Local Release of Sema3A Induces a Rapid GC Collapse and Retraction

The role of Rho-family GTPases in response to several guidance cue stimulations has been extensively studied in order to address their role in F-actin dynamics and organization that determine axon guidance, GC behavior and axon extension (Gallo and Letourneau, 2004). Attractive cues such as brain-derived neurotrophic factor (BDNF) activate Cdc42 and Rac (Yuan et al., 2003; Cheung et al., 2007; Myers et al., 2012; Tep et al., 2012), whereas repulsive cues like Slit or Eph/ephrin have been shown to induce a reduction of Cdc42 activity at GC periphery and an activation of RhoA/ROCK pathway respectively (Wahl et al., 2000; Myers et al., 2012; Takeuchi et al., 2015). However, it is well-established that small GTPases are important components of Semaphorin (Sema)/plexin axon guidance signaling (Kruger et al., 2005; Tran et al., 2007). The Sema family of secreted, transmembrane and GPI-linked proteins is one of the largest families of axon guidance cues and guides the growing axons by repelling them or preventing them from entering certain regions (Yazdani and Terman, 2006). The prototypic member of this family is the diffusible repulsive guidance cue Sema3A that induces collapse of GCs through the interaction with its receptor plexinA1 (Fan and Raper, 1995; Nakamura et al., 2000; Brown and Bridgman, 2009). In our experiments, Sema3A local delivery leads to a rapid GC collapse and retraction in NG108-15 neuroblastoma cell line (**Figure 4**) in agreement with similar experiments in DRG neurons (Brown et al., 2009).

Sema3A Local Stimulation Activates RhoA and Cdc42 with Specific Spatio-temporal Dynamics

Previous findings have indicated an inhibitory role for RhoA in inducing neurite extension (Kozma et al., 1997; Dickson, 2001; Wu et al., 2005). Consistently, we found that Sema3A local release leads to RhoA activation within 30 s, causing a delayed GC retraction (100–120 s from stimulation) with a correlation between the levels of RhoA activity and Sema3A-induced morphological changes (**Figure 5**). This delay suggests that GC collapse and

retraction could require RhoA recruitment of its binding partners.

In Cdc42 transfected cells, local delivery of Sema3A caused a decrease of Cdc42 activity within 60 s from the stimulation (**Figure 6**). Cdc42 showed a wave behavior with a retrograde flow that proceeded almost in synchrony with cell retraction toward the repulsive cue (**Figure 6**). In a few cases, Sema3A local release induced the formation of active Cdc42 propagating waves away from Sema3A stimulation that generated new lamellipodia and filopodia suggesting a role for Cdc42 as an important component of actin *t*-waves (Lim et al., 2008; Flynn et al., 2009; Mori et al., 2011; Allard and Mogilner, 2013) (**Figure 6**).

Local stimulation with Sema3A coated beads induced the formation of active Cdc42 waves that propagated from the edge of the GC to the center of the cell with a period of 70 s (**Figure 7**). The same active Cdc42 waves were found in spontaneous GC collapse and retraction in response to repellent signals naturally occurring in neuronal cell culture, but with a mean period of 110 s (Rauch et al., 2013). How differently Sema3A stimulation can influence Cdc42 wave behavior is still an open question. One possibility is that these different Cdc42 dynamic wave patterns reflect the heterogeneity of the cell population or differential activity states of the cell. Alternatively, bead mechanical stimulation could induce calcium oscillations within the cell that influence actin *t*-waves through the modulation of Cdc42 activity (Wu et al., 2013). Although previous models have highlighted a fine spatio-temporal crosstalk between Rho GTPases that exhibit sustained polarization by a wave-pinning mechanism (Mori et al., 2008; Holmes et al., 2012; Marèe et al., 2012), our data show a wave-propagation mechanism for Cdc42 but not for RhoA and provide clear evidence for a higher degree of complexity in Rho GTPase signaling network (Pertz, 2010).

Our findings clearly indicate that the combination of the FRET technique with local stimulation provides new tools for the study of cytoskeleton rearrangements in response to guidance cue stimulations, highlighting the dynamic spatial and temporal regulation of Rho GTPases.

Acknowledgments

We acknowledge the financial support of the NEUROSCAFFOLDS Project n.604263 within the Seventh Framework Programme for Research of the European Commission. We also acknowledge the financial support of the SI-CODE project of the Future and Emerging Technologies (FET) programme within the Seventh Framework Programme for Research of the European Commission, under FET-Open grant number: FP7-284553.

Supplementary Material

The Supplementary Material for this article can be found online at: http://journal.frontiersin.org/article/10.3389/fncel.2015.00333

References

Adams, R. H., Lohrum, M., Klostermann, A., Betz, H., and Püschel, A. W. (1997). The chemorepulsive activity of secreted semaphorins is regulated by furin-dependent proteolytic processing. *EMBO J.* 16, 6077–6086. doi: 10.1093/emboj/16.20.6077

Ahmed, I., Calle, Y., Iwashita, S., and Nur-E-Kamal A. (2006). Role of Cdc42 in neurite outgrowth of PC12 cells and cerebellar granule neurons. *Mol. Cell. Biochem.* 281, 17–25. doi: 10.1007/s11010-006-0165-9

Ahnert-Hilger, G., Höltje, M., Grosse, G., Pickert, G., Mucke, C., Nixdorf-Bergweiler, B., et al. (2004). Differential effects of Rho GTPases on axonal and dendritic development in hippocampal neurones. *J. Neurochem.* 90, 9–18. doi: 10.1111/j.1471-4159.2004.02475.x

Allard, J., and Mogilner, A. (2013). Traveling waves in actin dynamics and cell motility. *Curr. Opin. Cell Biol.* 25, 107–115. doi: 10.1016/j.ceb.2012.08.012

Boureux, A., Vignal, E., Faure, S., and Fort, P. (2007). Evolution of the Rho family of ras-like GTPases in eukaryotes. *Mol. Biol. Evol.* 24, 203–216. doi: 10.1093/molbev/msl145

Brown, J. A., and Bridgman, P. C. (2009). Disruption of the cytoskeleton during Semaphorin 3A induced growth cone collapse correlates with differences in actin organization and associated binding proteins. *Dev. Neurobiol.* 69, 633–646. doi: 10.1002/dneu.20732

Brown, J. A., Wysolmerski, R. B., and Bridgman, P. C. (2009). Dorsal root ganglion neurons react to semaphorin 3A application through a biphasic response that requires multiple myosin II isoforms. *Mol. Biol. Cell* 20, 1167–1179. doi: 10.1091/mbc.E08-01-0065

Cheung, Z. H., Chin, W. H., Chen, Y., Ng, Y. P., and Ip, N. Y. (2007). Cdk5 is involved in BDNF-stimulated dendritic growth in hippocampal neurons. *PLoS Biol.* 5:e63. doi: 10.1371/journal.pbio.0050063

Dent, E. W., Gupton, S. L., and Gertler, F. B. (2011). The growth cone cytoskeleton in axon outgrowth and guidance. *Cold Spring Harb. Perspect. Biol.* 3:a001800. doi: 10.1101/cshperspect.a001800

D'Este, E., Baj, G., Beuzer, P., Ferrari, E., Pinato, G., Tongiorgi, E., et al. (2011). Use of optical tweezers technology for long-term, focal stimulation of specific subcellular neuronal compartments. *Integr. Biol. (Camb.)* 3, 568–577. doi: 10.1039/c0ib00102c

Dickson, B. J. (2001). Rho GTPases in growth cone guidance. *Curr. Opin. Neurobiol.* 11, 103–110. doi: 10.1016/S0959-4388(00)00180-X

Etienne-Manneville, S., and Hall, A. (2002). Rho GTPases in cell biology. *Nature* 420, 629–635. doi: 10.1038/nature01148

Fan, J., and Raper, J. A. (1995). Localized collapsing cues can steer growth cones without inducing their full collapse. *Neuron* 14, 263–274. doi: 10.1016/0896-6273(95)90284-8

Flynn, K. C., Pak, C. W., Shaw, A. E., Bradke, F., and Bamburg, J. R. (2009). Growth cone-like waves transport actin and promote axonogenesis and neurite branching. *Dev. Neurobiol.* 69, 761–779. doi: 10.1002/dneu.20734

Gallo, G., and Letourneau, P. C. (2004). Regulation of growth cone actin filaments by guidance cues. *J. Neurobiol.* 58, 92–102. doi: 10.1002/neu.10282

Gomez, T. M., and Letourneau, P. C. (2014). Actin dynamics in growth cone motility and navigation. *J. Neurochem.* 129, 221–234. doi: 10.1111/jnc.12506

Goshima, Y., Ito, T., Sasaki, Y., and Nakamura, F. (2002). Semaphorins as signals for cell repulsion and invasion. *J. Clin. Invest.* 109, 993–998. doi: 10.1172/JCI0215467

Goshima, Y., Ohsako, S., and Yamauchi, T. (1993). Overexpression of Ca2+/calmodulin-dependent protein kinase II in Neuro2a and NG108-15 neuroblastoma cell lines promotes neurite outgrowth and growth cone motility. *J. Neurosci.* 13, 559–567.

Govek, E. E., Newey, S. E., and Van Aelst, L. (2005). The role of the Rho GTPases in neuronal development. *Genes Dev.* 19, 1–49. doi: 10.1101/gad.1256405

Haesman, S. J., and Ridley, A. J. (2008). Mammalian Rho GTPases: new insights into their functions from *in vivo* studies. *Nat. Rev. Mol. Cell. Biol.* 9, 690–701. doi: 10.1038/nrm2476

Hall, A. (1998). Rho GTPases and the actin cytoskeleton. *Science* 279, 509–514. doi: 10.1126/science.279.5350.509

Hall, A., and Lalli, G. (2010). Rho and Ras GTPases in axon growth, guidance, and branching. *Cold Spring Harb. Perspect. Biol.* 2:a001818. doi: 10.1101/cshperspect.a001818

Hengst, U., Cox, L. J., Macosko, E. Z., and Jaffrey, S. R. (2006). Functional and selective RNA interference in developing axons and growth cones. *J. Neurosci.* 26, 5727–5732. doi: 10.1523/JNEUROSCI.5229-05.2006

Holmes, W. R., Carlsson, A. E., and Edelstein-Keshet, L. (2012). Regimes of wave type patterning driven by refractory actin feedback: transition from static polarization to dynamic wave behaviour. *Phys. Biol.* 9:046005. doi: 10.1088/1478-3975/9/4/046005

Ichikawa, M., and Yoshikawa, K. (2001). Optical transport of a single cell-sized liposome. *Appl. Phys. Lett.* 79, 4598–4600. doi: 10.1063/1.1430026

Jaffe, A. B., and Hall, A. (2005). Rho GTPases: biochemistry and biology. *Annu. Rev. Cell Dev. Biol.* 21, 247–269. doi: 10.1146/annurev.cellbio.21.020604.150721

Jin, Z., and Strittmatter, S. M. (1997). Rac1 mediates collapsin-1-induced growth cone collapse. *J. Neurosci.* 17, 6256–6263

Jongbloets, B. C., and Pasterkamp, R. J. (2014). Semaphorin signalling during development. *Development* 141, 3292–3297. doi: 10.1242/dev.105544

Kozma, R., Sarner, S., Ahmed, S., and Lim, L. (1997). Rho family GTPases and neuronal growth cone remodelling: relationship between increased complexity induced by Cdc42Hs, Rac1, and acetylcholine and collapse induced by RhoA and lysophosphatidic acid. *Mol. Cell. Biol.* 17, 1201–1211.

Kruger, R. P., Aurandt, J., and Guan, K. L. (2005). Semaphorins command cells to move. *Nat. Rev. Mol. Cell. Biol.* 6, 789–800. doi: 10.1038/nrm1740

Kuhn, T. B., Brown, M. D., Wilcox, C. L., Raper, J. A., and Bamburg, J. R. (1999). Myelin and collapsin-1 induce motor neuron growth cone collapse through different pathways: inhibition of collapse by opposing mutants of rac1. *J. Neurosci.* 19, 1965–1975.

van Leeuwen, F. N., Kain, H. E., Kammen, R. A., Michiels, F., Kranenburg, O. W., and Collard, J. G. (1997). The guanine nucleotide exchange factor Tiam1 affects neuronal morphology; opposing roles for the small GTPases Rac and Rho. *J. Cell Biol.* 139, 797–807. doi: 10.1083/jcb.139.3.797

Lim, L. B., Bu, W., Goh, W. I., Koh, E., Ong, S. H., Pawson, T., et al. (2008). The Cdc42 Effector IRSp53 generates filopodia by coupling membrane protrusion with actin dynamics. *J. Biol. Chem.* 283, 20454–20472. doi: 10.1074/jbc.M710185200

Luo, L. (2000). Rho GTPases in neuronal morphogenesis. *Nat. Rev. Neurosci.* 1, 173–180. doi: 10.1038/35044547

Marèe, A. F., Grieneisen, V. A., and Edelstein-Keshet, L. (2012). How cells integrate complex stimuli: the effect of feedback from phosphoinositides and cell shape on cell polarization and motility. *PLoS Comput. Biol.* 8:e1002402. doi: 10.1371/journal.pcbi.1002402

Mori, Y., Jilkine, A., and Edelstein-Keshet, L. (2008). Wave-pinning and cell polarity from a bistable reaction-diffusion system. *Biophys. J.* 94, 3684–3697. doi: 10.1529/biophysj.107.120824

Mori, Y., Jilkine, A., and Edelstein-Keshet, L. (2011). Asymptotic and bifurcation analysis of wave-pinning in a reaction-diffusion model for cell polarization. *SIAM J. Appl. Math.* 71, 1401–1427. doi: 10.1137/10079118X

Murakoshi, H., Wang, H., and Yasuda, R. (2011). Local, persistent activation of Rho GTPases during plasticity of single dendritic spines. *Nature* 472, 100–104. doi: 10.1038/nature09823

Myers, J. P., Robles, E., Ducharme-Smith, A., and Gomez, T. M. (2012). Focal adhesion kinase modulates Cdc42 activity downstream of positive and negative axon guidance cues. *J. Cell Sci.* 125, 2918–2929. doi: 10.1242/jcs.100107

Nakamura, F., Kalb, R. G., and Strittmatter, S. M. (2000). Molecular basis of semaphorin-mediated axon guidance. *J. Neurobiol.* 44, 219–229. doi: 10.1002/1097-4695(200008)44:2<219::AID-NEU11>3.0.CO;2-W

Nalbant, P., Hodgson, L., Kraynov, V., Toutchkine, A., and Hahn, K. M. (2004). Activation of endogenous Cdc42 visualized in living cells. *Science* 305, 1615–1619. doi: 10.1126/science.1100367

Nobes, C. D., and Hall, A. (1995). Rho, rac and cdc42 GTPases: regulators of actin structures, cell adhesion and motility. *Biochem. Soc. Trans.* 23, 456–459. doi: 10.1042/bst0230456

Ohnami, S., Endo, M., Hirai, S., Uesaka, N., Hatanaka, Y., Yamashita, T., et al. (2008). Role of RhoA in activity-dependent cortical axon branching. *J. Neurosci.* 28, 9117–9121. doi: 10.1523/JNEUROSCI.1731-08.2008

Peng, J., Wallar, B. J., Flanders, A., Swiatek, P. J., and Alberts, A. S. (2003). Disruption of the Diaphanous-related formin Drf1 gene encoding mDia1 reveals a role for Drf3 as an effector for Cdc42. *Curr. Biol.* 13, 534–545. doi: 10.1016/S0960-9822(03)00170-2

Pertz, O. (2010). Spatio-temporal Rho GTPase signaling - where are we now? *J. Cell Sci.* 123, 1841–1850. doi: 10.1242/jcs.064345

Pinato, G., Cojoc, D., Lien, L. T., Ansuini, A., Ban, J., D'Este, E., et al. (2012). Less than 5 Netrin-1 molecules initiate attraction but 200 Sema3A molecules are necessary for repulsion. *Sci. Rep.* 2:675. doi: 10.1038/srep00675

Pinato, G., Raffaelli, T., D'Este, E., Tavano, F., and Cojoc, D. (2011). Optical delivery of liposome encapsulated chemical stimuli to neuronal cells. *J. Biomed. Opt.* 16, 095001. doi: 10.1117/1.3616133

Raftopoulou, M., and Hall, A. (2004). Cell migration: Rho GTPases lead the way. *Dev. Biol.* 265, 23–32. doi: 10.1016/j.ydbio.2003.06.003

Rauch, P., Heine, P., Goettgens, B., and Käs, J. A. (2013). Different modes of growth cone collapse in NG 108-15 cells. *Eur. Biophys. J.* 42, 591–605. doi: 10.1007/s00249-013-0907-z

Ridley, A. J., and Hall, A. (1992). The small GTP-binding protein rho regulates the assembly of focal adhesions and actin stress fibers in response to growth factors. *Cell* 70, 389–399. doi: 10.1016/0092-8674(92)90163-7

Sarner, S., Kozma, R., Ahmed, S., and Lim, L. (1997). Phosphatidylinositol 3-Kinase, Cdc42, and Rac1 act downstream of ras in integrin-dependent neurite outgrowth in N1E-115 neuroblastoma cells. *Mol. Cell. Biol.* 20, 158–172. doi: 10.1128/MCB.20.1.158-172.2000

Sit, S. T., and Manser, E. (2011). Rho GTPases and their role in organizing the actin cytoskeleton. *J. Cell Sci.* 124, 679–683. doi: 10.1242/jcs.064964

Smalheiser, N. R. (1991a). Cell attachment and neurite stability in NG108-15 cells: what is the role of microtubules? *Brain Res. Dev. Brain Res.* 58, 271–282. doi: 10.1016/0165-3806(91)90015-B

Smalheiser, N. R. (1991b). Role of laminin in stimulating rapid-onset neurites in NG108-15 cells: relative contribution of attachment and motility responses. *Brain Res. Dev. Brain Res.* 62, 81–89. doi: 10.1016/0165-3806(91)90192-L

Takahashi, T., Nakamura, F., and Strittmatter, S. M. (1997). Neuronal and non-neuronal collapsin-1 binding sites in developing chick are distinct from other semaphorin binding sites. *J. Neurosci.* 17, 9183–9193.

Takeuchi, S., Katoh, H., and Negishi, M. (2015). Eph/ephrin reverse signalling induces axonal retraction through RhoA/ROCK pathway. *J. Biochem.* pii: mvv042. doi: 10.1093/jb/mvv042

Tep, C., Kim, M. L., Opincariu, L. I., Limpert, A. S., Chan, J. R., Appel, B., et al. (2012). Brain-derived neurotrophic factor (BDNF) induces polarized signaling of small GTPase (Rac1) protein at the onset of Schwann cell myelination through partitioning-defective 3 (Par3) protein. *J. Biol. Chem.* 287, 1600–1608. doi: 10.1074/jbc.M111.312736

Thies, E., and Davenport, R. W. (2003). Independent roles of Rho-GTPases in growth cone and axonal behavior. *J. Neurobiol.* 54, 358–369. doi: 10.1002/neu.10135

Tran, T. S., Kolodkin, A. L., and Bharadwaj, R. (2007). Semaphorin regulation of cellular morphology. *Annu. Rev. Cell Dev. Biol.* 23, 263–292. doi: 10.1146/annurev.cellbio.22.010605.093554

Tsuji, T., Higashida, C., Yoshida, Y., Islam, M. S., Dohmoto, M., Koizumi, K., et al. (2011). Ect2, an ortholog of Drosophila's pebble, negatively regulates neurite outgrowth in neuroblastoma x glioma hybrid NG108-15 cells. *Cell. Mol. Neurobiol.* 31, 663–668. doi: 10.1007/s10571-011-9668-3

Wahl, S., Barth, H., Ciossek, T., Aktories, K., and Mueller, B. K. (2000). Ephrin-A5 induces collapse of growth cones by activating Rho and Rho kinase. *J. Cell Biol.* 149, 263–270. doi: 10.1083/jcb.149.2.263

Wong, J. T., Wong, S. T., and O'Connor, T. P. (1999). Ectopic semaphorin-1a functions as an attractive guidance cue for developing peripheral neurons. *Nat. Neurosci.* 2, 798–803. doi: 10.1038/12168

Worzfeld, T., and Offermanns, S. (2014). Semaphorins and plexins as therapeutic targets. *Nat. Rev. Drug Discov.* 13, 603–621. doi: 10.1038/nrd4337

Wu, K. Y., Hengst, U., Cox, L. J., Macosko, E. Z., Jeromin, A., Urquhart, E. R., et al. (2005). Local translation of RhoA regulates growth cone collapse. *Nature* 436, 1020–1024. doi: 10.1038/nature03885

Wu, M., Wu, X., and De Camilli, P. (2013). Calcium oscillations-coupled conversion of actin travelling waves to standing oscillations. *Proc. Natl. Acad. Sci. U.S.A.* 110, 1339–1344. doi: 10.1073/pnas.1221538110

Yazdani, U., and Terman, J. R. (2006). The semaphorins. *Genome Biol.* 7:211. doi: 10.1186/gb-2006-7-3-211

Yuan, X. B., Jin, M., Xu, X., Song, Y. Q., Wu, C. P., Poo, M. M., et al. (2003). Signalling and crosstalk of Rho GTPases in mediating axon guidance. *Nat. Cell Biol.* 5, 38–45. doi: 10.1038/ncb895

Zhou, Y., Gunput, R. A., and Pasterkamp, R. J. (2008). Semaphorin signaling: progress made and promises ahead. *Trends Biochem. Sci.* 33, 161–170. doi: 10.1016/j.tibs.2008.01.006

Conflict of Interest Statement: The authors declare that the research was conducted in the absence of any commercial or financial relationships that could be construed as a potential conflict of interest.

Supplementary Information:

Cdc42 and RhoA reveal different spatio-temporal dynamics upon local stimulation with Semaphorin-3A

Federico Iseppon[1], Luisa M.R. Napolitano[1,2], Vincent Torre[1,*] and Dan Cojoc[3,*]

[1]Neurobiology Sector, International School for Advanced Studies (SISSA), Trieste, Italy.
[2]Structural Biology Laboratory, Elettra-Sincrotrone Trieste S.C.p.A., Area Science Park, Basovizza, Trieste, Italy.
[3]Institute of Materials – National Research Council (IOM-CNR), Area Science Park-Basovizza, Italy

***Correspondence:** Vincent Torre, Neurobiology Sector, International School for Advanced Studies (SISSA), via Bonomea 265, Trieste 34136, Italy. E-mail: torre@sissa.it.
Dan Cojoc, Institute of Materials – National Research Council (IOM-CNR), Area Science Park- Basovizza, Trieste 34149, Italy. E-mail: cojoc@iom.cnr.it

Keywords: RhoA, Cdc42, FRET, local stimulation, Semaphorin3A, growth cone retraction, NG108-15 cell line

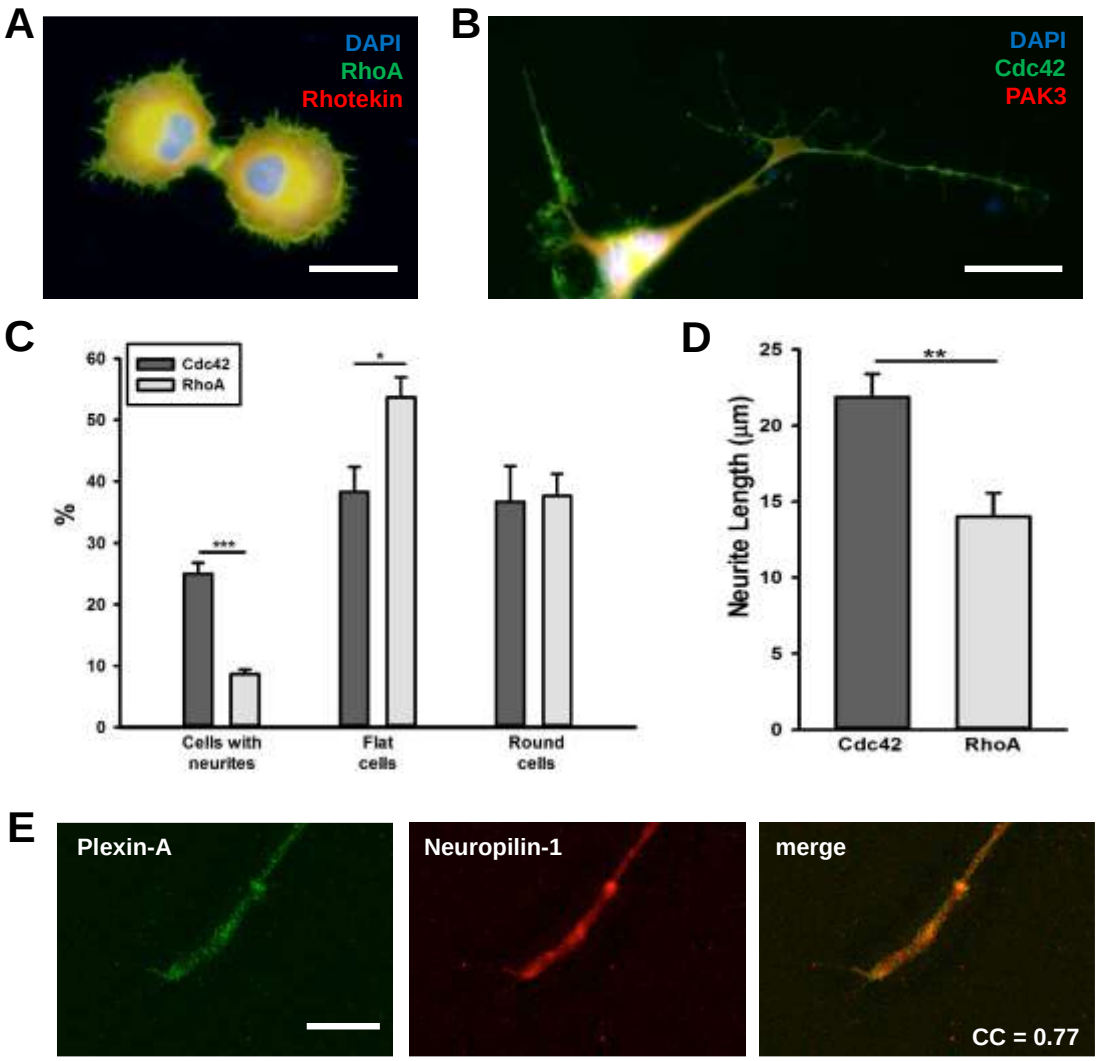

Figure S1: Cdc42 and RhoA expression in NG108-15 cell line. NG108-15 neuroblastoma cells were plated on laminin and transfected with either RhoA/Rhotekin **(A)** or Cdc42/Pak3 **(B)**. The values in **(C)** and **(D)** represent the percentage of transfected cells that exhibit neurite (C) and the neurite lenght (D) of 500 cells from four experiments. *p<0.05; **p<0.01; ***p<0.001 using ANOVA test **(E)** Immunostaining of NG108-15 growth cones with antibodies for plexinA1 (green) and neuropilin1 (red). As shown in the merged image, NG108-15 cells express both subunits needed to form a functional Sema3A receptor widely in the growth cones. Scale Bar: 5µm. Co-localization percentage: 77%.

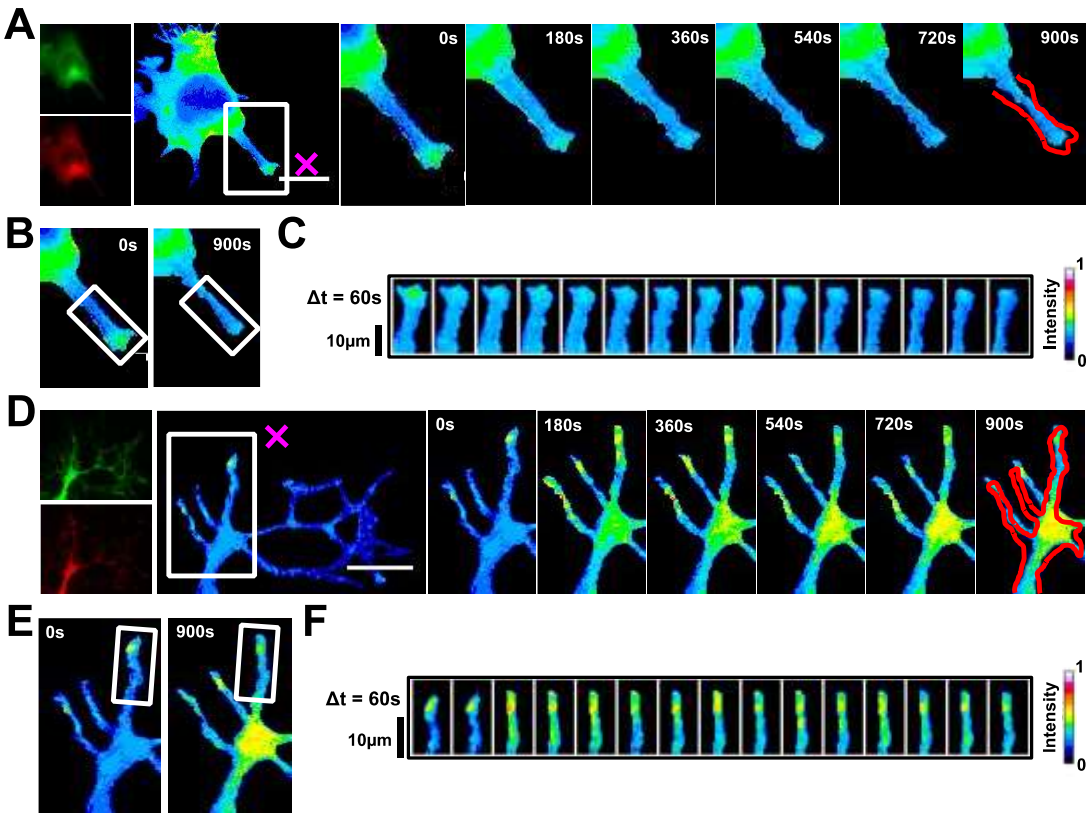

Figure S2: RhoA and Cdc42 dynamics in NG108-15 cells upon local stimulation with BSA-filled liposome. (A) RhoA activity determined by ratiometric FRET live imaging. Frames were taken every second (left: generation of a ratiometric image) for 15 minutes after the stimulation (the cross indicates the position of the lipid vesicle encapsulating BSA). Insets on the right show a time serie (1 frame every 3 minutes) of the magnified region denoted by the white box in the left image. The red line shows the initial edge profile. Scale Bar: 20µm. **(B** and **C)** Montage images showing RhoA dynamics in the stimulated cell growth cones. (B) Images showing the region of interest selected for the montage (white boxes). (C) Montage images highlighting a slight increase of RhoA activity in the region of the growth cone that shows a mild collapse. **(D)** Cdc42 activity determined by ratiometric FRET live imaging. Frames were taken every second (left: generation of a ratiometric image) for 15 minutes after the stimulation (the cross indicates the position of the lipid vesicle encapsulating BSA). Insets on the right show a time serie (1 frame every 3 minutes) of the magnified region denoted by the white box in the left image. The red line shows the initial edge profile. Scale Bar: 20µm. **(E** and **F)** Montage images showing Cdc42 activation dynamics in the stimulated cell growth cones. (E) Images showing the region of interest selected for the montage (white boxes). (F) Montage images highlighting a higher activation in the growing filopodium. Intensity scales on the right in (C, F) apply to (A – F).

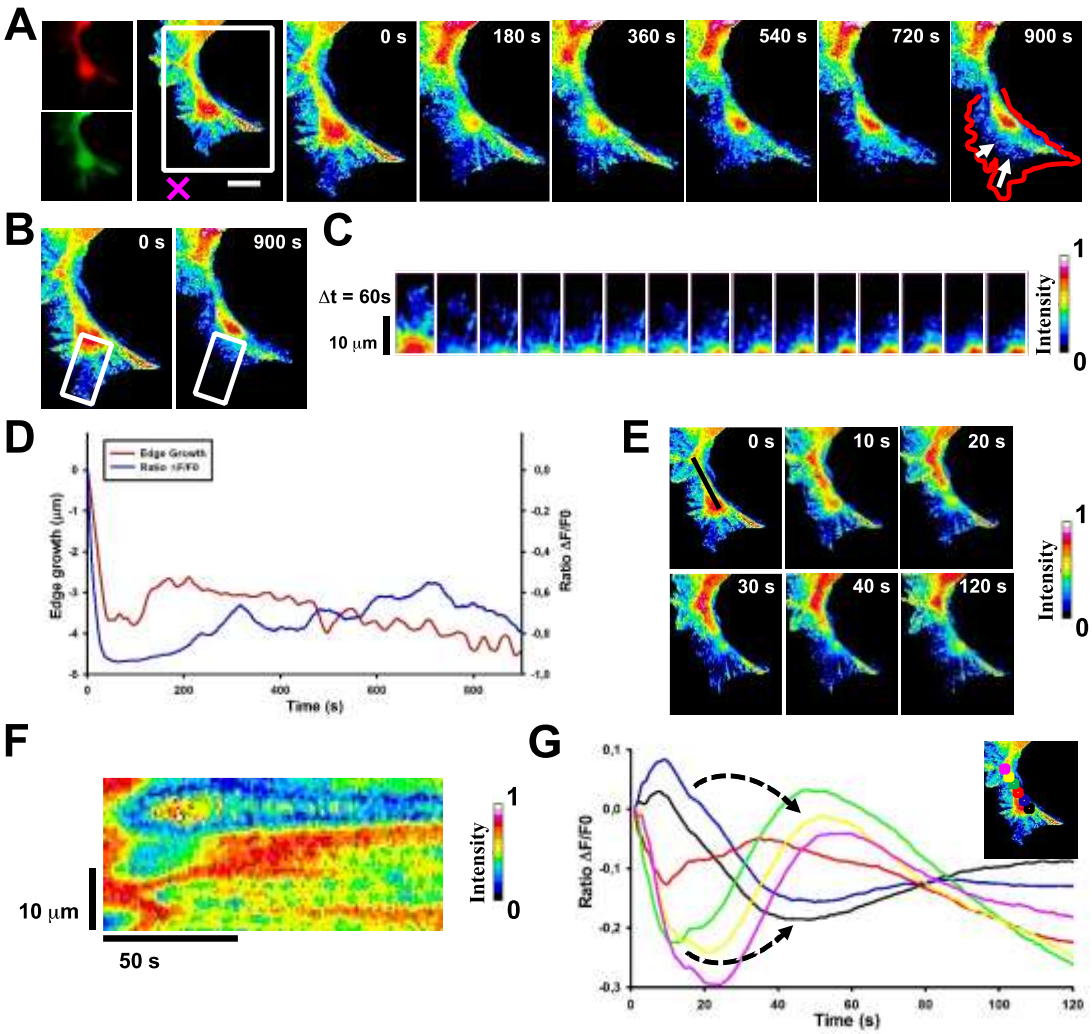

Figure S3: Cdc42 activity in a cell neurite upon stimulation with lipid vesicles encapsulating Sema3A. **(A)** Cdc42 activity determined by ratiometric FRET live imaging. Frames were taken every second (left: generation of a ratiometric image) for 15 minutes after the stimulation (the cross indicates the position of the lipid vesicle encapsulating Sema3A). Insets on the right show a time serie (1 frame every 3 minutes) of the magnified region denoted by the white box in the left image. Arrows indicate retraction directions. The red line shows the initial edge profile. Scale Bar: 20µm. **(B** and **C)** Montage images showing Cdc42 activity in the retracting region. (B) Images showing the region of interest selected for the montage (white boxes). (C) Montage images highlighting a decrease of Cdc42 activity in the retracting region of the cell facing the lipid vesicle filled with Sema3A. Images are taken at 60s intervals. In this case we observed a strong decrease of Cdc42 activity within 60 seconds from Sema3A delivery that proceeds simultaneously with the growth cone retraction. **(D)** Plot of average Cdc42 activity ($\Delta F/F_0$) versus edge growth from the area selected in (B). Negative values are defined as retraction. FRET ratio is represented as a blue line; edge growth is defined as a red line. **(E)** Legend as in (A), but the time span is 120 seconds. Black line indicates the area selected for kymograph analysis in **(F)** that highlights Cdc42 wave behavior. Intensity scales on the right in (C), (E), (F) apply to (A), (B), (C), (E) and (F). **(G)** Plot of average Cdc42 activity ($\Delta F/F_0$) in the regions defined by the colored squares in the inset image on the top right. The analyzed cell is the same shown in (E). Arrows indicate the temporal progression of the waves.

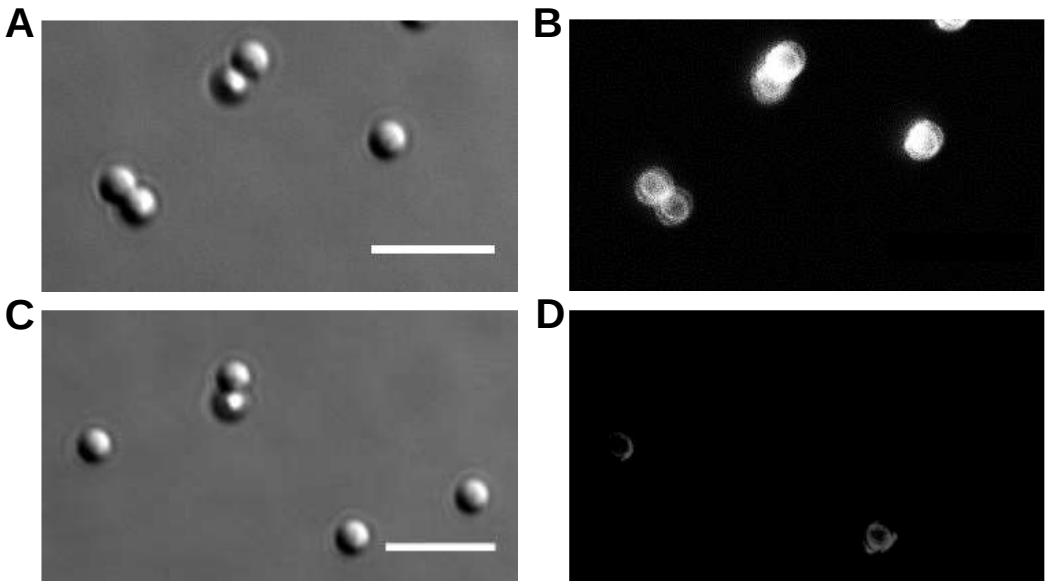

Figure S4. Sema3A-coated beads. Immunofluorescence images of Sema3A-beads (B) and of un-functionalized beads (D) incubated with the anti-Sema3A antibody following the protocol indicated in the Materials and Methods section. (A) and (C) are DIC images of the beads. Scale bar 5μm.

Supplementary Movie 1: Sema3A local stimulation leads to an activation of RhoA followed by growth cone collapse and retraction.
This movie shows the RhoA activation dynamics upon local stimulation by breaking of a lipid vescicle (magenta cross in the image) filled with 1 μM of Sema3A.
Frame interval: 4 s. Duration of original sequence: 15 min. Frames are color-coded 8 bit: warm colors represent higher activation and cold colors represent lower activation.

Supplementary Movie 2: Sema3A local stimulation induces an activation of Cdc42 in the region opposite to the stimulus
This movie shows the Cdc42 activation dynamics upon local stimulation by breaking of a lipid vescicle (magenta cross in the image) filled with 1 μM of Sema3A.
Frame interval: 4 s. Duration of original sequence: 15 min. Frames are color-coded 8 bit: warm colors represent higher activation and cold colors represent lower activation.

2

Combining FRET and Optical Tweezers to study RhoGTPases spatio-temporal dynamics upon local stimulation.

Federico Iseppon, Luisa Maria Rosaria Napolitano, Vincent Torre and Dan Cojoc

Journal of Biological Methods – Under Review

TITLE:

Combining FRET and Optical Tweezers to study RhoGTPases spatio-temporal dynamics upon local stimulation.

RUNNING TITLE:

FRET and Optical Tweezers for local stimulation.

AUTHORS:

Federico Iseppon[1], Luisa MR Napolitano[1], Vincent Torre[1], Dan Cojoc[2]

AFFILIATIONS:

[1] Neuroscience Area, International School for Advanced Studies, Trieste, IT

[2] Optical Manipulation Lab, CNR-IOM, the National Research Council of Italy - Institute Of Materials, Basovizza (TS), IT

CORRESPONDING AUTHOR:

Dan Cojoc, PhD, Optical Manipulation Lab, CNR-IOM, the National Research Council of Italy - Institute Of Materials, Area Science Park Basovizza, SS14, Km 163.5, 34149 Basovizza TS, Italy. Tel: 040 3758772; E-mail: cojoc@iom.cnr.it

ABSTRACT:

Local stimulation with optical tweezers has been used to mimic natural stimuli that occur in biological processes such as cell migration or differentiation. Carriers (beads and lipid vesicles) with sizes down to 30 nm can be manipulated with a high spatial and temporal resolution: they are positioned with a sub-micrometric precision on a specific cell compartment and the beginning of the stimulation can be triggered with millisecond precision. RhoGTPase are a Ras-related family of proteins that regulate many different functions including cell polarity, microtubule dynamics and membrane transport pathways. Here we combine local stimulation with FRET technique to study RhoGTPase spatial and temporal activation following guidance cue local stimulation. We used two different vectors for local delivery: silica micro-beads and micro-sized lipid vesicles. The experimental methods associated with neuronal growth cone local stimulation are discussed in detail, as well as the analysis methods. Here we present a protocol that enables to study neuronal growth cone cytoskeleton rearrangements in response to a gradient of molecules in a way that better mimics

physiological conditions, and it can be similarly applied to each secreted molecule involved in cell signalling.

KEYWORDS:
FRET, growth cones, guidance molecules, local stimulation, Optical Tweezers.

BACKGROUND:

RhoGTPases are a Ras-related family of proteins that play a major role in many physiological processes including cell polarity, microtubule dynamics, membrane transport pathways and transcription factor activity. They act as molecular switches that cycle between two conformational states: one bound to GTP (“active” state); the other one bound to GDP (“inactive” state)[1]. In the activated form, they bind different effector proteins leading to the activation of myriad downstream signals[2]. The best-characterized function of Rho GTPases is in the regulation of F-actin dynamics in both non-neuronal cells and neuronal growth cones [3,4]. During axon guidance, RhoGTPases translate signals from extracellular cues into growth-cone movement and axon guidance: RhoA increases the actomyosin contractility, whereas Rac1 and Cdc42 induce the polymerization of actin to form lamellipodial and filopodial protrusions, respectively [5,6]. RhoGTPases ability to regulate so many different functions, in highly dynamic cellular contexts, implies that they are tightly regulated at the spatio-temporal level. This has led to the development of fluorescent probes for the direct monitoring of their activation state in living cells based on the principle of Förster Resonance Energy Transfer (FRET) [7-9].

Most of the *in vitro* neuron stimulation experiments employ bath or micropipette administration of molecules to change the cell environment [10]. Hence, new strategies to address specific compartments of neuronal cells with spatial and temporal gradients of molecules, which better reflect cellular physiological conditions, should be considered [11]. Focal stimulation of neurons using optical tweezers and single micro-beads functionalized with a secretory molecule, the neurotrophin brain-derived neurotrophic factor (BDNF), demonstrated to induce focal increase of calcium signaling in the stimulated dendrite, with a specific activation of the TrkB receptor pathway and influenced the development of growth cones [12]. An elegant demonstration of the role of molecular gradients for cell stimulation has been reported for neutrophils by using optically manipulated microsources releasing soluble molecules that act as chemoattractants or perturb the actin cytoskeleton [13]. Another type of optically manipulated carriers are the lipid micro-vesicles encapsulating active molecules which are released by photolysis of the vesicle membrane using a laser pulse [14]. An optimization of this technique allowed to study the effect of a very small number

of different guidance cues on hippocampal neurons [15]. In principle, the number of molecules can be scaled down to a single molecule for a micron size vesicle at 1 nM concentration. Stimulation can be triggered with very high temporal precision, providing steep gradients over length scales from sub-micrometer to tens of micrometers and at time-scales from milliseconds to seconds.

Here, we present an experimental protocol that combines the FRET technique with local stimulation to observe the spatial and temporal activation of RhoA and Cdc42 following localized stimulation with Sema3A, a negative secreted guidance cue that steers a growth cone by inducing partial or local collapse [16,17]. We used two different vectors for Sema3A local delivery: silica micro-beads and micro-sized lipid vesicles. The former were covalently functionalized with Sema3A and placed on the selected neuronal growth cone for a controlled time (30 s); the latter were trapped with optical tweezers in front of the exploring Growth Cone and broken with short UV laser pulse, releasing the Sema3A in its native form. The combination of FRET technique with local stimulation provides new tools for the study of the cytoskeleton rearrangements in response to guidance cues stimulation, underlying the dynamic spatial and temporal activation of RhoGTPases.

MATERIALS:

Cells:

- NG108-15 Neuroblastoma cell line (Sigma-Aldrich, cat # 88112302)

Reagents:

- Bicinchoninic Acid Protein Assay kit (Sigma-Aldrich, cat # BCA1)
- Biomag Plus carboxyl coupling kit (Bangs Laboratories Inc., cat # BP611)
- $CaCl_2$ (Sigma-Aldrich, cat # C1016)
- DMEM (Thermofisher Scientific, cat # 31966-021)
- Ethanol (Sigma-Aldrich, cat # 02860)
- Fetal Bovine Serum (FBS) (Sigma-Aldrich, cat # F6178)
- Glass Coverslips (12mm round) (Chemglass, cat # 89167-106)
- Glucose (Sigma-Aldrich, cat # G0350500)
- HCl (Sigma-Aldrich, cat # 318949)
- HEPES (Sigma-Aldrich, cat # H3375)
- KCl (Sigma-Aldrich, cat #P9333)
- Laminin from Engelbreth-Holm-Swarm murine sarcoma basement membrane (Sigma-Aldrich, cat # L2020)

- Liposome Kit (Sigma-Aldrich, cat # L4395)
- mCherry-Pak3(60-113)/S74A/F84A-mCherry-C1 (Addgene, plasmid # 29676)
- mCherry-Rhotekin(8-89)-mCherry-C1 (Addgene, plasmid # 29675)
- mEGFP-Cdc42-C1 (Addgene, plasmid # 29673)
- mEGFP-RhoA-C1 (Addgene, plasmid # 29674)
- Metafectene Easy + transfection reagent (Biontex Laboratories, cat # T090)
- $MgCl_2$ (Sigma-Aldrich, cat # M8266)
- NaCl (Sigma-Aldrich, cat # S9888)
- PBS 10X, pH 7,4 (Thermofisher Scientific, cat # 70011044)
- Penicillin/Streptomycin (Biochrom AG, cat # A2213)
- Sucrose (Sigma-Aldrich, cat # S0389)

Recipes:

- *NG108-15 culture medium*: Add FBS and Penicillin-Streptomycin to respectively 10% and 1% of volume of DMEM. Store at 4°C for up to 8 weeks.
- *Ringer Solution*: Add NaCl 145 mM, KCl 3 mM, $CaCl_2$ 1.5 mM, $MgCl_2$ 1 mM, Glucose 5 mM, HEPES10 mM to 1L of MilliQ Water. Adjust the pH to 7,4.

Equipment:

- Cell culture incubator (humidified, 5% CO_2)
- Biological hood with laminar flow
- Cell counter chamber
- Nikon Eclipse inverted fluorescence microscope (Nikon)
- IR laser 1064nm (IPGphotonics)
- UV laser 355nm (Molecular Machines & Industries)
- Donor Filterset (Ex: 455/30, DM: 495LP) (Chroma Technology)
- Acceptor Filterset (Ex: 530/20, DM: 585LP) (Chroma Technology)
- Dual View FRET Filterset (DM: 585LP, Em1: 515/30, Em2: 625/30) (Chroma Technology)
- Emission/Excitation filter cube for 25mm filters (Cairn Research, cat # P290/000/200)
- Optosplit II LS Image Splitter (Cairn Research, cat # P280/210/MLS)
- ORCA-Flash 4.0 LT Digital CMOS camera (Hamamatsu, cat # C11440-42U)
- MATLAB Software (Mathworks) (download Biosensors 2.1 package from http://lccb.hms.harvard.edu/software.html)

PROCEDURE:

1. Preparation of coverslips

1.1 Wash glass coverslips overnight in 0,5 N hydrochloric acid (HCl) in a dedicated glass jar or beaker.

1.2 Remove the coverslips from HCl and wash twice in deionized water, then put them in 70% ethanol for 1,5 hr.

1.3 Separate the coverslips and sterilize them in a laminar flow hood or biosafety cabinet for 3 hours at 180 °C.

1.4 Place the coverslips in a 12-well plate and coat them with **2 µg/cm² of Laminin** for 2-3 hr. Rinse them twice with 1 ml of pre-warmed cell culture medium. Leave the coverslips in 1 ml of pre-warmed medium.

NOTES: Grow and maintain NG108-15 neuroblastoma cell line following standard protocols. All cell incubations are performed at 37°C, 5% CO_2 incubator. Equipment and reagents coming into contact with cell line must be sterile.

2. Cell transfection

NOTES: This protocol has been optimized for the transfection of Cdc42 and RhoA **inter-molecular** FRET probes developed by Murakoshi *et al.* [18] using **Metafectene Easy+** reagent. Single probe transfection is required for the image correction (Step 6).

2.1 Seed 0.2 X 10^5 cells into the coverslips in DMEM medium supplemented as described above and leave them in the incubator for 24 hr.

2.2 Prepare Buffer Solution 1X in sterile H_2O. Calculate 100 µl of buffer solution for each coverslip to be transfected. Add 1 µg of plasmid DNA for each transfection.

2.3 Put 2.5 µl of transfection reagent in each tube and mix gently. Remember to **Vortex** the reagent before adding it to the DNA-buffer solution.

2.4 After 15 min incubation at RT, add the transfection mixture dropwise to the cells. Leave them in the incubator for 18-24 hr to ensure the complete protein expression.

3. Beads Functionalization

3.1 Dilute 3 µl of bead **stock solution** in 1.8 ml Coupling Buffer.

3.2 Pipette 60 µl of the diluted beads in a polypropylene micro-centrifuge tube.

3.3 Centrifuge for 10 min at 1000 x g.

3.4 Discard the supernatant and suspend the pellet in 100 µl of Coupling Buffer.

3.5 Centrifuge for 10 min at 1000 x g.

3.6 Discard the supernatant and suspend the pellet in 50 µl of Coupling Buffer.

3.7 Prepare a **200 mg/ml 1-Ethyl-3-(3-dimethylaminopropyl)carbodiimide (EDAC) solution** in Coupling Buffer and add 10 µl of this solution to the beads suspension.

3.8 Mix gently and **leave to rest** at RT for 1 hr.

3.9 Add the protein of choice at saturation. For the right amount of protein calculate 20-500 µg of protein for each mg of particles.

3.10 **Leave to rest** for 1 hr at RT with gentle mixing.

3.11 Centrifuge for 10 min at 1000 x g, then remove the supernatant and suspend the pellet in 400 µl of Wash/Storage Buffer. **Repeat** this washing procedure twice.

3.12 Store the particles at 4 °C for up to two weeks.

NOTES (Step 3.11): Keep the supernatant for the calculation of the amount of protein linked to the bead with the BCA protein assay.

NOTES: This protocol is **optimized for** the BioMag Plus Carboxyl Coupling Kit.

4. Lipid Vesicles Preparation

4.1 Prepare a 6 ml solution of chloroform:methanol in proportion 2:1 (v/v).

4.2 Add the chloroform:methanol solution to the liposome kit vial. **Saturate the vial with N_2** (lipid vials can be stored at -20 °C until expiration date).

4.3 Put 50 µl of the lipid solution in a glass vial and proceed to the lipid desiccation in the vacuum oven (18 hr).

4.4 Remove the glass vial from the oven and **immediately saturate with N_2**. Proceed with the lipid film rehydration preparing a solution (Solution A) with 20 µl PBS + 5 µl Sucrose at 1M concentration for each lipid film to rehydrate.

4.5 Prepare a 25 µl solution in sterile PBS containing the protein of choice at the desired concentration (Solution B) for each lipid film to rehydrate. We used 1 µM Sema-3A final concentration [17,19].

4.6 **Mix well together** Solution A and Solution B (50 µl in total). Add **gently** the 50µl rehydrating solution to each glass vial containing the lipid film.

4.7 Vortex for about 1 minute and **leave them** overnight at 4 °C.

4.8 The day after, prepare a 100 mM Glucose washing solution in PBS.

4.9 Add 500 µl of washing solution in a 500 µl micro-centrifuge tube.

4.10 Add gently 10 µl of the lipid vesicles solution previously prepared on the surface.

4.11 Pellet the lipid vesicles in a table top centrifuge for 3 min at 1500 x g. Add 500 µl of washing solution and repeat this process again.

4.12 Resuspend the final pellet in 50µl of washing solution. Add the lipid vesicles directly in the plate to perform the local stimulation experiments.

TIPS (Step 4.11): Be cautious when removing the supernatant because the pellet is **not visible** and **very delicate**.

5. Local Stimulation and FRET imaging

NOTES: For these experiments the setup is equipped with an InfraRed (IR) and an UltraViolet (UV) laser together with an image splitter to record both channels needed for FRET at the same time. The microscope needs to be equipped also with two filtersets: a filterset with Donor excitation and no emission, since the image splitter will have both Donor and FRET channels, and a filterset with Acceptor excitation for FRET crosstalk correction (Fig.1).

5.1 Prepare the Ringer's solution at pH 7.4: NaCl 145 mM, KCl 3 mM, $CaCl_2$ 1.5 mM, $MgCl_2$ 1 mM, Glucose 5 mM, HEPES10 mM.

5.2 Record a set of 30-50 images **with no light** and then another set of 30-50 images with the **fluorescence light ON** and Donor molecule excitation but **no sample to use in the following offline correction steps (see 6.3-6.4 step)**.

5.3 Carefully remove the coverslip with the sample cells from the plate and place it into the recording chamber. Fill the recording chamber with Ringer's solution and put it under the microscope onto the pre-heated stage at 37°C.

5.4 Focus the cells under the microscope and search for a transfected one.

NOTES (Step 5.4): The **optimal** transfection efficiency is around 40-60%. For these experiments search for an isolated cell with neurite-like protrusions and growth cones.

5.5 Put 5-8 µl of lipid vesicles or beads into the sample medium and **wait** for them to sink, then turn the InfraRed (IR) laser ON.

5.6 To stimulate with lipid vesicles adopt the following procedure.

5.6.1 Move the focus **upwards** with respect to **the cell level**, find the focal point of the IR laser and then follow a lipid vesicle until it's trapped into the IR laser's focal point.

5.6.2 Gently move the trapped vesicle in the **proximity** (10-20 µm) of the cell compartment to stimulate. (Fig.2 A-C).

5.6.3 When all is set up, acquire a fluorescence video of about 90 sec to assess the viability of the

cell and its basal dynamics.

5.6.4 Acquire a video in Differential Interference Contrast (DIC) of the **lipid vesicle breaking** and perform it by giving pulses of 50-100 msec with an UltraViolet (UV) laser.

5.6.5 Acquire a fluorescence video of the cell after the stimulation for 15 min.

5.7 To stimulate with beads adopt the following procedure.

5.7.1 Acquire a fluorescence video of about 90 sec to assess the viability of the cell and its basal dynamics.

5.7.2 Move the focus upwards with respect to the cell level, find the focal point of the IR laser and then **trap a bead** into the IR laser's focal point.

5.7.3 Gently move the bead onto the cell compartment to stimulate it, then **move slowly the bead downwards** until it touches the cell membrane. In this case move the bead to the central part of the growth cone or onto filopodia and lamellipodia (Fig.2 D-F).

5.7.4 **Leave the trap ON** for the time of the stimulation, while acquiring a video in DIC, then turn the IR laser OFF. For this protocol we stimulated the cells for 30 sec.

5.7.5 Acquire a fluorescence video of the cell after 15 min stimulation.

NOTES: For these experiments, all the videos were acquired with **binning X4** and **1 sec** of **exposure time**.

CAUTION: This protocol involves the use of class 3b lasers and will require proper training and safety guidelines to be followed.

6. Offline Image Processing, Correction and Ratio Analysis

NOTES: FRET imaging data can be analysed offline at any time after the experiment using most imaging software dedicated to microscopy. Here is described the protocol using a custom Matlab software for processing together with the **Biosensors 2.1** Matlab package for correction and ratio analysis. This process involves offline correction of technical noise from the camera together with noise coming from uneven illumination and specific noise of the FRET technique. The final **ratio** between the corrected Acceptor channel and the Donor channel (upon Donor excitation) reflects the amount of activated protein.

6.1 **Split** the two channels from the raw sample video into Donor and FRET channels, then **align** them to match perfectly. This step uses custom-made Matlab software for the channels separation and alignment.

6.2 Carry out the following correction steps using **Biosensors 2.1 Matlab package**.

6.3 Correct the dark current noise with the control images taken with no light at step 5.2.

6.4 Correct for the uneven illumination with the control images taken with the fluorescence light ON at step 5.2.

6.5 Threshold the image to **create a mask** of the cell contour. It can be done automatically by choosing one of the algorithms in the programs or by manually setting up the threshold.

6.6 Subtract the background from the selected mask.

6.7 **Subtract the bleed-through and crosstalk noises using the following method:**

6.7.1 Open the images of all the channels of the cells transfected with only the single DNAs for either Donor or Acceptor. For this part use ImageJ software.

6.7.2 Select **at least 3 Regions of Interest (ROIs)** of the cells in all the channels and calculate the average intensity.

6.7.3 In case of cells transfected only with the Donor fluorophore, calculate the bleed-through coefficient by dividing the mean ROI intensity of the FRET channel and the one of the Donor channel.

6.7.4 Calculate the crosstalk coefficient by dividing, for the cells transfected only with the Acceptor fluorophore, the mean ROI intensity of the FRET channel and the one of the Acceptor channel.

6.7.5 Insert these coefficients in the Biosensors package to eliminate bleed-through and crosstalk noises.

6.8 **Calculate and correct** the photobleaching by choosing one of the algorithms in the package.

6.9 **Calculate the ratio** between corrected channels (FRET / Donor) and then create a file .tiff with the obtained result.

ANTICIPATED RESULTS:

Local stimulation based on optically manipulated carriers containing active molecules is a flexible technique easy to integrate with the optical microscope for live cell analysis. Different imaging techniques can thus be used in parallel with optical manipulation, as phase contrast, fluorescence, or FRET microscopy. Micro-carriers are generally employed since it is easier to observe and monitor them by bright field imaging inside the sample chamber. Both carriers used in this work (beads and lipid vesicles) can deliver any type of active proteins, which makes them practical for a very wide range of applications.

By using the method described herein, we were able to stimulate neuronal growth cones by mimicking the natural stimuli that lead to neuronal cell migration. We observed morphological rearrangements within the growth cones upon local Sema3A release.

Figure 4 shows an example of the morphological changes occurred in NG108-15 cells upon Sema3A local stimulation with beads (Fig. 3 A and B) and lipid vesicles (Fig. 3 C and D) in comparison with a cell that is not stimulated (Fig. 3 E and F). The plot of the mean edge growth of stimulated cells shows that both local stimulation methods are effective ways to trigger growth cone collapse and retraction, since there is no significant difference in the morphological response to either stimulation methods (Fig. 3 G).

The combination of FRET imaging with local stimulation allows the monitoring of the spatial and temporal activation of signaling molecules (e.g. RhoGTPases) in response to local extracellular stimuli (e.g guidance cues). The dynamics of the ratio between Donor and FRET channels reflect the spatio-temporal activation of the proteins studied.

Figure 4 shows that Sema3A repulsive stimulus triggers an activation of RhoA in both the center of the growth cone that diffuses to the leading edge and in filopodia causing growth cone collapse and retraction. The dynamic changes can be further investigated by using image montages (Fig. 5 A-C) or by performing Area Intensity Analysis to plot the ratio changes versus the leading edge dynamics (Fig. 5 D).

In summary, this methodology can be used to study the dynamic growth cone rearrangement in response to different guidance cues, and has been recently defined as a very promising method for guidance cues delivery [20]. Since a great variety of FRET probes have been created to study the dynamics of many proteins [21-24], this combination provides a very useful tool for investigating intra-cellular signalling pathways at the basis of major cell dynamics.

However, the development of new vectors - for which the molecules release can be timely tuned - and of more sensitive FRET probes will represent important optimizations of this technique in the future to broaden even more its potential applications.

TROUBLESHOOTING:

Table 1 presents issues and problems that are most likely to be encountered during this procedure and some hints and solutions to solve them. The setup configuration, alongside IR and UV relative alignment are the most delicate and should be always checked and addressed carefully, since a misalignment between the two beams brings to impossibility in trapping the beads and breaking the lipid vesicles.

Step	Problems	Causes	Suggestions
2	Poor transfection efficiency	DNA quantity is too low	Modify the transfection reagent/DNA ratio by adding more DNA to the mixture.
2	Low cell viability	- DNA quantity is too high - Incubation time is too high	- Decrease the amount of transfection solution and DNA added to the cells - Decrease the incubation time. NOTE: longer incubation times may result in higher efficiency but higher toxicity also.
3	Low BCA result	Low protein linked to the bead	Check that the amount of protein added is at saturation for the linker reaction to successfully take place
4	No lipid vesicles detected in the solution	- No lipid vesicles present - Wrong molarity of the solutions	- Be careful in all the washing procedures - Check the correct molarity of the glucose and sucrose solutions
5	No fluorescence intensity is detected in the FRET channel	FRET signal is very low	Increase the exposure time or the light intensity; this may bring to excessive photobleaching or phototoxicity, adjust these parameters to optimize the image acquisition.
5	Lipid vesicles and beads cannot be trapped	- IR laser is out of focus - IR laser power is too low	- Check the IR laser focus and align the beam - Increase the laser power
5	Lipid vesicles cannot be broken	UV an IR laser are not overlapping	Check the UV and IR laser relative position and focus and align the beam

6	Biosensors 2.1 package doesn't run	MATLAB version does not support it	This package works on MATLAB 2012b or below.

Table 1: Troubleshooting.

ACKNOWLEDGEMENTS:

We acknowledge the financial support of the NEUROSCAFFOLDS Project n.604263 within the Seventh Framework Programme for Research of the European Commission. We also acknowledge the financial support of the SI-CODE project of the Future and Emerging Technologies (FET) programme within the Seventh Framework Programme for Research of the European Commission, under FET-Open grant number: FP7-284553.

DISCLOSURES:

The authors declare that they have no competing financial interests.

REFERENCES:

1. Etienne-Manneville, S., Hall, A. RhoGTPases in cell biology. *Nature.* **420**, 629 – 635, 10.1038/nature01148, (2002).
2. Pertz, O. Spatio-temporal RhoGTPases signaling – where are we now? *J. Cell Sci.* **123**, 1841 - 1850, doi: 10-1242/jcs.064345, (2010).
3. Luo, L. RhoGTPases in neuronal morphogenesis. *Nat. Rev. Neurosci.* **1**, 173 – 180, doi: 10.1038/35044547, (2000).
4. Dickinson, B. J. Rho GTPases in growth cone guidance. *Curr. Opin. Neurobiol.* **11**, 103 – 110, doi: 10.1016/S0959-4388(00)00180-X, (2001).
5. Gallo, G., Letourneau, P. C. Regulation of growth cones actin filaments by guidance cues. *J. Neurobiol.* **58**, 92 – 102, 10.1002/neu.10282, (2003).
6. Ridley, A. J. RhoGTPases and cell migration. *J. Cell Sci.* **114**(Pt 15), 2713 – 2722, (2001).
7. Kraynov, V. S., Chamberlain, C., Bokoch, G. M., Schwartz, M. A., Slabaugh, S., Hahn, K. M. Localized Rac activation dynamincs visualized in living cells. *Science.* **290**(5490), 333-337, doi: 10.1126/science.290.5490.333, (2000).

8. Mochizuki, N., Yamashita S., Kurokawa K., Ohba Y., Nagai T. *et al.* Spatio-temporal images of growth-factor-induced activation of Ras and Rap1. *Nature.* **411**(6841), 1065 – 1068, (2001).
9. Itoh, R. E., Kurokawa, K., Ohba, Y., Yoshizaki, H., Mochizuki, N., Matsuda, M. Activation of rac and cdc42 video imaged by fluorescence resonance energy transfer-based single-molecule probes in the membrane of living cells. *Mol. Cell Biol.* **22**(18), 6582-6591, doi: 10.1128/MCB.22.18.6582.6592.2002, (2002).
10. Pujic, Z., Giacomantonio, C. E., Unni, D., Rosoff, W. J., Goodhill, G. J. Analysis of the growth cone turning assay for studying axon guidance. *J. Neurosci. Methods.* **170,** 220 – 228, (2008).
11. Dupin, I., Dahan, M., Studer, V. Investigating axonal guidance with microdevice-based approaches. *The Journal of neuroscience: the official journal of the Society for Neuroscience* **33**, 17647 – 17655, (2013).
12. D'Este, E., Baj, G., Beuzer, P., Ferrari, E., Pinato, G., Tongiorgi, E., Cojoc, D. Use of optical tweezers technology for long-term, focal stimulation of specific subcellular neuronal compartments, *Integr. Biol.* **3**, 568 – 577, (2011).
13. Kress, H., Park GJ., Mejean CO., Forster JD., Park J. *et al.* Cell stimulation with optically manipulated microsources. *Nature methods* **6**, 905 – 909, doi: 10.1038/nmeth.1400, (2009).
14. Sun, B., Chiu, D. T. Determination of the encapsulation efficiency of individual vesicles using single-vesicle photolysis and confocal single-molecule detection. *Analytical chemistry* **77**, 2770-2776, doi: 10.1021/ac048439n, (2005).
15. Pinato, G., CojocD., Lien LT., Ansuini A., Ban J. *et al.* Less than 5 Netrin-1 molecules initiate attraction but 200 Sema3A molecules are necessary for repulsion. *Scientific reports* **2**, 675, doi: 10.1038/srep00675, (2012).
16. Wong, J. T., Wong, S. T., O'Connor, T. P., Ectopic Semaphorin-1A functions as an attractive guidance cue for developing peripheral neurons. *Nature Neuroscience* **2**, 798 – 803, doi: 10.1038/12168, (1999).
17. Iseppon, F., Napolitano, L. M. R., Torre, V., Cojoc, D. Cdc42 and RhoA reveal different spatio-temporal dynamics upon local stimulation with Semaphorin-3A. *Fron. Cell. Neurosci.* **9**(333), doi: 10.3389/fncel.2015.00333, (2015).
18. Murakoshi, H., Wang, H., Yasuda, R. Local persistent activation of RhoGTPases during plasticity of single dendritic spines. *Nature*. **472**, 100 – 104, doi: 10.1038/nature09823, (2011).

19. Pinato, G., Raffaelli, T., D'Este, E., Tavano, F., Cojoc, D. Optical delivery of liposome encapsulated chemical stimuli to neuronal cells. *J. Biomed. Opt.* **16**(9), 095001, doi: 10.1117/1.3616133, (2011).
20. Dupin, I., Dahan, M., Studer, V. Investigating axonal guidance with microdevice-based approaches. *J. Neurosci.* **33**(45), 17647-17655, doi: 10.1523/JNEUROSCI .3277-13.2013, (2013).
21. Fritz, R.D., Letzelter M., Reimann A., Martin K., Fusco L. *et al.* A versatile toolkit to produce sensitive FRET biosensors to visualize signaling in time and space. *Sci. Signal.* **6**(285), rs12, doi: 10.1126/scisignal.2004135, (2013).
22. Lam, A.J., St-Pierre F., Gong Y., Marshall JD., Cranfill PJ. *et al.* Improving FRET dynamic range with bright green and red flurescent proteins. *Nat. Methods.* **9**(10), 1005-1012, doi: 10.1038/nmeth.2171, (2012).
23. Grashoff, C., Hoffman BD, Brenner MD, Zhou R., Parsons M. *et al.* Measuring mechanical tension across vinculin reveals regulation of focal adhesion dynamics. *Nature.* **466**(7303), 263-266, doi: 10.1038/nature09198, (2010).
24. Wang, Y., Botvinick EL., Zhao Y., Berns MW., Usami S. *et al.* Visualizing the mechanical activation of Src. *Nature*. **434**(7036), 1040-1045, doi: 10.1038/nature03469, (2005).

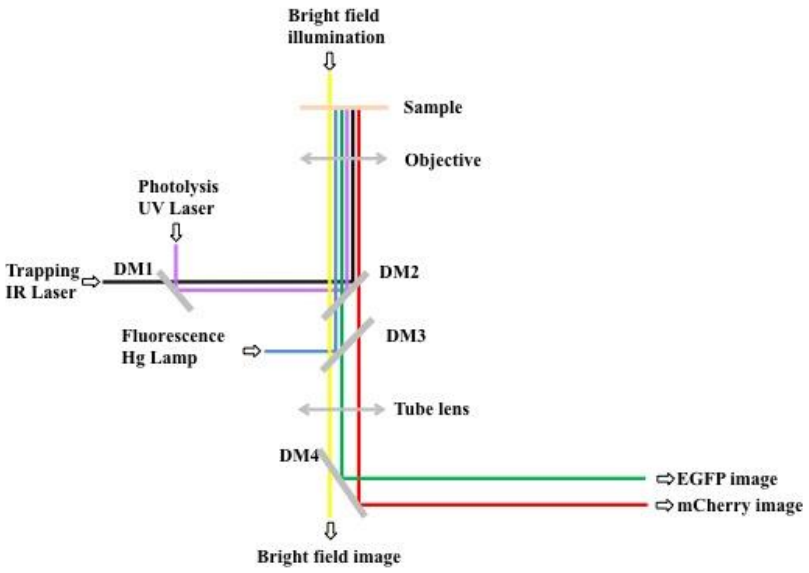

Figure 1: Schematic representation of the optical manipulation and FRET imaging setup. The InfraRed (IR) laser used for trapping micro-particles is aligned with the UltraViolet (UV) laser used for photolysis and then they are both directed into the objective pupil (60X, 1.2 NA). The sample is illuminated both by a white light source and a Hg fluorescence lamp. The light coming from the excited sample is then separated into the two emissions of the Donor and Acceptor fluorophores for

FRET imaging by the beam splitter (DM4, 585 LP) and directed onto the two halves of the camera sensor.

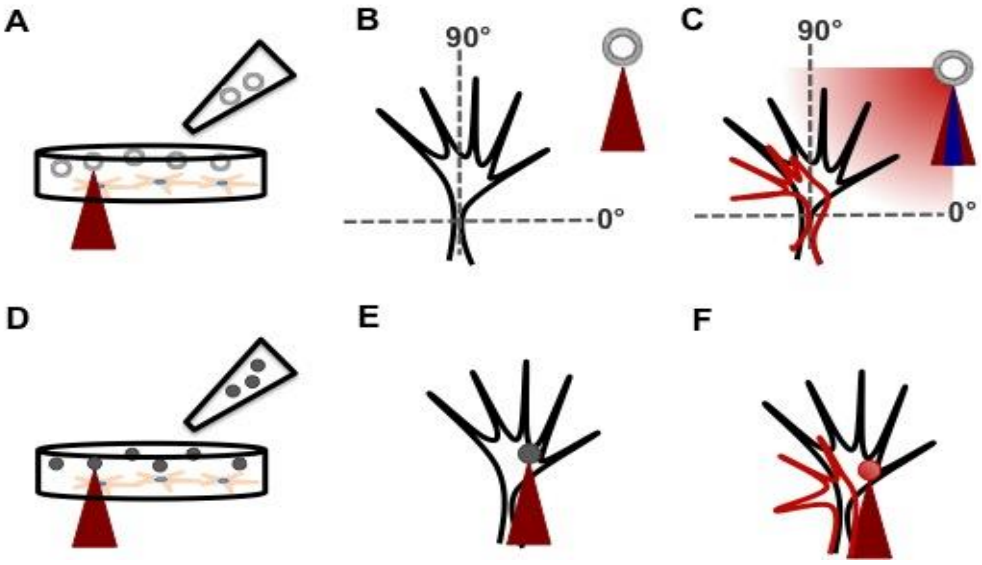

Figure 2: Schematic representation of the local stimulation protocols. (A) Pipette 5-8 µl of solution containing lipid vesicles into the imaging chamber, wait for them to sink and trap one of them by focusing the IR laser in the center of the vesicle. **(B)** Gently move the trapped lipid vesicle in the proximity (10-20 µm) of the cell compartment (growth cone in this case) to stimulate, with an angle between 0-90°. **(C)** Break the lipid vesicle to release its content and locally deliver the protein to the growth cone. In this case, a repulsive cue triggers collapse and retraction from the source. **(D)** Same as in (A), but pipette 5-8 µl of coated beads into the chamber. **(E)** Gently move the trapped bead over the cell compartment (central part of the growth cone in this case) to stimulate and leave it there for the chosen amount of time. **(F)** In this case, a repulsive cue mediates collapse and retraction of the stimulated region.

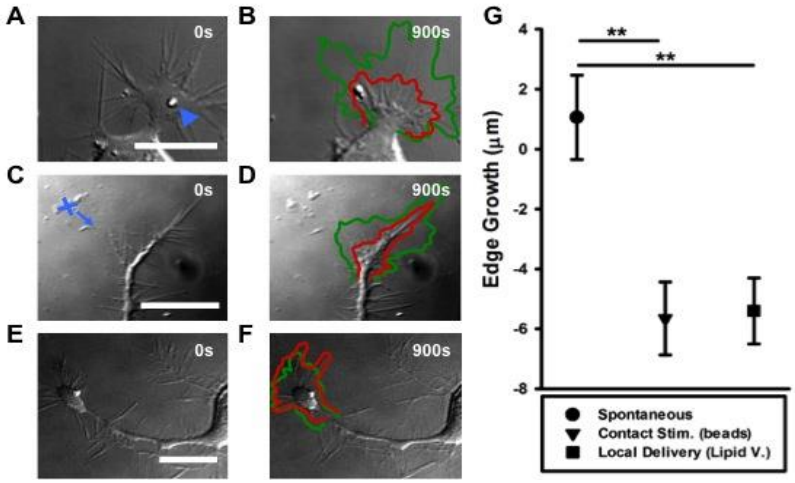

Figure 3: Representative results of a repulsive local stimulation experiment on NG108-15 cells. (A,B) DIC images of a cell undergoing spontaneous motion at 0s (A) and after 900s from the acquisition (B). The green line represents the initial profile (0s) and the red line represents the final profile (after 900s). **(C,D)** DIC images of a cell during local repulsive stimulation with Sema3A-coated beads (the blue arrowhead indicates the bead position). **(C)** Stimulated cell at the beginning of the stimulation. **(D)** Stimulated cell after 900s from the stimulation. The green line represents the initial profile (0s) and the red line represents the final profile (after 900s). **(E,F)** DIC images of a cell during local delivery of 1μM of Sema3A (the blue cross and arrow indicate the position of the lipid vesicle). **(E)** Stimulated cell at the breaking of the lipid vesicle. **(F)** Stimulated cell after 900s from the breaking. The green line represents the initial profile (0s) and the red line represents the final profile (after 900s). Scale Bars: 20 μm. **(G)** Plot of the mean edge growth of cells undergoing spontaneous motion (circle), and cells stimulated locally with a repulsive stimulus with beads (triangle) and lipid vesicles (square). There is a significant difference between the non-stimulated cells ((n=12) mean edge growth: 1.1±1.4 μm) and the cells stimulated with beads ((n=6) mean edge growth: -5.7±1.1 μm) and lipid vesicles ((n=12) mean edge growth: -5.4±1.0 μm).

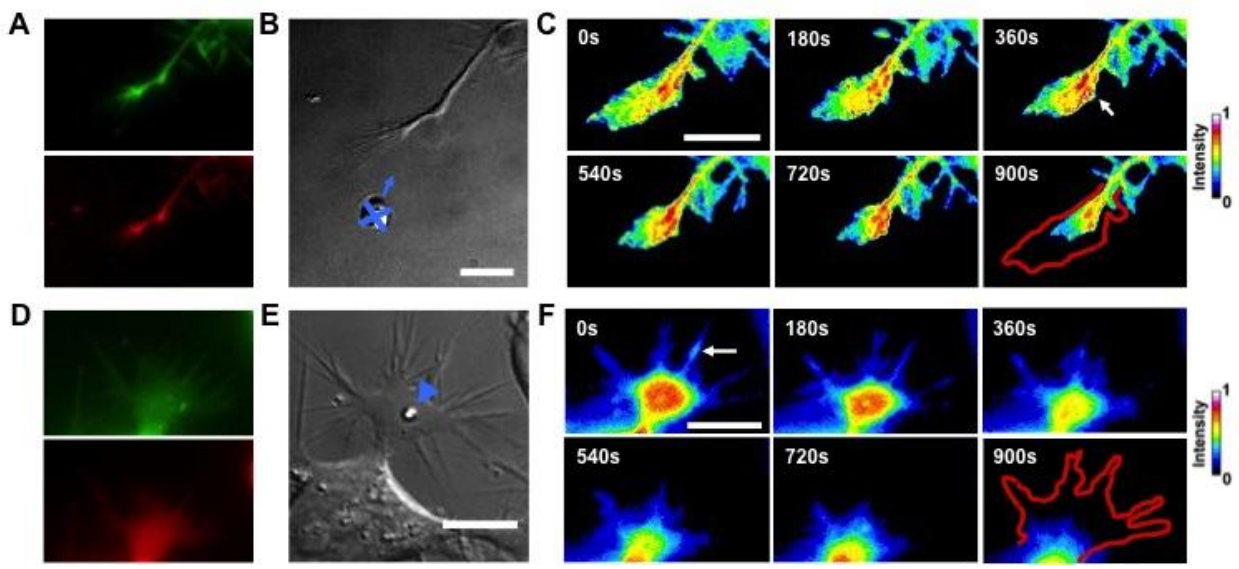

Figure 4: Representative results of FRET imaging of RhoA after local repulsive stimulation. (A) Example images of EGFP (green) and mCherry (red) fluorescence channels that are separated and corrected offilne to obtain the final ratiometric video (mCherry/EGFP). **(B)** DIC image of the growth cone undergoing local delivery of 1 μM Semaphorin-3A. The blue cross and arrow indicate the position of the lipid vesicle. **(C)** Ratiometric FRET live imaging of a representative cell transfected with RhoA inter-molecular probe. The insets show a time series (1 frame every 3 minutes) for 900s after the stimulation. The white arrow highlights the increase of FRET signal in the center of the

growth cone subsequent to its retraction. The red line shows the initial edge profile. The intensity scale on the right applies to all the images. **(D)** Same as in (A). **(E)** Same as in (B), but the cell is locally stimulated by a Semaphorin-3A-coated bead. The arrowhead indicates the position of the bead. **(F)** Raw FRET signal for a representative cell transfected with RhoA inter-molecular probe. The white arrow here indicates a peak of RhoA activity. Scale Bars: 20 µm.

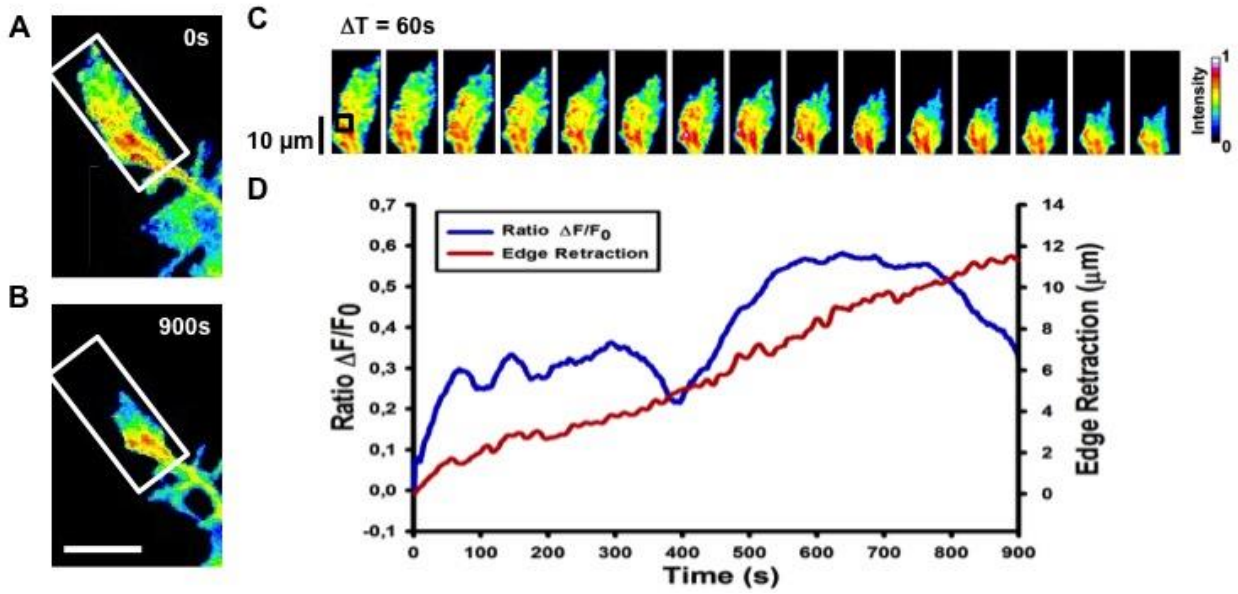

Figure 5: Further analysis of FRET ratiometric images. (A,B) Example FRET ratiometric images of the cell in Figure 4 (A), (B), (C) taken at 0s (A) and 900s (B) from the stimulation. The white box in both images refers to the area used in the image montage in (C). Scale Bar in (B) refers to (A) and (B): 20 µm**. (C)** Image montage of the region highlighted by the white box in (A) and (B). Images are taken every 60s. The intensity scale in (C) refers to (A), (B) and (C). **(D)** Plot of the RhoA activity (DF/F_0) in the edge region highlighted by the black square in (C) vs. edge retraction that shows the increase of RhoA activity as the growth cone retracts. FRET ratio is represented as a blue line: edge retraction is defined as a red line.

3

Acto-myosin contractility and membrane tension regulate growth cone-like actin waves morphology and dynamics.

Federico Iseppon, Simone Mortal, Luisa Maria Rosaria Napolitano and Vincent Torre

In preparation

Acto-myosin contractility and membrane tension regulate morphology and dynamics of growth cone-like actin waves

F Iseppon[1,*], S Mortal[1,*], LMR Napolitano[1], E D'Este[3], D Cojoc[2], V Torre[1]

[1] International School for Advanced Studies, Trieste 34126, Italy;

[2] Optical Manipulation Lab, IOM-CNR, Basovizza, Trieste 34149, Italy;

[3] Department of NanoBiophotonics, Max Planck Institute for Biophysical Chemistry, Göttingen, Germany

[*]These authors equally contributed to this work

To whom correspondence should be addressed: Vincent Torre; e-mail: torre@sissa.it.

Keywords: Actin Waves (AWs); Growth Cones (GCs); Myosin IIB; ß-cyclodextrin; RhoGTPases.

ABSTRACT

Actin Waves (AWs) are growth cone–like structures that emerge at the base of developing neurites and migrate up to the tip and contribute to growth cone (GC) dynamics. Using live-cell imaging, we have identified new dynamical properties of AWs: when AWs approach the distal neurite, GCs retract several microns fusing with the incoming AWs. Subsequently, following the arrival of the AW the GC advances. This "pulling" effect is abolished by addition of blebbistatin, an inhibitor of myosin II. Treatment with ß-cyclodextrin, a compound responsible for cholesterol extraction from the membrane and reducing the membrane tension of the neurite, abolishes the growth cone-like shape of AWs and influence their dynamicity. Inhibition of both Rac1 and Cdc42 decreased the waves' frequency and velocity affecting the dynamics of actin travelling waves along the neurite shaft as well. Taken together, our results suggest a major role of both myosin II and membrane cholesterol in the morphology and the dynamics of AWs and confirm an important role of the RhoGTPases in AWs inception and propagation along the neurite shaft.

INTRODUCTION

The actin cytoskeleton is a highly dynamical system that facilitates the transduction of mechanical signals and generates the intracellular forces required for many cellular functions like cell motility,

polarization, active cell shape control, neurite outgrowth and exocytosis (Madden and Snyder, 1998; Morales et al., 2000; Pollard and Borisy, 2003; Lowery and Van Vactor, 2009). A characteristic feature of all these processes is the dynamics and assembly of filamentous actin (F-actin) from its subunits (G-actin) that undergoes a constant and rapid reshaping of actin network. Actin filaments arise and grow through a complex and well-understood process (Devreotes and Horwitz, 2015) in which the Arp2/3 complex has a key role in nucleating actin branches that are seen in broad protrusions (Insall and Machesky, 2009). In cell migration, contraction forces generated by Myosin II motor proteins are needed mainly to promote retrograde movement of actin filaments away from the zone of active actin polymerization in the lamellipodium (Devreotes and Horwitz, 2015).

Different types of wave phenomena have been observed in the actin system of motile cells (Vicker, 2002; Gerisch et al., 2004; Weiner et al., 2007; Bretschneider T et al., 2009). Actin Waves (AWs) are growth cone–like structures that emerge at the base of neurites, migrating slowly up to the tip with a speed of ~2–3 μm/min, flaring the plasma membrane during transit and capable of changing directions (Fig. 1; Ruthel and Banker, 1998,1999; Flynn et al., 2009; Katsuno et al., 2015). They have been found more prevalent in early neurons compared to mature neurons and are present in cultured organotypic slices as well as primary hippocampal neurons (Flynn et al., 2009; Katsuno et al., 2015; Ruthel and Banker, 1998). Waves are critically dependent on actin dynamics, but are also disrupted by microtubule-depolymerizing agents (Ruthel and Banker,1998). Indeed, it has been proposed that they promote anterograde and kinesin-based transport driving neurite extension (Winans AM et al., 2016).

In previous works, signalling proteins such as the Rho family members of small GTPases (Rac, RhoA, and Cdc42) have been considered as putative Nucleation Promoting Factors (NPFs) (Holmes et al., 2012; Weiner OD, 2007) that modulate actin filament nucleation. The Rho GTPases act as molecular switches to control signal transduction pathways by cycling between a GDP-bound, inactive form, and a GTP- bound, active form (Raftopoulou and Hall, 2004). They act on a number of effectors that regulate cytoskeleton machinery: Rac and Cdc42 regulate actin polymerization via Arp2/3; RhoA activates ROCK leading to Myosin II stimulation (Ridley 2006, 2011; Heasman and Ridley, 2008). Machacek et al (Machacek et al, 2009) provided quantitative evidence for the correlation of Cdc42, Rac1, and RhoA wave dynamics with F-actin mediated edge protrusion and in (Wu M et al., 2013), waves of Cdc42 were shown to be correlated in both space and time with waves of F-actin.

Here, we use live-cell imaging to investigate the dynamic of AWs and of AWs constituent proteins in hippocampal neurons and provide evidence for a direct role of the actomyosin complex in the AWs' generation. Our results show that as an AW approaches the distal neurite, the growth cone retracts several microns to fuse with the wave and advances following the AW arrival. Furthermore, when we treated cells with either Blebbistatin, a cell permeant inhibitor of myosin II (Kovàcs et al., 2004), or ß-Cyclodextrin, a drug that reduces the cholesterol concentration in biological membrane

(Vladislav I et al., 2013), the AWs lose their characteristic growth-cone like shape and the “pulling effect” is completely abolished, suggesting that both myosin II and membrane surface tension have a major role in the travelling of AWs along the neurite shaft. We also investigated the cross-talk between AWs and RhoGTPases and our data support the idea that cytoskeletal dynamics and Rac1/Cdc42 activities are tightly coupled at sub-cellular levels.

RESULTS

The dynamic of Actin Waves (AWs)

We performed long-term live cell imaging of AWs on rat hippocampal cells using mCherry-LifeAct that selectively labels F-actin (Riedl et al., 2008). Individual neurons were imaged at 10 s intervals for 10 hours to have a complete picture of the wave phenomena. Consistent with previous studies (Ruthel and Baker, 1998; Flynn et al., 2009; Katsuno et al., 2015; Winans et al., 2016), the AWs exhibit a growth-cone like morphology and behavior forming filopodia and lamellipodia on one or both sides of the neurite shaft and travel mainly in an anterograde fashion in our DIV2 imaging window (Figure 1A). They are generated at a median frequency of 2-3 AWs per hour and move at an average speed of 2-3 μm/min. An analysis of edge dynamics highlighted that, when an AW approaches the distal neurite, the GC retracts several microns so to approach the incoming AW, then fuses with it and advances following the AW arrival (Figure 1B-1C). The continuous AW arrival generates retraction/growth cycles that do not result in a net neurite elongation in our culture conditions, although it increases its size and dynamicity (Figure 1C, Figure S1).

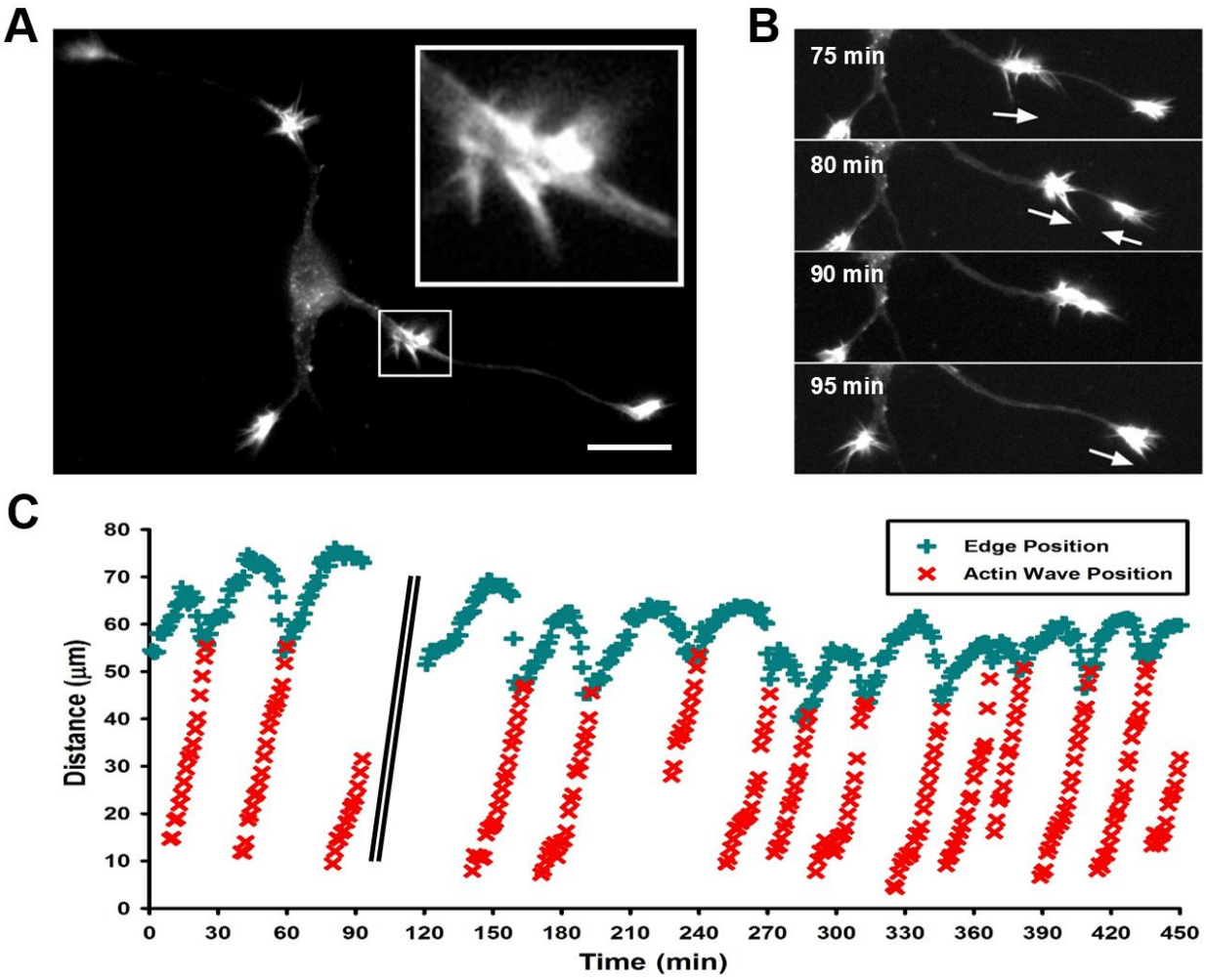

Figure 1: AWs dynamics. (A) Fluorescence image of F-actin showing a wave advancing down a neurite with its characteristic growth-cone like shape (white square). The insert shows a higher magnification of the growth-cone like AW. (**B)** Time-lapse images of the F-actin expressing primary hippocampal neurite showed in A). When an AW approaches the distal neurite, the growth cone retracts several microns to reach the wave, then fuses with it and advances following the wave arrival. White arrows indicate AW direction. Images were taken every 10 s. Scale bar refers to (A) and (B)= 20µm. (**C)** Plot showing the progression of several AWs (red) along the neurite shaft of the cell in (A). The edge trace (light blue) shows the retraction of the GC at the arrival of the AW. The mean velocity of AWs is 2,2 ± 0,4 µm/min.

The role of myosin and membrane tension

Myosin IIA and IIB are the most prominent type II myosin molecules expressed in migrating neurons within the CNS (Golomb et al., 2004): myosin IIB is required for maintaining normal growth cone shape and traction force, polarization size, and actin organization (Bridgman et al., 2001). We therefore employed two-colour STED nanoscopy (Gottfert et al., 2013) to verify whether and where myosin IIB is present in AWs (Figure 2) with a sub-diffraction resolution. All three colour channels (see Materials and Methods) were bright and well resolved, with the respective structures identified unequivocally (Figure 2). Actin and myosin IIB images were acquired via STED nanoscopy, whereas β-III tubulin image was collected by confocal microscopy (Figure 2A). Previous reports have localized myosin II mainly to the T zone and the C domain of the GC and in the contractile node region

(Burnette et al., 2008; Loudon et al., 2006; Rochlin et al., 1995). A comparison between STED images of an AW and of a GC on the same neurite showed that myosin IIB appeared as fluorescent spots localized in the transition and central regions of the GC, with a semi-circular organization corresponding to contractile acto-myosin arcs. A similar localization was found in AWs, where myosin IIB is mostly present at the sides of the neurite shaft from where erupt the lamellipodia and filopodia forming the wave (Figure 2B-2C). We also observed spots of myosin IIB along actin bundles in the thicker filopodia structures. A line-scan analysis of Myosin IIB fluorescence intensity over distance highlighted that myosin IIB is prominent at the rear of all the proceeding actin waves suggesting that its activity strongly correlates with actin wave organization and dynamics (Figure 2D).

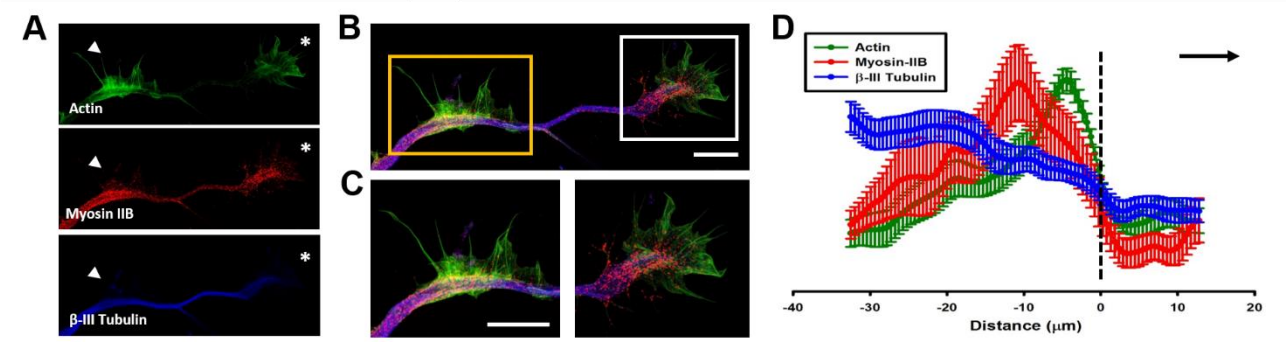

Figure 2: STED microscopy reveals Myosin IIB in AWs. (A) Representative single-channel STED images of rat hippocampal neurons at 1 DIV stained with actin (phalloidin), non-muscle myosin IIB and ß-III tubulin show the presence of myosin IIB in the growth-cone like waves. Scalebars in (A) and (B) = 10µm. White arrowheads indicate the AW; white asterisks indicate the GC. (**B)** A comparison between the actin growth-cone like wave (yellow square) and the growth-cone itself (white square) highlighting that in both cases myosin IIB is brightest in the central regions of the cone and in the rear region of the AW. Myosin IIB can be also seen more peripherally along actin bundles in filopodia. (**C)** Averaged line scans (see Methods) show that myosin IIB is highly concentrated at the rear of advancing actin wave. Dashed line indicates AW front, and black arrow highlights wave direction. N=16 neurites. Measurements are taken from STED images. All traces were normalized by mean intensity and smoothed before averaging (Winans et al., 2016). Data are shown as Mean ± SEM

To test this hypothesis, we treated our DIV2 hippocampal cultures with the cell permeant inhibitor blebbistatin, which inhibits the ATP activity of the A and B isoforms of non-muscle myosin II (Kovàcs et al., 2004). Blebbistatin treatment (20µM) abolished the growth-cone like shape of the AWs without affecting their area, indicating a rearrangement of the actin assembly after myosin inhibition (Figure 3B, 3F). Live-cell imaging experiments highlighted also the disappearing of the GC retraction preceding the wave arrival, together with a significant increase of neurons outgrowth 30 min after blebbistatin addition (Figure 3C). Finally, consistent with the data of Flynn et al. (2009) and Katsuno et al. (2015), blebbistatin increased significantly the frequency of wave appearance and, at the same time, reduced AWs velocity (Figures 3D, 3E). Taken as a whole, these data suggest a strong

involvement of myosin II in both structural and dynamical organization of AWs. Further analysis of the dynamicity of AWs showed that blebbistatin treatment affects both the velocity and the frequency of the AWs: the former decreases by about 20%, whereas the latter increases by about 10%.

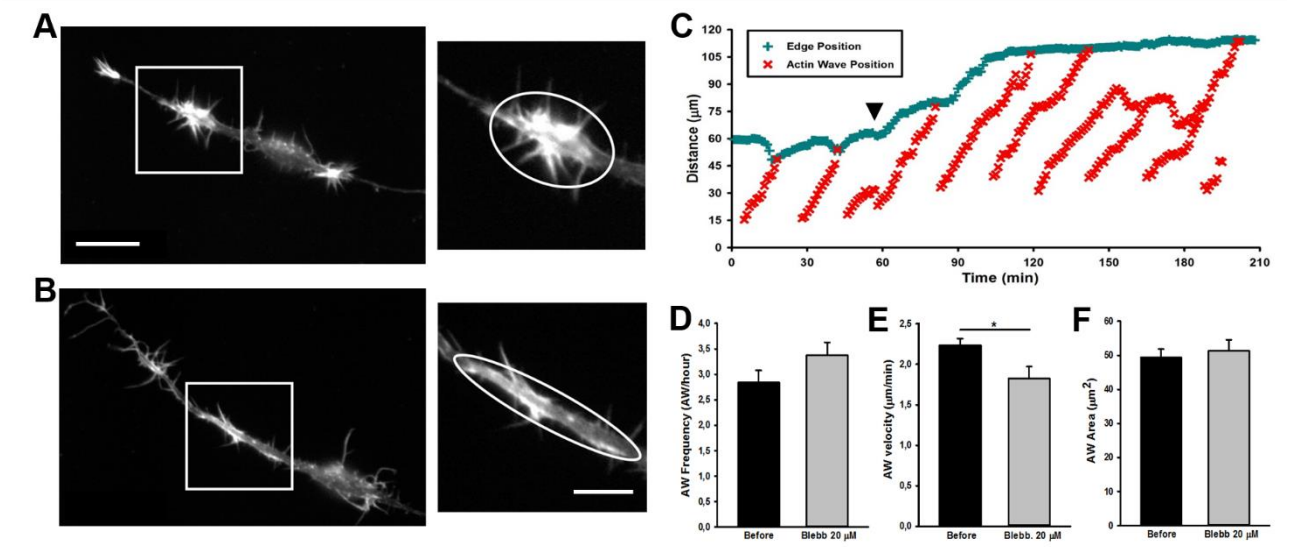

Figure 3. Blebbistatin treatment abolishes growth-cone like actin waves. (A, B) Live-cell images of a growth cone-like AW before **(A)** and after **(B)** Blebbistatin treatment (20µM). Insets on the right represent a magnified view of the AWs showed in (A) and (B). Blebbistatin treatment changes dramatically the morphology of the wave that loses the characteristic growth-cone shape. Scale bar in (A): 20 µm. Scalebar in (B) = 10 µm (**C)** Plot highlighting the progression of the AWs (red) showed in (A) and (B) along the neurite. The black arrowhead indicates blebbistatin addition: myosin II inhibition abolishes the average retraction distance. The edge trace (light blue) highlights the disappearing of the GC retraction upon the AW arrival after the Blebbistatin treatment. **(D)** Quantification of the AWs frequency calculated on neurons treated with or without blebbistatin for 4 hours and imaged like in (A) and (B). N = 4 neurites **(E)** Quantification of the AWs velocity (µm/min) calculated on neurons treated with or without blebbistatin for 4 hours and imaged like in (A) and (B). N = 18 AWs. (**F)** Quantification of the AWs mean area (μm^2) calculated on neurons treated with or without blebbistatin for 4 hours and imaged like in (A) and (B). N= 18 AWs. Student's and U-Man Whitney tests were performed for histograms: *P<0.05.

As inhibition of myosin II alters the shape of AW, the surface tension of the membrane surrounding the wave could have a role in its dynamics. A high cholesterol concentration increases the membrane tension and therefore its reduction has been demonstrated to reduce the stiffness of the cellular membrane enveloping the actin filament network (Amin L et al., 2012). To further verify the effect of the cholesterol depletion in the AWs dynamic, we treated the hippocampal neurons with the ß-cyclodextrin that has been reported to be the most efficient compound in extracting cholesterol from membranes (Vladislav I et al., 2013). Live-cell imaging showed a loss of the growth-cone like shape of the AW after adding the ß-cyclodextrin compound (Figures 4A, 4B) and a significant reduction of the AWs area of about 60% (Figure 4F). Further analysis highlighted that ß-cyclodextrin addition affects also AW dynamics: both velocity and frequency of AWs decreased after the treatment, of about 10% and 50% respectively (Figure 4D, 4E). These results clearly indicate that membrane has

a strong role in AWs structure and dynamicity, especially in in F-actin polimerization required for AWs initiation.

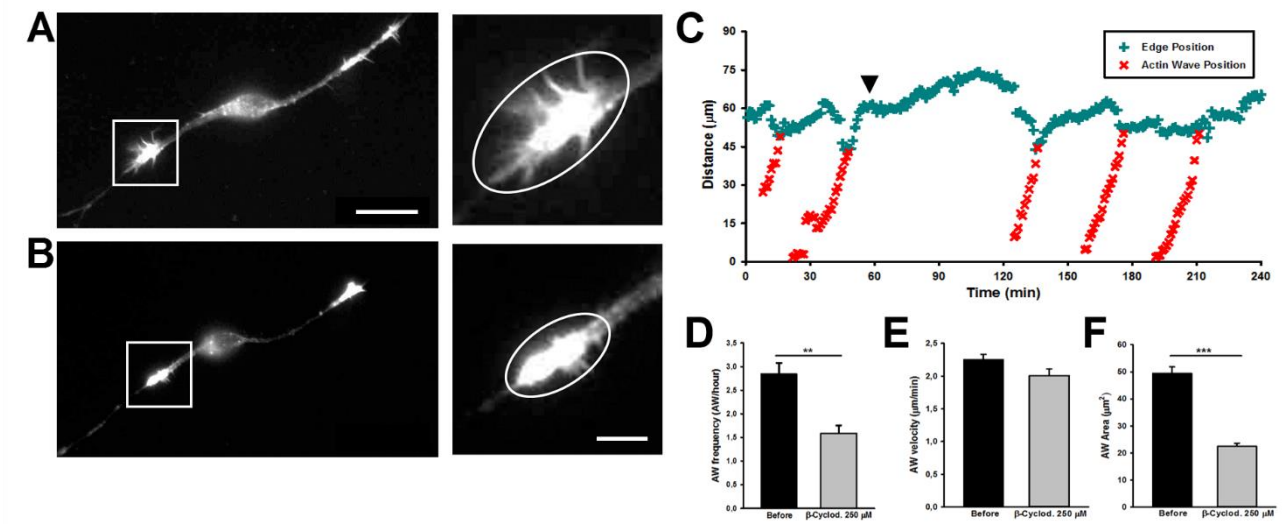

Figure 4. ß-cyclodextrin treatment affects AWs structure. (A, B) Live-cell images of a growth cone-like AW before **(A)** and after **(B)** ß-cyclodextrin treatment (250 µM). On the right, magnified views of the AWs showed in (A) and (B) before and after ß-cyclodextrin treatment that abolishes completely the growth-cone like shape. Scale bar in (A): 20 µm. Scalebar in (B) = 5 µm **(C).** Plot highlighting the progression of the AWs (red) showed in (A) and (B) along the neurite. The black arrowhead indicates ß-cyclodextrin addition. The edge trace (light blue) highlights that the GC retraction upon AW arrival seems unaffected. **(D)** Quantification of the AWs frequency calculated on neurons treated with or without ß-cyclodextrin for 4 hours and imaged like in (A) and (B). N = 4 neurites. **(E)** Quantification of the AWs velocity (µm/min) calculated on neurons treated with or without ß-cyclodextrin for 4 hours and imaged like in (A) and (B). N = 16 AWs. (**F)** Quantification of the AWs mean area (μm^2) calculated on neurons treated with or without ß-cyclodextrin for 4 hours and imaged like in (A) and (B). N = 16 AWs. Student's and U-Man Whitney tests were performed for histograms: *P<0.05.

The role of small Rho-GTPases

In order to evaluate the role of small RhoGTPases in the AWs, we used Cdc42 and Rac1 selective guanine nucleotide binding inhibitors (ML141 and EHT1864, respectively) to provide a reversible and non-competitive inhibition (Shutes A et al., 2007; Surviladze Z et al., 2010). DIV2 hippocampal neurons incubated with or without ML141 (10µM) were imaged at a 10 s time resolution (Figures 5A, 5B). We first sought to determine if Cdc42 inhibition changed growth cone-like shape of AWs affecting their dynamic. Live cell imaging experiments (Figure 5B) together with a measure of the Actin Wave Area (Figure 5F) revealed that Cdc42 inhibition decreased AWs size of 40% that appeared also less dynamic. As already observed after Blebbistatin treatment, ML141 addition led to an increase of neurite outgrowth suggesting a role for Cdc42 in controlling AWs merging with GC and neurite outgrowth (Figure 5C).

We then determined the frequency of the AWs calculating the numbers of complete waves (i.e waves able to reach the tip of the growth cone) in an hour. In control neurons, growth-cone like structures travelling from the base of the neurite to the tip were clearly visible with a frequency of almost 2 waves for hour (Figure 5D). Instead, neurons exposed to 10 µM of ML141 showed a 75% decrease

of the AWs frequency (Figure 5C,5D) 50 minutes after drug addition. When we added ML141 at 30 μM, we observed an almost complete depletion of the wave phenomena (Supplementary Figure S2). Furthermore, to evaluate the neurite dynamicity, we measured the velocity of the AWs, calculated as the time taken by the wave to reach the tip of the growth cone, normalized for the length of the axon (Tilve S, 2015). Neurons exposed to 10 μM of ML141 showed a 25% decrease in the velocity of AWs (Figure 5D).

A recent report has demonstrated that Rac1 activity is sufficient to generate an AW (Winans et al., 2016). As already showed for Cdc42 inhibition, the addition of EHT1864 at 10 μM caused Rac1 inhibition with a completely lost of the growth-cone like shape (Figure 6B) and a significant reduction of the Actin Wave Area (Figure 6F). Moreover, a reduction of 75% in AWs frequency (Figure 6D) together with a 50% decrease in the AWs velocity (Figure 6E) assessed an important role for Rac1 in modulating positively the actin polymerization required for the AWs generation.

Taken together these data support the hypothesis that Cdc42 and Rac1 have an important role in the AW architecture and dynamics and suggest a strongest role of Cdc42 in AW inception and of Rac1 in AW travelling.

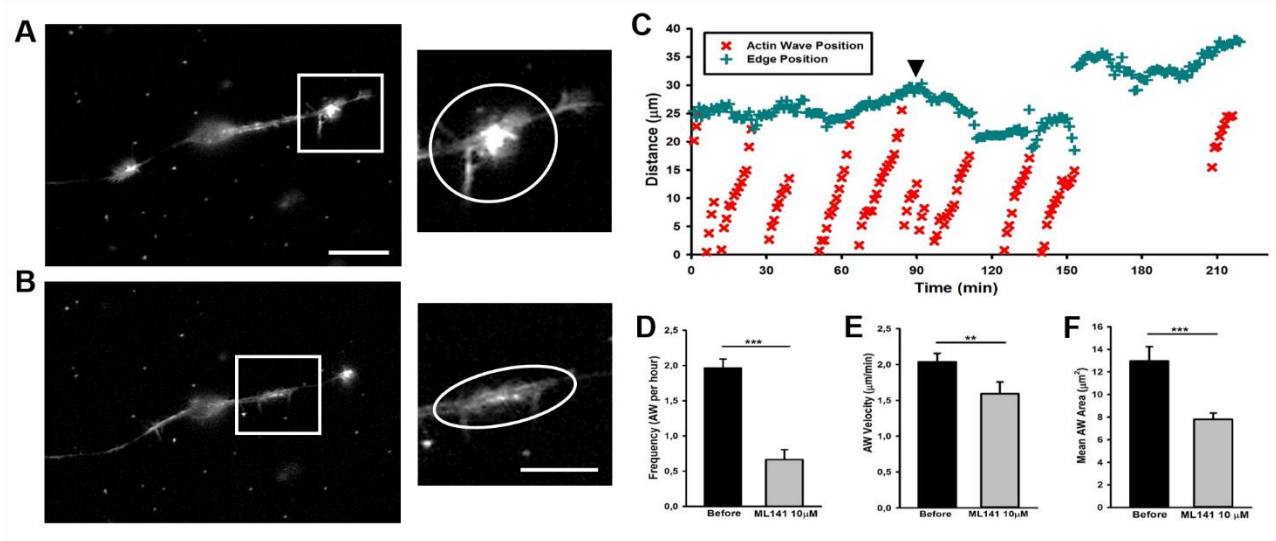

Figure 5. Cdc42 inhibition affects AW dynamicity. (A, B) Live cell imaging of DIV2 rat hippocampal neurons before (A) and after (B) addition of ML141 (10μM). White boxes indicate the growth-cone like AW. On the right, magnified views of the AW showed in (A) and (B) before and after ML141 treatment. Scale bar in (A): 20 μm. Scalebar in (B) = 10 μm. **(C)** Plot showing the progression of several AWs (red) along the neurite shaft. The edge trace (light blue) highlights a transient increase in neurite elongation after the ML141 treatment. Black arrowhead indicates ML141 addition. **(D)** Quantification of the AWs frequency calculated on neurons treated with or without ML141for 4 hours and imaged like in (A) and (B). N=10 neurites. **(E)** Quantification of the AWs velocity (μm/min) calculated on neurons treated with or without ML141for 4 hours and imaged like in (A) and (B). N=14 AWs. **(F)** Quantification of the AWs mean area (μm^2) calculated on neurons treated with or without ML141for 4 hours and imaged like in (A) and (B). N= 9AWs. Student's test was performed for all histograms: **P<0.01;***P<0.001.

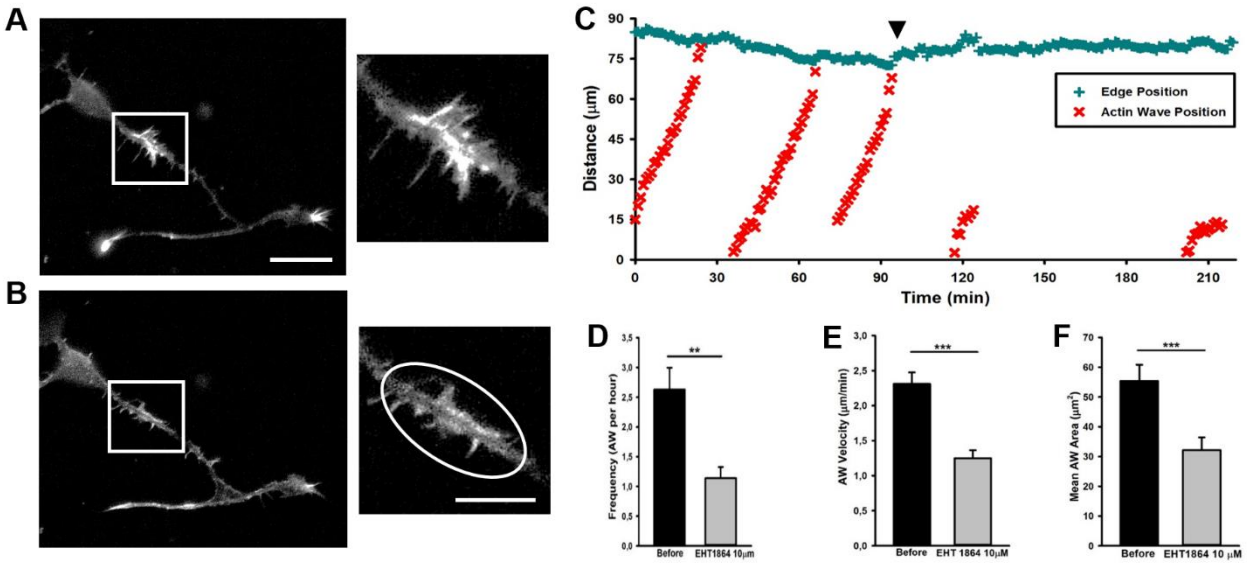

Figure 6. Rac1 inhibition affects actin wave propagation. (A, B) Live cell imaging of DIV2 rat hippocampal neurons before (A) and after (B) addition of EHT1864 (10µM). White boxes indicate the growth-cone like AW. On the right, magnified views of the AW showed in (A) and (B) before and after EHT1864 treatment. Scale bar in (A): 20 µm. Scalebar in (B) = 10 µm. **(C)** Plot showing the progression of several AWs (red) along the neurite shaft. The edge trace (light blue) highlights a stabilization of neurite length, concurrent with AWs propagation defects after EHT1864 treatment. Black arrowhead indicates EHT1864 addition. **(D)** Quantification of the AWs frequency calculated on neurons treated with or without EHT1864 for 4 hours and imaged like in (A) and (B). N=10 neurites. **(E)** Quantification of the AWs velocity (µm/min) calculated on neurons treated with or without EHT1864 for 4 hours and imaged like in (A) and (B). N=10 AWs. (**F)** Quantification of the AWs mean area (μm^2) calculated on neurons treated with or without EHT1864 for 4 hours and imaged like in (A) and (B). N= 10 AWs. Student's test was performed for all histograms: **P<0.01;***P<0.001.

DISCUSSION

In this study we have analysed the dynamics of AWs and AW constituent proteins to unravel the mechanism of wave inception and propagation. Using live cell imaging and STED, we have characterized their growth-cone like morphology and motility and we provide evidence that myosin II, membrane tension, as well as small RhoGTPases act as critical components of AW dynamics. Our study suggests the existence of a cross-talk between actin cytoskeleton and its upstream regulators such as RhoGTPases, the motor protein myosin and the cellular membrane integrity. These interactions are necessary to translocate the actin and associated proteins along the neurite. The waves investigated herein are generated at a frequency of 1-2 waves per hour, propagate with an average speed of ~2–3 µm/min and travel from the base of the neurites to the growth cone. They resemble the GC in size and appearance and present a mix of lamellipodia and filopodia structures that project outward from the neurite shaft, characteristic of the GCs. STED nanoscopy revealed the AWs ultrastructure with a sub-diffraction resolution. As in the GC, the F-actin is present in filopodia

(bundled F-actin) and lamellipodia (meshwork of F-actin) with spots of Myosin IIB along thicker filament bundles and in lamellipodia, where they appeared diffusely distributed. Moreover, myosin IIB appeared concentrated in the region close to the neurite shaft: in GCsthis pattern is critical to form the contractile arcs, and in AWs it may have a similar function. An averaged line scan analysis of STED images highlighted an enrichment of Myosin IIB at the rear and inside the wave with Tubulin behind it (Figure 2) suggesting a role for Myosin IIB in the morphological dynamic remodelling of the actin cytoskeleton. Furthermore, live cell imaging data showed that as an AW approaches the distal neurite, the growth cone retracts several microns to fuse with the incoming wave and advances following the AW arrival. After the treatment with Blebbistatin, retrograde flow is completely abolished with a significant neurite outgrowth (Figure 3). These findings strongly suggest that Myosin IIB activity normally regulates the rate of retrograde flow that pulls the neurite backward: its absence triggers a strong increase in actin-bundle length. This observation is consistent with the data of Medeiros and co-workers who hypotesized that the “push” of actin assembly and the “pull” of myosin combine to drive retrograde flow (Medeiros et al., 2006). Based on this scenario the AWs described herein could have a role in the maintenance of a dynamic equilibrium between all the growing neurites that is more like a competition, with large fluctuations in search for signals that would define the “winning” process that will became the axon. Indeed, the AWs bear more impact, in terms of growth promotion, to the maturating axon and their frequency is elevated in the axonal process after the polarization (Flynn et al., 2009; Katsuno et al., 2015). It is worth noticing that Blebbistatin leads to a complete destruction of the GC instead the AWs lose in part their actin-wave shape (i.e. no significant change in the GC area in observed before and after the blebbistatin treatment), while AW velocity and frequency are affected underlying differences in the intracellular machinery organization.

Actin has long been known to be associated with membranes and there have been a number of theoretical studies that focus on the interrelationships between the protrusive forces generated by actin polymerization and the dynamics of the membrane-bound activators. Indeed, F-actin network assembly, organization and dynamics are controlled by the spatial and temporal regulation of the activity of actin-binding proteins that are associated with the membrane in a multifaceted way (Bezanilla et al., 2015). To explore the influence of the membrane on the AWs’ dynamic, we treated our DIV2 hippocampal cells with ß-cyclodextrin, responsible for the depletion of cholesterol from the membrane (Amin L et al. 2012). Consistent with a role of the membrane in the AWs’ structure, the elimination of cholesterol slows down AWs’ area and causes a loss of the growth-cone shape. Interestingly, ß-cyclodextrin affects not only the morphology, but also the dynamics of wave phenomena: both frequency and velocity of AWs decreased after ß-cyclodextrin addition, suggesting a role for the membrane that goes beyond AW shape maintenance. Our data seem to suggest that the membrane may be important for the correct localization of actin filaments and actin-associated proteins in the propagating AWs, and any perturbation affects the dynamics of the signalling

pathways involved in F-Actin polymerization/depolymerisation. The same morphological effect was observed when selective inhibitors of the RhoGTPases Rac1 and Cdc42 were added to the cellular medium. Indeed, the Rho-family GTPases represent a key node for connecting extracellular signals to regulated actin dynamics and, by stimulating actin dynamics, they induce plasma membrane protrusion like lamellipodia and filopodia (Burridge and Wennerberg, 2004; Hall and Nobes, 2000). Recently Winans and co-authors demonstrated that Cdc42 exhibited a higher activity in front of an AW and that Rac1 activity is sufficient to initiate AWs (Winans et al., 2016). We observed that Cdc42 inhibition induced a burst in the neurite outgrowth suggesting that it could contribute to the actomyosin contractility required for modulation of the neurite outgrowth (Wilkinson et al., 2005). Moreover, we found that the frequency and the velocity of the AWs, used as parameters of neurite dynamicity, were decreased in the presence of both the RhoGTPases inhibitors. This significant decrease in AW initiation capacity and propagation kinetics can be explained with a putative role of these two RhoGTPases in the regulation of both actin polymerization and assembly through the Arp2/3 complex or formins and adhesions strength through an increase in shootin-1 phosphorylation that has been shown to mediate the linkage between F-actin retrograde flow and cell adhesion in GCs (Kubo et al., 2015). A cascade downstream of Cdc42, Rac and subsequently PAK1 can be accounted responsible to modulation of the balance between adhesion strength and myosin mediated retrograde flow in maintaining anterograde stable unidirectional motion. Taken together these results seem to indicate that Cdc42 and Rac1 could promote AWs migration toward the leading edge and could be involved in the assembly and disassembly of F-actin network.

Our study provides evidence for a holistic picture of the AW phenomena by demonstrating that AW dynamic is a consequence not only of the actin polymerization dynamics, but also of the interplay between the membrane itself, the activators that reside on it like the RhoGTPase proteins and the contractility of the motor protein myosin II. In conjugation with previous studies, our results argue that a combination of F-actin polimerization and F-actin retrograde flow, both “orchestrated” by multiple cytoskeletal and membrane effectors, play a crucial role in the mechanism that allows the neurite to explore the surrounding space. The data presented here underscore the importance of analyzing the organization and dynamics of the AWs into a holistic picture that takes into account the membrane-actin system.

MATHERIALS AND METHODS

DNA constructs

mCherry-Lifeact-7 was a gift from Micheal Davidson (Addgene plasmid #54491) and was verified by full-length sequencing.

Primary culture and hippocampal neurons transfection

Hippocampal neurons from Wistar rats (P2-P3) were prepared in accordance with the guidelines of the Italian Animal Welfare Act, and their use was approved by the Local Veterinary Service, the SISSA Ethics Committee board and the National Ministry of Health (Permit Number: 2848-III/15) in accordance with the European Union guidelines for animal care (d.1.116/92; 86/609/C.E.). The animals were anaesthetized with CO_2 and sacrificed by decapitation, and all efforts were made to minimize suffering. The coverslips were coated with 50µg/ml poly-L-ornithine (Sigma-Aldrich, St. Louis, MO, USA) overnight and with Matrigel just before cells seeding (Corning, Tewksbury MA, USA). Dissociated cells were plated at a concentration of 4×10^4 cells/ml in minimum essential medium (MEM) with GlutaMAX$_{TM}$ supplemented with 10% foetal bovine serum (FBS, all from Invitrogen, Life Technologies, Gaithersburg, MD, USA), 0.6% D-glucose, 15mM Hepes, 0.1mg/ml apo-transferrin, 30µg/ml insulin, 0.1µg/ml D-biotin, 1 µM vitamin B12 (all from Sigma-Aldrich), and 2.5 µg/ml gentamycin (Invitrogen). The neuronal cultures were maintained in an incubator at 37°C, 5% CO_2 and 95% relative humidity. Hippocampal neurons were transfected 24h later with the LifeAct plasmid using Lipofectamine 3000® reagent (Invitrogen) following the manufacturer's protocol and imaged 1 day after transfection.

Drug Application

Blebbistatin and ß-cyclodextrin were used at a final concentration of 20 µM and 250 µM respectively. ML141 (TOCRIS bioscience) was used at a final concentration of 10µM for low concentration and 30µM for high concentration experiments; EHT1864 (TOCRIS) was used at a final concentration of 10µM concentration.

STED

Cells were washed with PBS and fixed in 4% PFA and 0.25% Glutaraldehyde in PHEM buffer (60 mM PIPES, 25 mM HEPES, 10 mM EGTA, 2 mM $MgCl_2$, pH 6.9) for 20 min at room temperature, quenched with ammonium chloride and glycine (100 mM each) for 5 min, permeabilized with 0.1% Triton X-100 for another 5 min and blocked in PBS supplemented with 1% BSA for 30 min. Primary antibodies against β-III Tubulin (Abcam, cat. ab7759), Myosin-IIB (Sigma, cat. M 7939) and actin (Phalloidin) were incubated in PBS for 1 hour or overnight at 4 °C. Secondary antibodies (sheep anti-mouse, Dianova, cat. 515-005-003; goat-anti-rabbit, Dianova, cat. 111-005-003) were labeled with STAR580 (Abberior, cat. 1-0101-005-2), or Atto490LS (Attotech, cat. AD 490LS-31). Phalloidin was coupled to STAR635 (Abberior, cat. 2-0205-002-5). Both secondary antibody, and phalloidin incubations were performed in PBS for 1 hour at room temperature or overnight at 4 °C. Samples were then mounted in Mowiol supplemented with DABCO. Imaging was performed on a two-color Abberior STED 775 QUAD scanning microscope (Abberior Instruments GmbH, Göttingen, Germany)

equipped with 488 nm, 561 nm, and 640 nm pulsed excitation lasers, a pulsed 775 nm STED laser, and a 100x oil immersion objective lens (NA 1.4).

Live Cell Imaging

Live imaging experiments were performed on an epi-fluorescence microscope (Olympus IX-83, Olympus) equipped with LED illumination (λ = 590 nm, Thorlabs). During all imaging cells were kept at 37°C, 5,0% CO_2, 95% humidity by using an imaging chamber incubator (Okolab). Time-lapse images were taken every 10s with 1s exposure up to 10 hours using a 40X oil immersion objective (Olympus, NA=1.3), and all acquisitions were done with a CCD sensor at 12bit depth (ORCA-D2, Hamamatsu). All inhibitors used were added after about 60-90 minutes imaging, and the acquisition continued for at least 90 minutes after addition at the conditions previously stated.

Image Analysis

Image analysis was performed using ImageJ software (NIH) and custom-build MATLAB codes (Mathworks).

Morphological analysis of actin waves and growth cones

For the morphological analysis of the AW, the area was determined manually at different time-points of the wave progression along the neuritis, both before and after the drug addition. The mean AW area throughout the neuritis was then obtained by averaging the areas previously collected. For the morphological analysis of the GCs, the area was determined manually at different time-points of the wave progression and also every minute for about 5-10 minutes after the arrival and fusion of the AW with the growth cone. The mean GC areas were then obtained by averaging the areas previously calculated.

Intensity Line Scans

Line scans were performed with ImageJ software. Images were background subtracted and thresholded to select the neurite of interest, and then a line was traced in the neurite to have an intensity profile trace. Traces were then aligned to the half-maximum value of the front of the actin wave (oriented towards the growth cone). Half maximum values were determined by manual identification of the maximum actin signal on the front half of the actin curve. Traces were then computationally aligned using a custom-built Matlab software.

Analysis of the actin wave position along the neuritis, velocity and frequency.

The analysis of the AW position was performed using a custom-built MATLAB code. Time-lapse sequences were background corrected and thresholded to select the neurite of interest. The position of the soma and of the end of the neurite was tracked automatically, whereas the AW position along

the neurite was tracked manually. The distances calculated from the soma were then extrapolated and plotted as a function of time. The time-points when no wave is travelling along the neurite were eliminated. The velocity of the AW was calculated by extracting the distance travelled and the time taken from the position data previously described and dividing distance over time. The frequency of AW was calculated as AW per hour by manually counting all the AW events before and after the drug addition.

Statistical Analysis

All results have been obtained from at least three independent experiments and expressed as the mean ± S.E.M. Experimental data were analysed by Paired t-test or U-Mann Whitney test using SigmaPlot 10.0 software (Systat Software Inc.). Differences among samples were considered statistically significant when $p < 0.05$.

REFERENCES

1. Amin, L., Ercolini, E., Shahapure, R., Migliorini, E. & Torre, V. The role of membrane stiffness and actin turnover on the force exerted by DRG lamellipodia. *Biophys. J.* **102,** 2451–2460 (2012).
2. Bezanilla, M., Gladfelter, A. S., Kovar, D. R. & Lee, W.-L. Cytoskeletal dynamics: a view from the membrane. *J. Cell Biol.* **209,** 329–337 (2015).
3. Bretschneider, T. *et al.* The three-dimensional dynamics of actin waves, a model of cytoskeletal self-organization. *Biophys. J.* **96,**2888–2900 (2009).
4. Bridgman, P. C., Dave, S., Asnes, C. F., Tullio, A. N. & Adelstein, R. S. Myosin IIB is required for growth cone motility. *J. Neurosci.* **21,**6159–6169 (2001).
5. Burnette, D. T. *et al.* Myosin II activity facilitates microtubule bundling in the neuronal growth cone neck. *Dev. Cell* **15,** 163–169 (2008).
6. Burridge, K. & Wennerberg, K. Rho and Rac take center stage. *Cell* **116,** 167–179 (2004).
7. Devreotes, P. & Horwitz, A. R. Signaling networks that regulate cell migration. *Cold Spring Harb Perspect Biol* **7,** a005959 (2015).
8. Flynn, K. C., Pak, C. W., Shaw, A. E., Bradke, F. & Bamburg, J. R. Growth cone-like waves transport actin and promote axonogenesis and neurite branching. *Dev Neurobiol* **69,** 761–779 (2009).
9. Gerisch, G. *et al.* Mobile actin clusters and traveling waves in cells recovering from actin depolymerization. *Biophys. J.* **87,** 3493–3503 (2004).

10. Golomb, E. *et al.* Identification and characterization of nonmuscle myosin II-C, a new member of the myosin II family. *J. Biol. Chem.* **279,** 2800–2808 (2004).
11. Göttfert, F. *et al.* Coaligned dual-channel STED nanoscopy and molecular diffusion analysis at 20 nm resolution. *Biophys. J.* **105,**L01–03 (2013).
12. Hall, A. & Nobes, C. D. Rho GTPases: molecular switches that control the organization and dynamics of the actin cytoskeleton. *Philos. Trans. R. Soc. Lond., B, Biol. Sci.* **355,** 965–970 (2000).
13. Heasman, S. J. & Ridley, A. J. Mammalian Rho GTPases: new insights into their functions from in vivo studies. *Nat. Rev. Mol. Cell Biol.* **9,**690–701 (2008).
14. Holmes, W. R., Carlsson, A. E. & Edelstein-Keshet, L. Regimes of wave type patterning driven by refractory actin feedback: transition from static polarization to dynamic wave behaviour. *Phys Biol* **9,**046005 (2012).
15. Insall, R. H. & Machesky, L. M. Actin dynamics at the leading edge: from simple machinery to complex networks. *Dev. Cell* **17,** 310–322 (2009).
16. Katsuno, H. *et al.* Actin Migration Driven by Directional Assembly and Disassembly of Membrane-Anchored Actin Filaments. *Cell Rep* **12,**648–660 (2015).
17. Kovács, M., Tóth, J., Hetényi, C., Málnási-Csizmadia, A. & Sellers, J. R. Mechanism of blebbistatin inhibition of myosin II. *J. Biol. Chem.* **279,** 35557–35563 (2004).
18. Kubo, Y. *et al.* Shootin1-cortactin interaction mediates signal-force transduction for axon outgrowth. *J. Cell Biol.* **210,** 663–676 (2015).
19. Loudon, R. P., Silver, L. D., Yee, H. F. & Gallo, G. RhoA-kinase and myosin II are required for the maintenance of growth cone polarity and guidance by nerve growth factor. *J. Neurobiol.* **66,** 847–867 (2006).
20. Lowery, L. A. & Van Vactor, D. The trip of the tip: understanding the growth cone machinery. *Nat. Rev. Mol. Cell Biol.* **10,** 332–343 (2009).
21. Machacek, M. *et al.* Coordination of Rho GTPase activities during cell protrusion. *Nature* **461,** 99–103 (2009).
22. Madden, K. & Snyder, M. Cell polarity and morphogenesis in budding yeast. *Annu. Rev. Microbiol.* **52,** 687–744 (1998).
23. Medeiros, N. A., Burnette, D. T. & Forscher, P. Myosin II functions in actin-bundle turnover in neuronal growth cones. *Nat. Cell Biol.* **8,**215–226 (2006).
24. Morales, M., Colicos, M. A. & Goda, Y. Actin-dependent regulation of neurotransmitter release at central synapses. *Neuron* **27,** 539–550 (2000).
25. Pollard, T. D. & Borisy, G. G. Cellular motility driven by assembly and disassembly of actin filaments. *Cell* **112,** 453–465 (2003).
26. Raftopoulou, M. & Hall, A. Cell migration: Rho GTPases lead the way. *Dev. Biol.* **265,** 23–32 (2004).

27. Ridley, A. J. Life at the leading edge. *Cell* **145,**1012–1022 (2011).
28. Ridley, A. J. Rho GTPases and actin dynamics in membrane protrusions and vesicle trafficking. *Trends Cell Biol.* **16,**522–529 (2006).
29. Riedl, J. *et al.* Lifeact: a versatile marker to visualize F-actin. *Nat. Methods* **5,** 605–607 (2008).
30. Rochlin, M. W., Itoh, K., Adelstein, R. S. & Bridgman, P. C. Localization of myosin II A and B isoforms in cultured neurons. *J. Cell. Sci.* **108 (Pt 12),** 3661–3670 (1995).
31. Ruthel, G. & Banker, G. Actin-dependent anterograde movement of growth-cone-like structures along growing hippocampal axons: a novel form of axonal transport? *Cell Motil. Cytoskeleton* **40,** 160–173 (1998).
32. Ruthel, G. & Banker, G. Role of moving growth cone-like 'wave' structures in the outgrowth of cultured hippocampal axons and dendrites. *J. Neurobiol.* **39,** 97–106 (1999).
33. Shutes, A. *et al.* Specificity and mechanism of action of EHT 1864, a novel small molecule inhibitor of Rac family small GTPases. *J. Biol. Chem.* **282,** 35666–35678 (2007).
34. Surviladze, Z. *et al.* in*Probe Reports from the NIH Molecular Libraries Program* (National Center for Biotechnology Information (US), 2010).
35. Tilve, S., Difato, F. & Chieregatti, E. Cofilin 1 activation prevents the defects in axon elongation and guidance induced by extracellular alpha-synuclein. *Sci Rep* **5,**16524 (2015).
36. Toriyama, M., Kozawa, S., Sakumura, Y. & Inagaki, N. Conversion of a signal into forces for axon outgrowth through Pak1-mediated shootin1 phosphorylation. *Curr. Biol.* **23,** 529–534 (2013).
37. Vicker, M. G. F-actin assembly in Dictyostelium cell locomotion and shape oscillations propagates as a self-organized reaction-diffusion wave. *FEBS Lett.* **510,** 5–9 (2002).
38. Vladislav, I. T., Gökmen-Polar, Y., Kesler, K. A., Loehrer, P. J. & Badve, S. The role of histology in predicting recurrence of type A thymomas: a clinicopathologic correlation of 23 cases.*Mod. Pathol.* **26,** 1059–1064 (2013).
39. Weiner, O. D., Marganski, W. A., Wu, L. F., Altschuler, S. J. & Kirschner, M. W. An actin-based wave generator organizes cell motility.*PLoS Biol.* **5,** e221 (2007).
40. Wilkinson, S., Paterson, H. F. & Marshall, C. J. Cdc42-MRCK and Rho-ROCK signalling cooperate in myosin phosphorylation and cell invasion. *Nat. Cell Biol.* **7,**255–261 (2005).
41. Wilson, C. A. *et al.* Myosin II contributes to cell-scale actin network treadmilling through network disassembly. *Nature* **465,**373–377 (2010).
42. Winans, A. M., Collins, S. R. & Meyer, T. Waves of actin and microtubule polymerization drive microtubule-based transport and neurite growth before single axon formation. *Elife* **5,**e12387 (2016).
43. Wu, M., Wu, X. & De Camilli, P. Calcium oscillations-coupled conversion of actin travelling waves to standing oscillations.*Proc. Natl. Acad. Sci. U.S.A.* **110,** 1339–1344 (2013).

SUPPLEMENTARY

Figure S1.

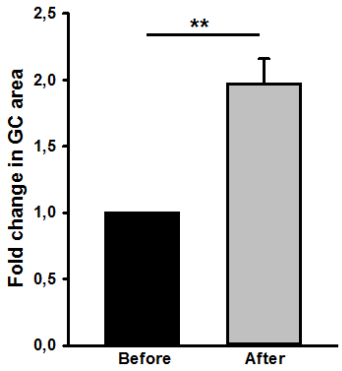

Wave arrival affects GC morphology. Histogram showing a significant increase in GC area after the arrival and fusion of an AW. Student's test was performed for histograms: **P<0.01.

Figure S2.

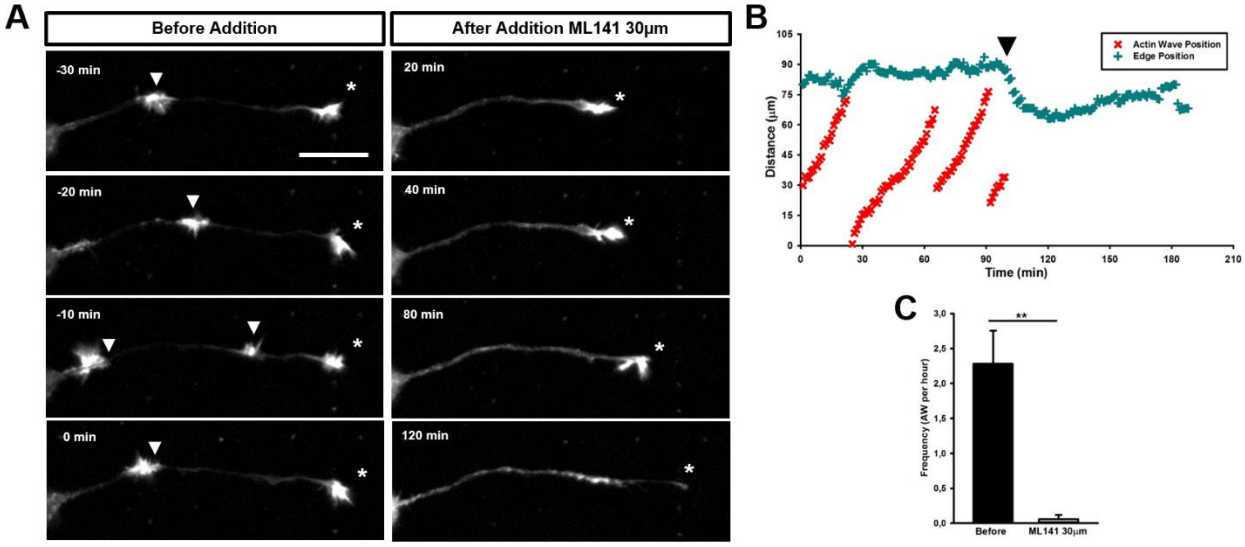

Cdc42 inhibition affects AW dynamicity. (A) Time-lapse live cell imaging of DIV2 rat hippocampal neurons before (left) and after (right) addition of ML141 (30µM). White arrow indicates the growth-cone like AW. The asterisk indicates the GC. Scale bars = 20µm. **(B)** Plot showing the progression of several AWs (red) along the neurite shaft. The edge trace (light blue) highlights neurite retraction concurrent with complete AW disappearing after the ML141 treatment. Black arrow indicates ML141 addition. **(C)** Quantification of the AWs frequency calculated on neurons treated with or without ML141 for 4 hours and imaged like in (A) and (B). N= 9AWs. Student's test was performed for histograms: **P<0.01.

RESULTS DISCUSSION AND FUTURE PROSPECTS

During these years of PhD I concentrated on investigating the spatio-temporal dynamics of neuronal cells and their response to localised chemical signals. The Growth Cone (GC) is one of the most studied structure of the neuronal cell, since it guides the growing axon to find its correct synaptic target. GC motility depends on the cytoskeleton dynamics that in turn are modulated by intracellular signalling cascades triggered by guidance cue receptors on the cell surface. One of the nodes of almost all pathways regulating actin cytoskeleton dynamics are the Rho family of GTPases, the principal focus of my research.

In the last 15 years a lot of effort was put into studying Rho-GTPases dynamics both in neuronal and non-neuronal cells (Itoh *et al.,* 2002; Nakamura *et al.,* 2005; Machachek *et al.,* 2009): one of the major breakthrough was the production of probes to follow their activation cycling in live cells with a high spatio-temporal resolution via Förster Resonance Energy Transfer (FRET) (Yoshizaki *et al.,* 2003). In this way it's been possible to observe in real time the compartmentalisation of Rho-GTPases activation during both spontaneous and evoked migration in fibroblasts and neutrophils (Machachek *et al.,* 2009; Yamao *et al.,* 2015), providing many insights on cell dynamics that are much more complex than what was previously thought (Pertz, 2010). Many studies focused also on the importance of Rho-GTPases in guidance-mediated signal processing, unraveling their importance in regulating cytoskeleton upstream of all the canonical guidance cues known so far.

The majority of these studies tended to use a global approach to stimulate the cells with guidance signals (Picard *et al.,*2009). However, *in vivo,* both neuronal and non-neuronal cells respond better to localised gradients of molecules, either by contact on the cell surface or secreted by distant targets and sensed by specific membrane-bound receptors. The signal, stimulating only specific cell locations, gives directionality to the cell movement. That's why I tried an approach that allowed me to localise the source of the stimulus and limit the guidance cue exposure to specific compartments. Different carriers can be utilised for local optical manipulation, like micro-beads or lipid vesicles. The former provide both a precise sub-cellular localisation of the stimulus, since the mean contact area with the cell is less than 1 μm, and control over the concentration of the stimulating molecule. The latter procure even more control over the molecule concentration, and with a mean vesicle volume of about 1 fL (for a 1 μm diameter lipid vesicle) gives the chance to deliver a very small number of molecules to precise sub-cellular locations (D'Este *et al.,* 2011; Pinato *et al.,* 2012). Optical manipulation of such micro-carriers containing active molecules provides thus both the sub-cellular precision and the versatility to operate in a more physiological manner on the cells object of study

(Pinato *et al.,* 2012; Difato *et al.,* 2013). Moreover different imaging techniques can be used in parallel with optical manipulation to monitor protein dynamics: phase contrast, fluorescence, or even FRET microscopy.

Hence I combined for the first time FRET imaging with optical manipulation to provide a strong tool to study dynamics of intracellular signalling molecules upon local delivery of chemical attractants and repellents. The precision of both techniques allowed me to evaluate the fine spatio-temporal regulation of the Rho-GTPases RhoA and Cdc42 in response to Semaphorin-3A (Sema-3A). Sema-3A is a repulsive secreted guidance cue that interacts with receptors on filopodia and lamellipodia of neuronal GCs. It is known to provoke retraction and affect RhoA and Rac1 activity in a variety of non-neuronal and neuronal cells (Burridge and Wennerberg, 2004). NG108-15 neuroblastoma cells responded to locally delivered Sema-3A with collapse and retraction of the GC. The nature of the carrier used (bead or lipid vesicle) did not affect the morphological response of the cells stimulated, indicating that both are effective ways to trigger local responses. FRET imaging highlighted, as expected, a rapid activation of RhoA in the central region of the GC within 30 seconds from the stimulation. This activation preceded the induced retraction by about 90s and activated RhoA levels correlated perfectly with the induced morphological changes.

On the other hand, an increase in Cdc42 activity is commonly correlated with growth and positive turning downstream of attractive molecules like Netrin-1 or Brain Derived Neurotrophic Factor (BDNF), whereas repulsion usually induces Cdc42 activity decrease, although Cdc42 is not yet clearly correlated with Sema-3A-dependent repulsion (Lowery and Van Vactor, 2009; Hall and Lalli, 2010). Consistent with this view, local delivery of Sema-3A triggered a rapid decrease of Cdc42 activity within 60s from the stimulation, concurrent with cell repulsion. Interestingly, the decrease in Cdc42 activation followed a wave-like behaviour that was almost in synchrony with the leading edge ruffling during retraction. Moreover, in few cases, Sema-3A release triggered a delayed increase in Cdc42 activation levels in the cell compartment away from the stimulus. Its activity propagated in a wave-like manner and generated new lamellipodia and filopodia structures to trigger growth away from the repulsive source.

Local repulsive stimulation with coated beads exerted active Cdc42 continuous waves propagating from the leading edge backwards with a period of about 70 s, similar to waves found in some cases of spontaneous GC collapse and retraction following repulsive stimuli spontaneously occurring *in vitro* (110 s period). If, and how these differences in Cdc42 activation dynamics are triggered by Sema-3A is still an open question. Besides reflecting the intercellular heterogeneity normally occurring in culture, there is a possibility that contact chemical stimulation with beads brings an

intrinsic and unavoidable mechanical component that affects intracellular dynamics. It is known that mechanical stimulation can induce Ca^{2+} oscillation that modify the travelling dynamics of actin and maybe its molecules upstream (Wu *et al.,* 2013), exceeding the fact that Ca^{2+} modulates RhoGTPases dynamics by affecting upstream regulators (Tojima *et al.,* 2011).

Although previous models described a precise spatio-temporal crosstalk between different Rho-GTPases that exhibit sustained polarisation by a wave-pinning mechanisms (Jilkine *et al.,* 2007), our results clearly show a wave-like behaviour only for Cdc42, indicating that there can be diverse crosstalk pathways for reciprocal Rho-GTPases regulation. This higher degree of complexity and signal compartmentalisation was unravelled thanks to the combination of high spatio-temporal resolution of FRET imaging and high subcellular precision of local manipulation.

Rho-GTPases have been considered as Nucleation Putative Factors (NPFs) for actin cytoskeleton dynamics in various mathematical models (Holmes *et al.,* 2012). These assumptions fit perfectly with the observed behaviour of Cdc42, that reminds stereotypical activation waves or wave-trains described in literature (Jilkine *et al.,* 2007; Holmes *et al.,* 2012). The wave-like nature of certain actin cytoskeletal structure can be correlated to the propagation of the oscillation of these NPFs and actin may possess feedback pathways to influence their activation levels. Propagating actin waves have been observed in a wide variety of neuronal and non-neuronal cells. Usually in non-neuronal cells the actin waves migrate along the leading edge causing local disassembly and reconstruction of the cytoskeleton to maintain the dynamicity of the cell in search for cues to direct its migration (Kunida *et al.,* 2012).

In neuronal cells, waves of actin travelling along the neurites shaft were discovered in the late 90's (Ruthel and Banker, 1998,1999). These Actin Waves (AWs) have a GC-like appearance, and originate at the boundary between soma and neurite. They proceed along the shaft in an anterograde fashion to reach the GC. When they arrive at close proximity to the neurite tip, the GC rapidly retracts and the two structures fuse together to form a new, bigger and more dynamic GC that protrude again (Flynn *et al.,* 2009; Katsuno *et al.,* 2015).

We characterised the morphology and dynamics of AWs and investigated the role Rho-GTPases in the inception and propagation of AWs in neuronal cells. The waves observed in hippocampal neurons have a GC-like morphology and dynamics similar to the ones previously described. They occur stochastically in all growing neurites with a mean frequency of 1-2 waves per hour and travel at a mean velocity of 2-3 μm/min. Our imaging setup allows the observation of single cells for multiple hours without disturbing the growth and retraction cycles of living cells. Thanks to that we were able

to highlight that, in early stages of neuron development, the arrival of AWs coincides with an increase of size and dynamicity of the growth cone, that may result in a more effective exploration of surrounding environment in search for directional cues. However, there was no evident increase in neurite length, even after 9 hours of imaging, whereas the elongation-retraction cycles caused by continuous AWs was clearly visible. This effect, that appears to go in contrast with previously reported work, can be explained with the early development stage of neurons used in our experiment. At 24-48 hours after plating most neurons have not yet polarised, and so AW occurrence is a stochastic process that randomly elongates neurites to explore the environment in the search for cues that will help break the symmetry to grow the axon (Winans *et al.,* 2016).

STED images revealed a strong presence of myosin-II in the AWs, in particular at the rear of the wave, with some myosin molecules spreading in the AW periphery, into thicker filopodia. This localisation recalls the one in the GC, where myosin-II is mostly present in the actin arcs at the transition zone, and suggests the presence of myosin-dependent contraction and filament disassembly. This contractility appears to be important for AWs morphology and dynamics, since the inhibition of myosin-II by blebbistatin disrupts their GC-like structure and abolish completely the pulling effect on the GC.

F-Actin network assembly and regulation is known to be associated with membranes and membrane dynamics, that control the compartmentalisation and activity of the plethora of membrane-associated actin-binding proteins in a multi-faceted manner (Bezanilla *et al.* 2015). Therefore, treatment with ß-cyclodextrin, which lowers membrane tension by sequestration of cholesterol (Amin *et al.,* 2012), strongly affects AW morphology and dynamics. Indeed the AW mean area decreases after addition, as well as frequency and velocity, markers we used for neurite dynamicity. These results suggest a role of the membrane that goes beyond shape maintenance, such as regulator of the correct assembly of actin network and localisation of actin-associated signalling in propagating AWs.

Rho-GTPases represent, as stated before, a key node for the regulation of intracellular actin cytoskeleton, inducing both filopodia and lamellipodia and controlling every aspect of actin filaments dynamics (Nobes and Hall, 1995). Recent work showed high activity of Cdc42 and Rac in the travelling AWs. Active Cdc42 level was higher also in front of the propagating AW, and optical activation of Rac molecules was sufficient to trigger AW inception (Winans *et al.,* 2016). We observed that both the frequency and the velocity of AWs, taken as parameters of dynamicity, were decreased in presence of inhibitors for both GTPases. Rac1 inhibition seems to affect the velocity parameter in particular, whereas Cdc42 inhibition has a more prominent effect on the AW frequency, with a complete stop of the waves initiation upon high inhibitor dosage. This effect on AW kinetics can be

explained postulating a role of these Rho-GTPases in the modulation of actin polymerisation and network assembly through the Arp2/3 complex and molecules of the formin family. Another explanation can derive from recent work describing a particular outgrowth pathway in neuronal GCs dependent on adhesions strength through activation of shootin-1 (Toriyama *et al.,* 2013). The mechanism, by which GCs elongate their structure in response to attractive cues like Netrin-1 that phosphorylate shootin-1, a molecules that links the actin filaments to adhesion molecules like L1-CAM, involves the same players recently found fundamental also in AW anterograde movement (Kubo *et al.,* 2015, Katsuno *et al.,* 2015). A cascade downstream of Cdc42, Rac1 and subsequently PAK1, may be responsible for the modulation of the balance between adhesion strength and myosin-dependent retrograde flow in to assure the movement a stable directionality towards the neurite tip. Taken together these results indicate that Cdc42 and Rac1 have a pivotal role AWs morphology and anterograde movement through fine spatio-temporal regulation of the actin cytoskeleton dynamics.

In conclusion, this work as a whole explores the importance of the RhoGTPases as one of the key switches that help regulate cell migration, motility and directional growth. Although the knowledge of these mechanisms is becoming clearer and clearer, especially with the help of high spatio-temporal resolution techniques, adequate dissection of these kinetics requires further study and technical improvements. First, we should explore the activation dynamics of all Rho-GTPases in AWs with FRET imaging, coupled with inhibition of single players to dissect the fine GTPases spatial and temporal regulation and highlight crosstalk and feedback mechanisms. Furthermore, in order to better understand their role in guidance-dependent dynamics, it seems necessary to couple imaging with local stimulation to evaluate the AW and GC changes upon chemical cues delivery and gain a better understanding of the processes that act together to build the complex network that is the nervous system.

References

Amin, L., Ercolini, E., Shahapure, R., Migliorini, E. & Torre, V. The role of membrane stiffness and actin turnover on the force exerted by DRG lamellipodia. *Biophys. J.* **102,** 2451–2460 (2012).

Bezanilla, M., Gladfelter, A. S., Kovar, D. R. & Lee, W.-L. Cytoskeletal dynamics: a view from the membrane. *J. Cell Biol.* **209,** 329–337 (2015).

Burridge, K. & Wennerberg, K. Rho and Rac take center stage. *Cell* **116,** 167–179 (2004).

D'Este, E. *et al.* Use of optical tweezers technology for long-term, focal stimulation of specific subcellular neuronal compartments. *Integr Biol (Camb)* **3,** 568–577 (2011).

Difato, F., Pinato, G. & Cojoc, D. Cell signaling experiments driven by optical manipulation. *Int J Mol Sci* **14,** 8963–8984 (2013).

Flynn, K. C., Pak, C. W., Shaw, A. E., Bradke, F. & Bamburg, J. R. Growth cone-like waves transport actin and promote axonogenesis and neurite branching. *Dev Neurobiol* **69,** 761–779 (2009).

Hall, A. & Lalli, G. Rho and Ras GTPases in axon growth, guidance, and branching. *Cold Spring Harb Perspect Biol* **2,** a001818 (2010).

Holmes, W. R., Carlsson, A. E. & Edelstein-Keshet, L. Regimes of wave type patterning driven by refractory actin feedback: transition from static polarization to dynamic wave behaviour. *Phys Biol* **9,**046005 (2012).

Jilkine, A., Marée, A. F. M. & Edelstein-Keshet, L. Mathematical model for spatial segregation of the Rho-family GTPases based on inhibitory crosstalk. *Bull. Math. Biol.* **69,** 1943–1978 (2007).

Katsuno, H. *et al.* Actin Migration Driven by Directional Assembly and Disassembly of Membrane-Anchored Actin Filaments. *Cell Rep* **12,**648–660 (2015).

Kubo, Y. *et al.* Shootin1-cortactin interaction mediates signal-force transduction for axon outgrowth. *J. Cell Biol.* **210,** 663–676 (2015).

Kunida, K., Matsuda, M. & Aoki, K. FRET imaging and statistical signal processing reveal positive and negative feedback loops regulating the morphology of randomly migrating HT-1080 cells. *J. Cell. Sci.* **125,** 2381–2392 (2012).

Lowery, L. A. & Van Vactor, D. The trip of the tip: understanding the growth cone machinery. *Nat. Rev. Mol. Cell Biol.* **10,** 332–343 (2009).

Machacek, M. *et al.* Coordination of Rho GTPase activities during cell protrusion. *Nature* **461,** 99–103 (2009).

Nakamura, T., Aoki, K. & Matsuda, M. FRET imaging in nerve growth cones reveals a high level of RhoA activity within the peripheral domain. *Brain Res. Mol. Brain Res.* **139,** 277–287 (2005).

Nobes, C. D. & Hall, A. Rho, rac, and cdc42 GTPases regulate the assembly of multimolecular focal complexes associated with actin stress fibers, lamellipodia, and filopodia. *Cell* **81,** 53–62 (1995).

Pertz, O. Spatio-temporal Rho GTPase signaling - where are we now?*J. Cell. Sci.* **123,** 1841–1850 (2010).

Picard, M. *et al.* Spatial and temporal activation of the small GTPases RhoA and Rac1 by the netrin-1 receptor UNC5a during neurite outgrowth. *Cell. Signal.* **21,** 1961–1973 (2009).

Pinato, G. *et al.* Less than 5 Netrin-1 molecules initiate attraction but 200 Sema3A molecules are necessary for repulsion. *Sci Rep* **2,** 675 (2012).

Ruthel, G. & Banker, G. Actin-dependent anterograde movement of growth-cone-like structures along growing hippocampal axons: a novel form of axonal transport? *Cell Motil. Cytoskeleton* **40,** 160–173 (1998).

Ruthel, G. & Banker, G. Role of moving growth cone-like 'wave' structures in the outgrowth of cultured hippocampal axons and dendrites. *J. Neurobiol.* **39,** 97–106 (1999).

Tojima, T., Hines, J. H., Henley, J. R. & Kamiguchi, H. Second messengers and membrane trafficking direct and organize growth cone steering. *Nat. Rev. Neurosci.* **12,** 191–203 (2011).

Toriyama, M., Kozawa, S., Sakumura, Y. & Inagaki, N. Conversion of a signal into forces for axon outgrowth through Pak1-mediated shootin1 phosphorylation. *Curr. Biol.* **23,** 529–534 (2013).

Winans, A. M., Collins, S. R. & Meyer, T. Waves of actin and microtubule polymerization drive microtubule-based transport and neurite growth before single axon formation. *Elife* **5,** e12387 (2016).

Wu, M., Wu, X. & De Camilli, P. Calcium oscillations-coupled conversion of actin travelling waves to standing oscillations. *Proc. Natl. Acad. Sci. U.S.A.* **110,** 1339–1344 (2013).

Yamao, M. *et al.* Distinct predictive performance of Rac1 and Cdc42 in cell migration. *Sci Rep* **5,** 17527 (2015).

Yoshizaki, H. *et al.* Activity of Rho-family GTPases during cell division as visualized with FRET-based probes. *J. Cell Biol.* **162,** 223–232 (2003).